EXPERIMENTAL STUDY OF POSITRON MODERATION AND TIMING

A thesis submitted to the University of London
for the degree of Philosophy

Jonathan Peter Merrison
Department of Physics and Astronomy
University College London

October 1992

ABSTRACT

The development of more intense and better resolved slow positron (e^+) beams is one of the major goals in e^+ research. One way to achieve this is by improving the efficiency of β^+ moderation techniques. Such improvements would allow the application of this unique probe to many areas of research which currently find the technology prohibitively complex and expensive. It may also open the way to more ambitious research projects requiring high intensity beams, for example the formation of anti-hydrogen.

A technique employed in e^+ physics which is often important in order to improve the quality of the detected signal is that of single particle timing. This technique relies on the fact that generally e^+ beams are of low intensity and by resolving interactions in time it becomes possible to reduce spurious (random) background counts. The development of a new method of timing has been carried out which utilises the secondary e^-s emitted on β^+ impact with the moderator. The success of this method lies in the fact that the same component of the β^+ energy spectrum which contributes most to the emitted slow e^+ yield (ie the those with low energy) is also most efficient at secondary e^- emission. Positron tagging efficiencies of greater than 20% were observed with a signal to background ratio much higher than that obtained with other β^+ tagging techniques. There was also no loss of beam intensity using this technique, unlike that of timing at a remoderator.

An investigation was performed on the e+ moderating properties of the rare gas solids (RGS). Neon has recently provided the highest currently quoted moderation efficiencies. The work presented in this thesis showed that the other RGS (Ar, Kr and Xe) could achieve comparable efficiencies and provide greater than a ten fold improvement on the commonly used metal foil or mesh type moderators. Importantly these RGS moderators are easily fabricated, rugged and may be replaced without loss of vacuum.

The first observation of electric field assisted e^+ extraction was made during the course of this study. This was achieved by surface charging of the RGS film by the trapping of electrons on overlayered oxygen molecules. Enhancement in the moderation efficiency of a factor of three was observed and was attributed to the electric field, of strength approximately 6kV/mm, across the film due to the trapped surface charge. This effect is not only of importance in the development of more efficient slow e^- moderators but may prove to be an interesting new field of research in its own right.

TABLE OF CONTENTS

ABSTRACT 1

TABLE OF CONTENTS 2

LIST OF FIGURES 5

LIST OF TABLES 9

ACKNOWLEDGEMENTS 10

CHAPTER 1 Background

1.1 Introduction 12

1.2 Basic positronic properties 13

1.3 Positrons in solids 16

1.3.1 Positron backscattering 17

1.3.2 Positron implantation 18

1.3.3 Slowing down 20

1.3.3a Metals 21

1.3.3b Insulators 21

1.3.3c Semiconductors and ionic solids 22

1.3.4 Diffusion 23

1.3.5 Ps in solids 25

1.3.5a Ore model 25

1.3.5b Spur model 26

1.3.6 Surface processes 27

1.3.6a Introduction 27

1.3.6b Work function e^+ emission from metal 27

1.3.6c Prompt energetic Ps emission 29

1.3.6d Thermally desorbed Ps 30

1.3.6e e^+ emission from insulators 31

1.3.6f		Ps emission from insulators	31
1.3.6g		Surface trapping	32
1.3.7		Secondary e^- emission	33
1.4	The effect of an externally applied electric field on e^+s in solids		34
1.4.1		Implantation and thermalisation	35
1.4.2		e^+ diffusion	35
1.4.3		Ps formation	37
1.4.3a		Gas phase	37
1.4.3b		Solids	38
1.4.3bi		Spur	39
1.4.3bii		Ore	40
1.5	Positron moderation and transport		41
1.5.1		Moderation	41
1.5.2		Magnetic transport	44
1.5.3		Electrostatic transport	45
1.5.4		Brightness enhancement	46
1.6	Positron beam timing		47
1.6.1		Introduction	47
1.6.2		β^+ tagging	48
1.6.3		Secondary e^- tagging at a remoderator	50
1.6.4		Pulsed/bunched beams from radioactive sources	50
1.6.5		Conclusion	51
1.7	Motivation for present work		52
CHAPTER 2	**Secondary electron timing at the primary moderator**		
2.1	Introduction		54
2.2	Experimental arrangement		54
2.3	Experimental procedure		56
2.4	Results		58
2.5	Discussion		65
CHAPTER 3	**Rare Gas Solid Moderators**		66

	3.1	Theoretical treatment	66
	3.2	Experimental arrangements	67
	3.2.1	Magnetic beam	67
	3.2.2	Electrostatic beam	69
	3.3	Experimental procedure	74
	3.3.1	Magnetic transport	74
	3.3.2	Electrostatic transport	75
	3.4	Results and discussion	76
	3.4.1	Magnetic beam	76
	3.4.2	Electrostatic beam	79
	3.5	Conclusion	83
CHAPTER	**4**	**Surface charging and field assisted moderation using Rare Gas Solids**	
	4.1	Introduction	86
	4.2	Surface charging	87
	4.3	Experimental arrangement	90
	4.4	Results	92
	4.4.1	Observation of e^+ enhancement and preliminary tests	92
	4.4.2	Other RGS/Overlayers and charge application	95
	4.4.3	Preliminary retarding spectra	97
	4.4.4	Precision retarding spectra	103
	4.4.5	Precision charging measurements under controlled conditions	106
	4.4.6	Conventionally applied electric field	112
	4.5	Discussion	113
	4.6	Conclusion	117
CHAPTER	**5**	**Conclusion**	119
REFERENCES			123

LIST OF FIGURES

1.1	The Feynman diagrams for annihilation into a)one, b)two, c)three and d)four photons.	15
1.2	Energy distribution of γ-ray emission from o-Ps decay (Ore and Powell 1949, Chang et al 1982, 1985)	16
1.3	Schematic of e^+ interaction with the near surface region ($E \leq 100$keV), following Schultz and Lynn (1988).	17
1.4	Re-emitted e^+ energy spectra from solid neon (Gullikson and Mills 1986)	23
1.5	Energy loss processes for different classes of materials represented schematically following Schultz and Lynn (1988).	24
1.6	e^+ surface potential for a metal; a)bulk potential, b)surface dipole, c)image potential and d)complete potential.	28
1.7	Angular emission of work function e^+s from a metal surface.	30
1.8	Positron emission spectra for solid Ar, Kr and Xe at incident energies of 4800 and 1800eV (Gullikson and Mills 1986).	31
1.9	Positron energy spectrum from a solid Ne moderator (Mills and Gullikson 1986).	32
1.10	Energy spectra of Ps emitted from solid Quartz and MgO (Sferlazzo et al 1987).	33
1.11	Variation of the secondary yield (δ^+, δ^-) as a function of incident e^+ and e^- energy (Bodin 1957).	34
1.12	Secondary e^- energy spectra from Nb induced by 400keV proton and 3keV electron impact (Musket 1975).	35
1.13	X-ray induced secondary electron energy spectra from solid Ar and Xe (Gullikson 1988).	36
1.14	Schematic of the motion of a diffusing e^+ a)without and b)with an applied electric field.	37
1.15	Relative Ps yield in polyethylene avrying with electric field (Bisi et al 1981), the solid curve is based on theory (Brandt 1982).	39
1.16	Comparison of moderated e^+ spectrum with the β^+ particle energy spectrum for ^{58}Co (normalised).	41

1.17	Different common source/moderator geometries.	43
1.18	Brightness per unit-energy phase space for slow e^+ moderation (Mills 1983).	48
1.19	Typical raw data using β^+ scintillator technique, Coleman et al (1973)	49
2.1	Schematic of the magnetically guided slow e^+ beam employed in these experiments.	55
2.2	Vacuum rig used for the annealing of the metal moderators.	55
2.3	Schematic of the electronics employed for the e^+ time of flight measurements.	56
2.4	Typical raw data time of flight spectrum recorded over 1000secs using this apparatus with four W mesh moderators.	59
2.5	Secondary e^- energy spectrum obtained by retardation using this apparatus.	60
2.6	Calibrating the ToF system by varying the slow e^+ energy and measuring the fast-slow e^+ component separation	61
2.7	Number of W moderator meshes vs ▵ secondary e^-, □ slow e^+ yield and • e^+ timing efficiency	62
3.1	Calculated solid Ar moderation efficiency as a function of film thickness using a diffusion equation.	68
3.2	Schematic of the magnetically guided slow e^+ beam	69
3.3	Schematic of the electronic employed for the coincidence measurments.	70
3.4	Source mount and cold head designs for RGS moderators; a)cup1, b)cup2, c)cone and d)flat plate.	72
3.5	Electrostatic guided slow e^+ beam arrangement.	73
3.6	SIMION simulation program of the electrostatic beam optics for 2eV e^+s emitted at ±20° from the cup source.	73
3.7	Slow e^+ yield from a cup mounted Ar moderator as a function of time at a pressure of $5x10^{-5}$Torr.	76
3.8	Slow e^+ yield as a function of pressure×time for Ar moderator deposition at ● 2×10^{-5} and ○ 10^{-4} Torr.	78
3.9	Slow e^+ yield from cup 2 as a function of ○ Xe, ▾▽ Kr and □■ Ar deposition time.	80
3.10	Slow e^+ yield from a conical source as a function of ○ Xe, ▾ Kr and □ Ar deposition time.	81

4.1	Secondary electron emission curve from Teflon (PTFE) as a function of incident energy.	88
4.2	Current transmitted by an uncharged (top) and charged (bottom) $Kr+O_2$ film with e^- beam energy (Sanche and Deschenes 1988)	90
4.3	Electron energy dependence of the surface charging coefficient A_S for a 0.1-L-O_2/Kr film.	91
4.4	Modified electrostatic beam arrangement employing an e^- filament.	92
4.5	Slow e^+ yield from an Ar/air moderator with time during which e^- irradiation (▲ filament activation) is performed.	93
4.6	Slow e^+ retarding spectra from an ○ Ar, ▽ $Ar+O_2$ and ▲ $Ar+O_2$ after e^- irradiation.	96
4.7	β^+ induced secondary e^- spectra from ○ Ar, □ $Ar+O_2$ and ▲ $Ar+O_2$ after e^- irradiatio	97
4.8	Slow e^+ retarding spectra taken ○ before and ▲ after e^- irradiation.	98
4.9	β^+ induced secondary e^- retarding spectra taken ○ before and ▲ after e^- irradiation.	100
4.10	e^+ retarding spectra from ○ Kr, □ Kr+O and ▲ $Kr+O_2$ after e^- irradiation.	101
4.11	β^+ induced secondary e^- retarding spectra from ○ Kr, □ $Kr+O_2$ and ▲ $Kr+O_2$ after e^- irradiation.	102
4.12	β^+ induced secondary e^- yield from a Kr moderator as a function of time.	104
4.13	e^+ retarding spectra taken ○ before and ● after O_2 exposure of a Kr film.	105
4.14	β^+ induced secondary e^- retarding spectra taken ○ before and ● after O_2 coverage of a Kr film.	106
4.15	e^+ energy spectra emitted from a Kr film derived from a retarding spectrum.	107
4.16	β^+ induced secondary e^- energy spectra emitted from a Kr film derived from retarding spectra.	109
4.17	e^+ retarding spectrum taken before and after low enrgy e^- bombardment of an Ar/O_2 moderator film	110
4.18	β^+ induced secondary e^- spectra taken before and after low energy e^- bombardment of an Ar/O_2 moderator	111
4.19	β^+ induced secondary e^- yield from an $Ar+O_2$ moderator film as a function of time.	112

4.20 Surface charge (e^+ energy shift) as a function of time of an e^- irradiated $Ar+O_2$ moderator film. 113

4.21 Slow e^+ yield as a function of surface charge (and estimated field strength) from an e^- irradiated $Ar+O_2$ film . 114

4.22 β^+ induced secondary e^- yield as a function of surface charge from an $Ar+O_2$ film. 115

4.23 Current (e^-s) striking the source mount during filament activation as a function of retarding voltage. 116

LIST OF TABLES

1.1	Positron moderation efficiencies	40
1.2	RGS moderator efficiences and e^+ emission energy widths (Mills and Gullikson 1986)	43
1.3	Positron moderator characteristics	45
2.1	Parameters of timed beam using different numbers of annealed meshes in the moderator.	61
2.2	Timed beam parameters for different moderator materials.	64
3.1	Summary of the maximum RGS moderator efficiencies determined for different copper source designs and RGS samples.	82
4.1	Positron/secondary e^- yield from an air coated Ar moderator after various surface activation processes.	95
4.2	Positron yield and moderation efficiency as a function of RGS depth (deposition time × pressure).	97
4.3	Positron and secondary e^- yields from (clean) RGS moderators and following O_2 coating and surface activation.	102

ACKNOWLEDGEMENTS

I would like to express my gratitude to the people who have provided help, support and encouragement during my postgraduate work.

For his years of supervision and tuition I would like to thank Dr Mike Charlton.

For lots of useful advice and discussion I thank Drs Nella Laricchia and Finn Jacobsen and, also for enabling much of this work, Prof. Bernie Deutch

I should like to express my appreciation for the technical assistance of Ivan Rangué, Ted Oldfield, Paul Ageholm and Sven Olesen.

I wish to thank the SERC and the Danish Research Academy for financial support.

Thanks also to my friends and colleagues who have tried to keep me happy, interested and have always been in the bar for a quick one: Jonathan, Michele, Mark, Selena, Tom, Geraint, Dave, Annette, Lars, Mogens, Jeppe, Jeremy, Nazrene, Pat and Dave.

To Mum and Dad,

Tim, Claire and Rachael

CHAPTER 1

BACKGROUND

1.1 Introduction

The existence of antiparticles was originally proposed by Dirac following the development of his relativistic wave equation in 1928 which was to account for the intrinsic angular momentum of the electron. The negative energy electron states predicted were interpreted as being an electron antiparticle, or positron, the existence of which was first observed by Anderson in 1932 using a cloud chamber apparatus observing cosmic rays.

The possibility of an electron-positron bound state, later named positronium, was suggested by Mohorovicic in 1934, It was finally observed by Deutsch in 1951 by which time many calculations had been performed on this light atomic system. The emission of positrons by certain radioactive materials provided a means of controlled experiment, initially in the late 1940's, involving 'swarm' type experiments where positrons of broad energy distribution (eV-MeV) were observed interacting in various media. A more elegant experimental technique, proposed in 1950 by Madanski and Rasetti, was demonstrated by Cherry in 1958 and involved the slowing down (moderation) and subsequent low energy re-emission (at a few eV) of positrons by certain solids in order to produce a mono-energetic beam of the particles. Much research is still in progress to develop more efficient positron moderators and better spatially and energy resolved beams.

The positron provides a useful probe in the fields of solid state, surface and atomic physics and displays both important similarities and differences to the behaviour found for electrons. Generally positrons show increased correlation with electrons present in the target and are not affected by exchange. In addition the instantaneous emission of γ-radiation on positron annihilation not only signals its decay, the basis of positron lifetime experiments, but provides information about the electron with which it annihilated such as its energy and momentum. This property is employed in studies of the angular correlation and Doppler broadening of the annihilation radiation.

In many cases high resolution may be obtained using positrons compensating somewhat for the present restrictions on beam intensity. One example is that of low energy positron

diffraction (LEPD) which, as with low energy electron diffraction (LEED), relies on coherent scattering from a lattice to produce diffraction effects. Lack of exchange processes and differences in scattering cross section make positrons more surface sensitive and give LEPD significant advantages over LEED. Rather than compete it is more common that positron studies are carried out to complement existing techniques, this is especially true in the case of atomic scattering where the use of electrons, positrons, protons and antiprotons as probes serve to critically test theoretical models and provide some separation of mass and charge effects (Charlton et al 1988).

Stringent tests of quantum electrodynamics (QED) have been, and will undoubtedly continue to be, performed using positronium. Being a purely leptonic system precision measurements of its lifetime and energy levels challenge theoretical calculation. With the advent of positronium beam production new avenues of experimentation have been opened (Laricchia et al 1992). Fundamental positron related research currently underway includes the production of antihydrogen which would enable the first observations to be made of atomic antimatter. Determination of the properties of antihydrogen may provide important tests of CPT invariance, a cornerstone of modern particle physics. Several other measurements which may be performed on H are discussed by Deutch (1992), one of which for example is its behaviour under gravity.

In the following sections a brief outline of the nature of positrons and positronium will be presented followed by a discussion of the behaviour of positrons in solids, positron beam production and particle timing techniques. A more detailed outline of the work presented in this thesis and the motivation for it is given at the end of this chapter.

1.2 **Basic positronic properties**

As mentioned earlier the e^+ is the antiparticle of the electron, it therefore has the same mass which is currently measured to be $511.0034\pm0.0014 keV/c^2$ by Cohen and Taylor (1973). It is stable in vacuum ($\tau>2*10^{21}$yrs Bellotti 1983) also and assuming CPT theory to be valid, it should have the same spin (1/2), but opposite charge and magnetic moment as the electron

Capture of an e^- by a e^+ produces a quasi-stable bound state called positronium (Ps) which possesses similar structural properties to those of hydrogen. Having about half of the reduced mass of hydrogen it has double the spatial dimensions (Bohr radius $\approx$1.05Å). The energy

levels are consequently at half of the values seen with hydrogen, this gives Ps an ionisation energy of roughly 6.8eV. In its ground state it is comprised, as is hydrogen, of one (singlet) spin zero and three (triplet) total spin one states. Splitting of these states occurs due to the spin-spin hyperfine interaction which is some 200 times larger than in hydrogen owing mainly to the increased magnetic moment of the positron compared with that of the proton.

Annihilation of Ps will normally involve the emission of a number of γ-ray photons with energy totalling that of the system; at rest this is approximately 1.022MeV. The process is subject to certain selection rules which require the singlet state (commonly called para-Ps) to decay by emission of an even number of photons (usually two) and the triplet (known as ortho-Ps) by an odd number (usually three). Positron annihilation processes may be represented in schematic form using Feynman diagrams which are also of some practical use since in order to obtain approximate interaction probabilities. Figure 1.1 depicts four Feynman diagrams representing 2, 3 and 4 γ decay as well as 1 γ decay involving interaction with a third body (a nucleus). The likelihood of each process b) - d) is given roughly by α^m where α is the fine structure constant ($\approx 1/137$) and m is the number of photons liberated. The presence of a third body required in a) drastically reduces the probability of this process.

Detailed calculation of the decay rates via b) and c) channels for the bound state have been made by Caswell and Lepage (1979) and values were obtained of λ(para-Ps)=7.9852ns^{-1} and λ(ortho-Ps)=7.0386μs^{-1}. In terms of average lifetime this gives para-Ps an expected value of $\approx$0.125ns, decaying to two γ-rays which, for the system at rest, have equal energy and are emitted at 180° to each other. O-Ps would be expected to live on average $\approx$142ns and liberate three coplanar photons with energies distributed from 0 to 511KeV. Figure 1.2 illustrates this distribution as calculated by Ore and Powell (1949) and measured by Chang et al (1985).

Many experimental measurements have been carried out determining the o-Ps decay rate with the most accurate being that of Nico et al (1991) who obtained 7.0482$\pm$0.0016μs^{-1}. It should be noted that this value significantly deviates from theoretical prediction which may require refinement of the calculation to include higher order terms or the addition of an exotic decay mode not considered in the QED treatment. Due to its short lifetime direct measurement of the decay rate of p-Ps is not presently possible, however an experiment based on singlet-triplet Zeeman mixing in a strong magnetic field, performed by Gidley et al (1982), has provided the most accurate determination of λ(p-Ps)=7.994$\pm$0.011ns^{-1}. This value is in agreement with theory. Despite its low probability, decay by four γ-ray emission, channel

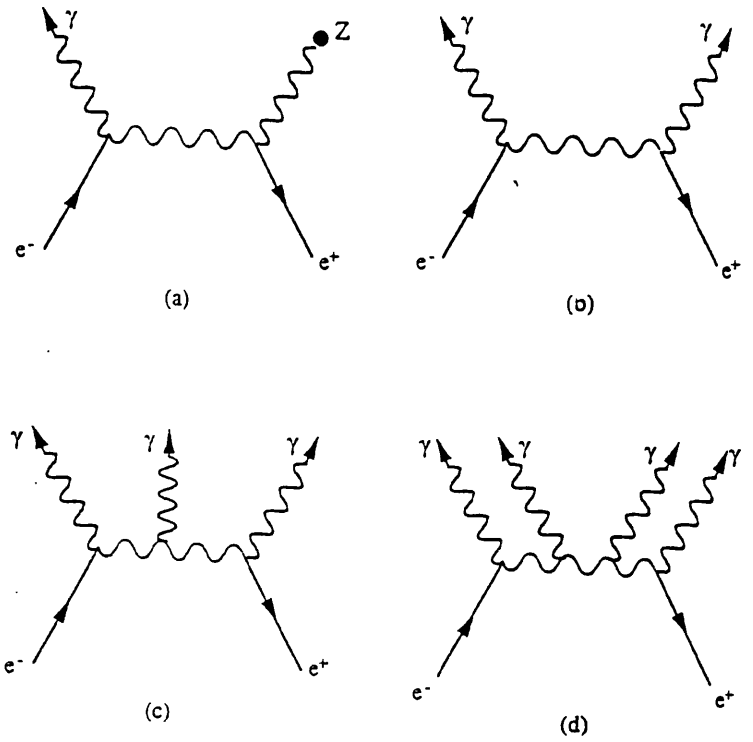

Figure 1.1 The Feynman diagrams for annihilation into a)one, b)two, c)three and d)four photons.

d), has recently been observed by Adachi et al (1990) at a branching ratio consistent with QED calculations.

The treatment of e^- interactions with matter began with Dirac (1930b) whose calculation of the 2-γ annihilation cross section with a free e^- yields, in the non-relativistic limit,

$$\sigma_{2\gamma} = \pi r_o^2 c/v \qquad 1.1$$

where r_0 is the classical electron radius, c and v are the speeds of light and the e^+ respectively. Modification of this equation allows an extension to be applied to e^+s within gases;

$$\sigma_{2\gamma} = \pi r_o^2 cZ_{eff}/v \qquad 1.2$$

where Z_{eff} is the effective number of e^- possessed by each atom as observed by the e^+. This differs from Z due to polarisation effects which become insignificant at high speeds.

Similarly for solids a simple expression has been derived for the e^+ 2-γ annihilation rate (Γ) as a function of the local e^- density as observed by the e^- ($\rho(r)$);

$$\Gamma = \pi r_0 \rho_- = \tau^{-1} \qquad 1.3$$

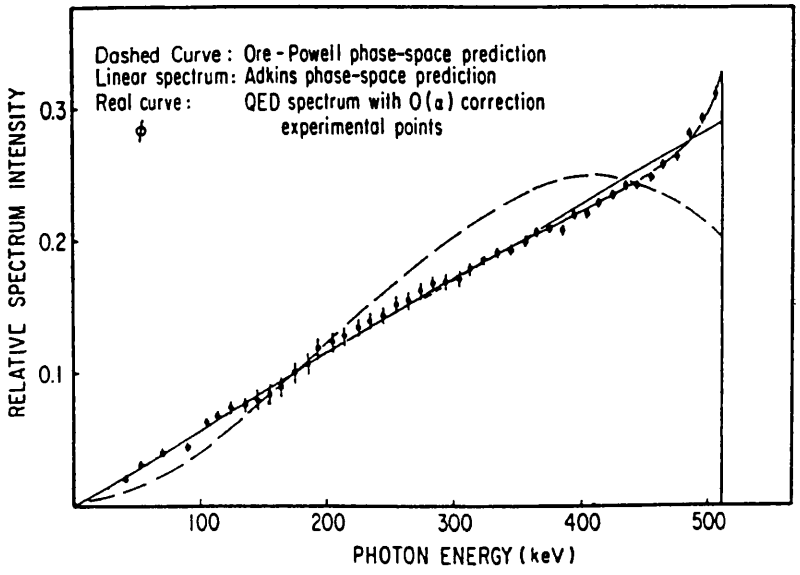

Figure 1.2 Energy distribution of γ-ray emission from o-Ps decay (Ore and Powell 1949, Chang et al 1982, 1985)

$$\rho_{-} = \int dr^3 \rho_{+}(r)\rho_{-}(r)$$

where $\rho_{+}(r)$ = e^{+} probability density at r and $\rho_{-}(r)$ = e^{-} probability density at r. The e^{+} annihilation rate, which is the inverse of the mean e^{+} lifetime (τ), may thus be used as a probe of the local e^{-} density though correction must be made for enhancements (in $\rho_{-}(r)$) due to the Coulomb interaction. For metals e^{+} lifetimes are typically around 150ps, although much variation is seen (Brandt and Dupasquier 1983). It should be noted that this time scale is large compared to other time scales within solids such as lattice relaxation ($\approx 10^{-13}$s), electronic de-excitation ($\approx 10^{-16}$s) and ,as will be discussed later, e^{+} thermalisation which normally take a few ps. The lower e^{-} densities found in insulators produce generally larger e^{+} lifetimes of several hundred ps, tending to ≈500ps for good insulators. Such low e^{-} densities may allow formation of bulk Ps, or quasi-Ps, which is observed by lifetime, angular correlation and 3-γ annihilation methods. The Ps formed within the solid is often highly perturbed by the surrounding lattice causing significant deviation of its lifetime from that in vacuum. This may also be reduced by pick-off processes involving other e^{-}s in the solid.

1.3 **Positrons in solids**

This section discusses the behaviour of e^{-} interactions with solids, beginning with back-

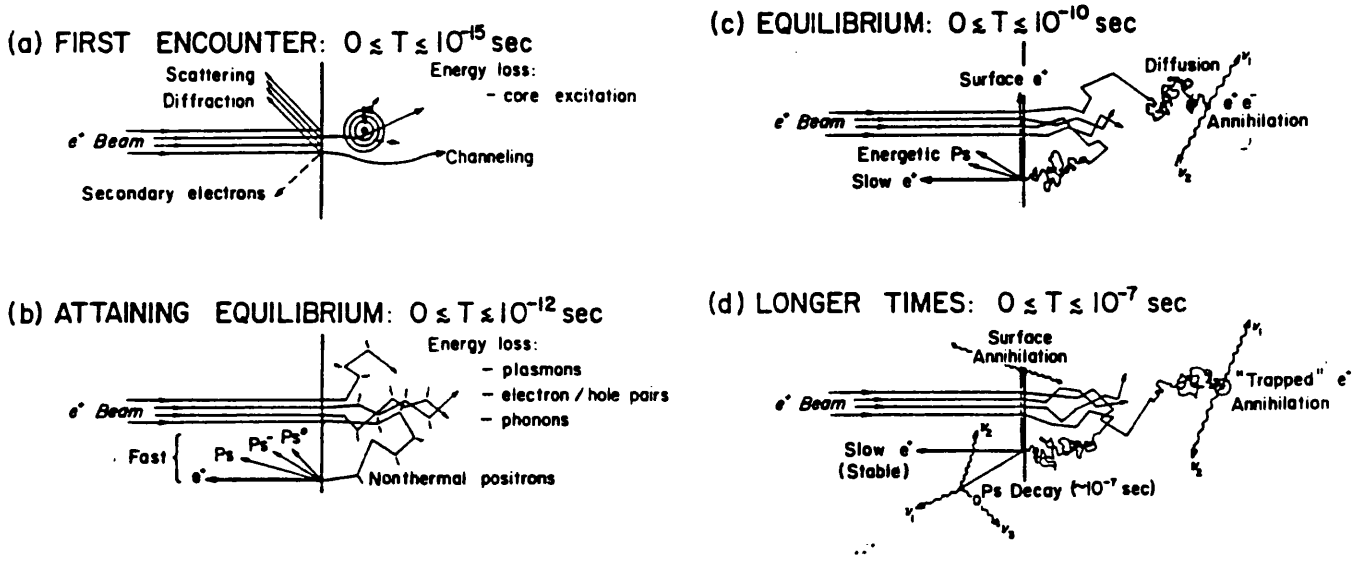

Figure 1.3 Schematic of e^+ interaction with the near surface region (E≤100keV), following Schultz and Lynn (1988).

scattering from or implantation into an incident surface. It will continue by covering the processes of slowing down and diffusion in the bulk followed by possible surface processes.

There is a strong energy dependence in the manner with which e^+s interact with surfaces. High energy particles generally penetrate deep into the solid and subsequently completely thermalise. At intermediate energies a significant fraction may return to the surface at epithermal energies, having incompletely slowed down. Lower energy e^+s (<100eV) have associated de Broglie wavelengths comparable to crystal lattice spacings and may thus undergo coherent scattering.

An important inelastic process for e^+s at a surface is that of secondary e^- production which will be discussed in some detail at the end of this chapter. Positrons returning to a surface may capture an e^- and be emitted in the form of positronium. A visual summary of e^+ interaction processes with solids is presented in figure 1.3.

1.3.1 Positron backscattering

The reflection of e^-s striking a surface is quantified by a coefficient (B) of backscattering which expresses the fractional loss of e^-s from an incident surface. This coefficient is highly dependent on both e^- energy and the atomic number of the target material (Z). MacKenzie et al (1973) measured the variation of B with Z for values ranging from 3 to 92 using β^+

particles and found that the data fitted the empirical relationship,

$$B = 0.342\log Z - 0.146 \qquad 1.4$$

Experiments have been carried out in order to investigate backscattering from metal samples, the first of these was performed by Mills and Wilson (1982) who measured the longitudinal energy spectra of e^+s re-emitted from an Al foil between 1 and 6keV. Baker and Coleman (1988) performed similar measurements using Cu, Ag, Al and W at energies ranging from 0.5-30keV and Massoumi et al (1991) carried out angular backscattering experiments at 35keV. The results from the these two studies differed from those obtained using β^+ particles and also differed from each other especially at lower energies (<10keV). Recently Mäkinen et al (1992) studied samples with Z ranging from 6 to 79 at energies from 2-30keV and found agreement with the results of Massoumi et al. Agreement was also found with Monte Carlo simulations.

1.3.2 Positron implantation

Positrons entering a surface may penetrate to various depths within the solid before being slowed down. In this context "slowed down" refers to degradation of the energy down to a few eV (the endpoint energy E_e) at which point phonon scattering becomes important as a thermalising process. At energies significantly above E_e little difference exists between the energy loss processes occurring in metals and insulators. The diffusion of the e^+s in the latter stages of thermalisation has only a small effect on the final penetration depth and leads only to a random walk blurring of the implantation distribution.

The probability of an implanted e^+ achieving the endpoint energy at a certain depth (x) is given by the stopping profile P(x). Implantation experiments using a variable energy (1-6keV) e^+ beam were carried out by Mills and Wilson (1982) on thin (up to 3000Å) films of Cu, Al and Si. Variation of the median implantation depth (x_o) for different materials was found to vary inversely with mass density (ρ). Also for Al and Cu x_o was found to vary as a function of implantation energy with a power law,

$$x_o = (A/\rho)\, E^n \quad \text{Å} \qquad 1.5$$

with n=1.6(+0.15, -0.08) and 1.3(+0.07, -0.11) respectively and A≈3.32 μg cm^{-1} keV^{-n}). Recently e^+ implantation experiments have been performed using a similar technique to that employed by Mills and Wilson (1982), but at the higher energies of 10-50keV. Here significant deviations were observed from this empirical power law relationship and this work also demonstrated that the simple mass density scaling is inadequate (Baker et al 1991a and b).

Monte Carlo simulations carried out by Valkealahti and Nieminen (1983 and 1984) of 1-10keV e^+ implantation found good agreement with experiment using a Makhovian stopping profile which was originally developed for e^- implantation. Recent experiments have confirmed the power of Monte Carlo simulations for modelling of e^+ implantation (Baker et al 1991c, Poulsen et al 1992). The Makhovian profile has the form,

$$P(x) = mx^{m-1}/x_0^m \exp[-(x/x_0)^m] \qquad 1.6$$

where parameter m is a shape parameter which when equal to 1 produces an exponential form and when 2 gives a gaussian derivative profile and x_0 is a quantity related to the median penetration depth, x, by x_o=1.13x. A value for the shape parameter m of 1.9 is predicted to give the best description of monoenergetic beam implantation (Valkealahti and Nieminen 1983), however the experimental results obtained by Mills and Wilson (1982) were fitted more closely by a value m≈1.4. Commonly a value of m=2 is used and it has been shown that this profile provides a better fit than an exponential (Vehanen et al 1987). It would appear that further analysis is required with respect to implantation profiles for monoenergetic beams before a consistent description emerges.

Absorption studies of β^+ and β^- particles implanted into various materials have been found to be well described by an exponential profile (eg. Knop and Paul 1966)

$$P(x) = \exp(-\alpha x) \qquad 1.7$$

where α is known as the absorption coefficient whose variation with endpoint energy (E_m) has been determined empirically and is given by Evans (1955) as

$$\alpha = 1.7\, E_m^{-1.14} \qquad 1.8$$

The consistency of the Makhovian profile, which describes mono energetic implantation, with the simple exponential discussed above was demonstrated by Vehanen and Mäkinen (1984) who folded the ^{22}Na β^+ energy spectrum with the Makhovian stopping profile and obtained quantitative agreement with equation 1.7. Brandt and Paulin (1977), while studying β^+ implantation profiles for various materials of different Z, observed a simple relation between the absorption coefficient α and the target density (ρ) as

$$\alpha = 29(\pm 1)\rho \ cm^2 g^{-1} \qquad 1.9$$

1.3.3 Slowing down

This sub-section discusses the energy loss processes which are involved in the slowing down of e^+s in solids begining at MeV energies and ending with thermalisation. A general treatment will be given for the highest energies since the processes are similar for most materials though at lower energies (keV) metals, semiconductors and insulators begin to reveal their different nature and are discussed individually.

Radiative slowing as a result of β^+-nucleus interaction is the dominant process at energies of a few MeV. This bremsstrahlung energy loss results in the emission of x-rays due to the e^+ repulsion of the positively charged nucleus. Comparison of this process between e^-s and e^+s has been performed by Kim et al (1986). At energies of several hundred keV energy loss by e^- scattering starts to be important while bremsstrahlung becomes inefficient. At these energies the β^+ trajectories are considerably affected by relativistic Mott scattering.

Below 100keV down to around 100eV core and valence electron excitation are the major energy loss processes for implanted e^+s and they generally take roughly 10^{-13} seconds to traverse this energy range. Discussion of energy loss within this energy regime has been tackled by several authors over different energy ranges and these studies rely predominantly on comparison to e^- energy loss mechanisms. At high energies (100's - 10's of keV) Schultz and Campbell (1985) analysed K-shell ionisation cross sections in thin metal foils. From 55-25keV L-shell cross sections were studied by Lennard et al (1988). At a few keV, as discussed in the previous section, Valkealahti and Nieminen (1984) performed Monte Carlo simulations of implanted e^+s and e^-s using Gryzinski's excitation function (1965). This

function makes no detailed account of e^--hole or plasmon processes which will be discussed later.

The process of channeling has not been discussed in this brief treatment of the subject since it is outside the scope of this thesis. The implications of channeling have not been studied with respect to implantation profiles.

1.3.3a Metals

Energy loss within metals at energies below, or close to, the ionisation threshold is characterised by inelastic scattering by free e^-s. Interaction with the Fermi e^- gas can be considered to occur either by a single particle interaction with the creation of an electron-hole pair (exciting an electron above the Fermi surface) or by producing a collective density oscillation (Zhang et al 1988). The latter is known as plasmon excitation which can be described by treating the conduction electrons as a plasma where coupling of a charged particle to this plasma may result in the excitation of oscillations with characteristic plasma frequencies. At higher energies this process can be quantitatively described by a dipole interaction; in the case of a e^+ this argues that while penetrating the solid free e^-s are attracted to the positively charged particle. More e^-s are however drawn along the path of the e^+ resulting in the accumulation of a greater negative concentration behind it than in front and the induced dipole has the effect of decelerating the e^+. This process is commonly treated by applying a charge dependent correction to the stopping power derived from the Bethe formula and is generally known as the Barkas effect (Lindhard 1976).

Inelastic scattering with conduction electrons is the most important energy loss process below the core ionisation threshold in metals. This however falls off below the Fermi energy level and in the last stage of thermalisation phonon scattering dominates over e^- interaction. Such processes are understandably temperature dependent and are slow compared to the processes previously discussed typically taking around 1-10ps.

1.3.3b Insulators

Positron energy loss below about 100eV is dominated by valence e^- interaction which essentially consists of electron-hole pair creation and Ps formation. The latter will be

discussed in some detail in section 1.3.5. The binding energy of excitons (electron-hole bound state) and Ps allow these processes to occur significantly below the band gap of an insulator. These also have a minimum threshold and at lower energies (typically a few eV) the only process open for e^+ cooling is phonon scattering. As mentioned above this is an inefficient process (especially at low temperatures) and thermalisation times can consequently be longer than the mean e^+ lifetime. The inability to thermalise e^+s is also expected to extend the lifetime of e^+s in insulators and semiconductors (Pendyala 1973).

The fact that e^+s stay 'hot' in insulators was first identified by Gullikson and Mills (1986) in their study of re-emission from the rare gas solids (RGS) and some of their data for solid Ar is presented in figure 1.4. Their results illustrate well the principle of hot e^+ diffusion. At the very lowest implantation energies very little re-emission is observed and this was interpreted as evidence for the existence of a small positive work function or possibly the presence of low energy surface trapping processes. Above this energy the re-emission probability becomes practically unity since the e^+s have a large diffusion length and long lifetime and thus have a good chance to return to the incident surface. The onset of Ps production is characterised by a sharp drop in re-emission and a rapid rise in the Ps fraction which susequently falls again as a result of competition with exciton production. The RGS are good insulators in that they have the widest of band gaps and their simple structure (weak bonding) makes them ideal for study. The absence of an optical phonon branch in these solids exacerbates the lack of cooling for epithermal e^+s with, for example, the average energy lost per collision in solid neon being only about 6meV.

1.3.3c Semiconductors and ionic solids

The existence of a finite band gap in these solids produces many similarities with e^+ behaviour at low energies in insulators. The hot positron model still appears to be valid with phonon scattering being dominant below the band gap. Ps production within these solids is the subject of much uncertainty since it is generally believed that, as in metals, its existence may not be possible due to screening of the attraction as a result of the high e^- density (Kahana 1960), see section 1.3.5.

A schematic of energy loss processes in the different classes of material outlined in this discussion is presented in figure 1.5 (Schultz and Lynn 1988).

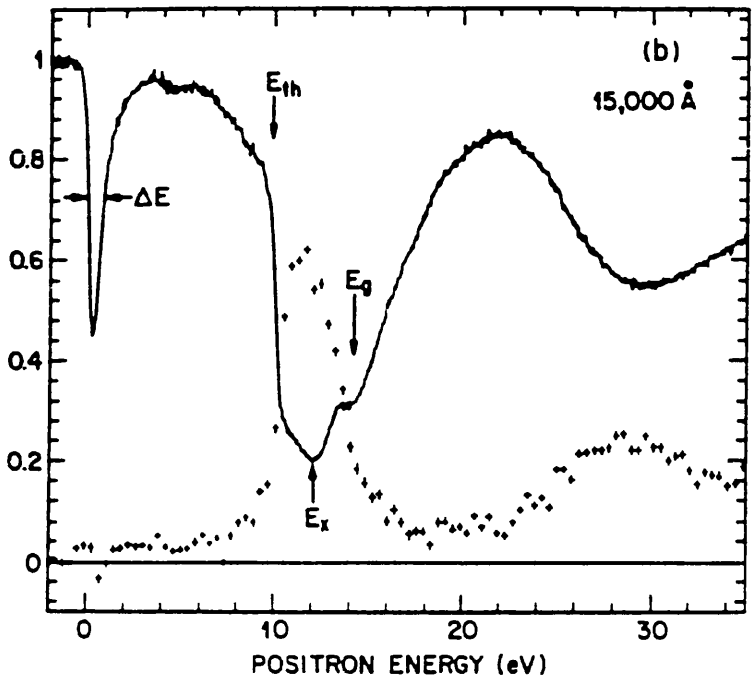

Figure 1.4 Re-emitted e^+ energy spectra from solid Ar (Gullikson and Mills 1986)

1.3.4 Diffusion

In this section the motion of thermalised e^+s in solids is considered. It is commonly treated as a diffusion process involving random scattering events. This section will deal mainly with metals and semiconductors since as discussed previously insulators generally cool e^+s rather poorly resulting in epithermal processes dominating the e^+ dynamics. Some of the principles of diffusion may, however, be applied in the case of epithermal particles.

The applicability of the Boltzmann diffusion equation to describe e^+ dynamics has been discussed by Brandt and Arista (1979). The constant D_+ is known as the diffusion coefficient and characterises the scattering process within a particular material. It is defined as,

$$D_+ = v_{th}^2 \, t_s/3 \qquad 1.10$$

where v_{th} is the average speed of the e^- and t_s is the mean time between collisions (Bergersen et al 1974).

Experimentally it is common to measure the fraction of implanted e^+s which return to the incident surface (or a transmission surface) and which are emitted as free e^+s or Ps. In order to obtain theoretical predictions of the reemitted/transmitted fractions one must not only solve

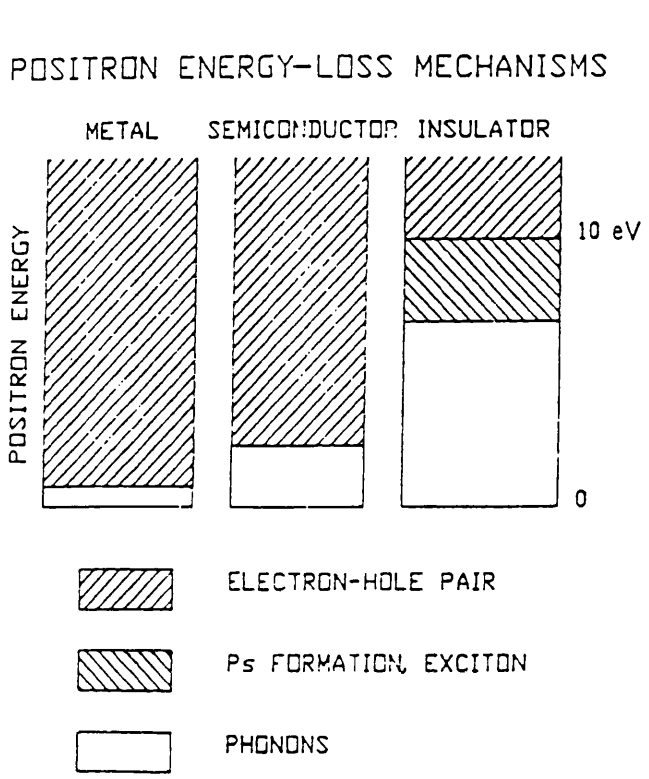

Figure 1.5 Energy loss processes for different classes of materials represented schematically following Schultz and Lynn (1988).

the diffusion equation but convolve this distribution with the stopping profile of the implanted e^+s. As has been discussed for beam work a Makhovian function provides an acceptable description (see equation 1.6). Generally good agreement can be found using this mathematical treatment for both e^+ and Ps emission. The Ps emitted yield can be calculated by assuming that a certain fraction of the e^+s reaching the surface form Ps (see section 1.3.6).

The diffusion constant D_+ can be related to several other important parameters which characterise e^+ dynamics in solids. One of these is the diffusion length L_+ given by

$$L_+ = (D_+ \tau)^{1/2} \qquad 1.11$$

where τ is the average e^+ lifetime. L_+ is essentially an estimate of the average distance that a e^- can diffuse through the bulk during one lifetime. If L_+ is of comparable size to the mean implantation depth, x, then a significant fraction of the incident e^+s will return to the surface. In defect free metals a typical value for L_+ is 1000Å. With x being of the order 10^5-10^6Å for implanted β^+ it is possible to appreciate why metal moderators are of low efficiency.

An estimate of 5000Å for the hot e^+ diffusion length in RGS (ie Ar) was made by Gullikson and Mills (1986). This large value results not only from the high epithermal speed of the diffusing e^+s but also their long lifetime when compared to most metals.

The majority of the discussion presented has centred around diffusion by acoustic phonon

scattering in metals and assumes that scattering events are predominantly elastic and isotropic. This argument can just as easily be applied to the epithermal diffusion of e^+s in the RGS, it is therefore expected that the diffusion equation (1.10) is also valid in this case.

1.3.5 Ps in solids

Bulk Ps formation is prevented in metals by the high conduction e^- density which acts to shield individual e^+-e^- correlation by the accumulation of negative charge around the attractive e^+ site. If a e^+-e^- pair were to become bound this would induce a dipole in the surrounding free e^- plasma and cause ionisation. Since the free e^- density is low in insulators bound e^+-e^- pairs may form and diffuse through these solids. Although in principle such a system has much in common with vacuum Ps the presence of the surrounding lattice distorts its atomic structure considerably. This affects most measurable quantities such as the lifetime and binding energy. A correlated e^+-e^- pair residing in the bulk is commonly called quasi-Ps (qPs) and has been observed in many insulators and ionic solids such as ice, SiO_2, NaF and most RGS. As measured by re-emission using low energy beams significant fraction of e^+s may form Ps in such solids, for example roughly 60% in the case of NaF (Mills and Crane 1984).

Two distinct formation processes have been suggested in order to explain qPs formation in solids and these are discussed separately below.

1.3.5a Ore model

This model was originated by Ore (1949) in order to describe Ps formation in gases and has subsequently been applied to solids. In this model Ps formation is only considered to be significant over a discrete range of e^+ energies. This is justified from a discussion of the energetics of the process. In forming qPs (in the ground state) a e^+ gains energy from binding to the e^- (E_b), but must expend sufficient energy in order to free a valence e^-, ie the band gap energy (E_g). The kinetic energy required by the e^+ (E_{th}), the threshold energy for qPs formation, is simply the difference of these components viz,

$$E_{th} = E_g - E_b \qquad 1.12$$

For e^+ impact energies in excess of E_{th} Ps will be created with some kinetic energy and when the e^+ energy is above E_g the Ps energy is greater than E_b. In this case the Ps has sufficient energy to dissociate (ionise) and is thus unstable if it interacts with another body. In dense media such as solids this is almost inevitable. Ps formation may therefore be treated as energetically favourable only in the e^+ energy range;

$$E_{th} < E_e < E_g \qquad 1.13$$

This range is termed the Ore gap and has a width of E_b.

1.3.5b Spur model

This second formation process was proposed by Mogensen (1974) specifically for Ps formation in dense media. The process is considered to occur in two distinct stages. The first involves the implantation of the high energy e^+ and considers that an ionisation spur will be created as a result of energy loss in the medium. In this region a considerable number of ions/free e^-s are created and it is in this environment that the e^+ slows down. At near thermal energies the e^+ may capture a diffusing e^- which has not recombined or escaped the spur region. This process is dynamic and involves several complex processes within the spur and is thus considerably more difficult to model mathematically than the Ore process.

Debate continues concerning the relative importance of each process in different circumstances, for a review see Dupasquier (1983).

Early e^+ lifetime measurements in liquid argon performed by Paul (1958) suggested a Ps formation fraction of $\approx$10% in the bulk. Recent work by Tuomisaari et al (1990) studied the energy distribution of emitted Ps from Ar, Kr and Xe following e^+ implantation. The emitted Ps energy spectra for Ar and Kr were well described by the Ore formation model followed by hot Ps diffusion during which energy loss occured.

Diffusion of Ps through solids has been considered to be similar to that of e^+s and to be essentially dependent on phonon scattering. Diffusion coefficients are generally observed to be small. Some work has been performed by Varlashkin (1970) on the possible self trapping of Ps in solid and liquid Ar, Kr and Xe in which the particle localises on a self induced

bubble in the material. Although this phenomenon was observed in the liquid, no evidence was observed for self trapping in the solid phase in agreement with the theoretical prediction of Cohen and Jortner (1969). A more recent study by Stewart et al (1990) extended this work to Ne. Gullikson and Mills (1989) studying e^- (and e^+) emission from Ar, Kr and Xe following e^+ implantation observed a peak in the energy spectrum of emitted e^-s which they concluded to be characteristic of Ps pick-off by valence e^-s. Their observation also of an anomalously short Ps diffusion length at low energies led them to suggest self trapping of Ps.

An important technique in the study of the Ps formation process in gases and insulators has been the effect of an applied electric field on the Ps yield and this will be discussed in section 1.4.

1.3.6 Surface Processes

1.3.6a Introduction

In this subsection a brief discussion is presented concerning the fate of e^+s which have diffused through the bulk and arrived at a surface. Qualitative differences are seen between metals and insulators which will therefore generally be treated seperately. Several distinct processes of emission may occur from metals including work function e^+ emission, prompt Ps formation and thermal Ps desorption. In the case of insulators it is more suitable to consider epithermal e^+ and physisorption of Ps. Surface trapping at impurities or defects will be discussed mainly with respect to metals, since more work has been performed in this field though some of the arguments presented can be applied to insulators.

1.3.6b Work function e^+ emission from metals

As an introduction to e^+ or Ps emission from a metal surface it is useful to discuss the potential energy variation of e^+s and e^-s in the near surface region. Beginning with e^+s, the simple jellium model can be applied to describe the bulk solid and in this case there are two components to the bulk potential. The first is a positive contribution resulting from the average repulsion of the positive ion cores (Vi) whilst the second arises from attraction to the conduction e^- continuum (Ve^-) and is by convention negative (see figure 1.6a).

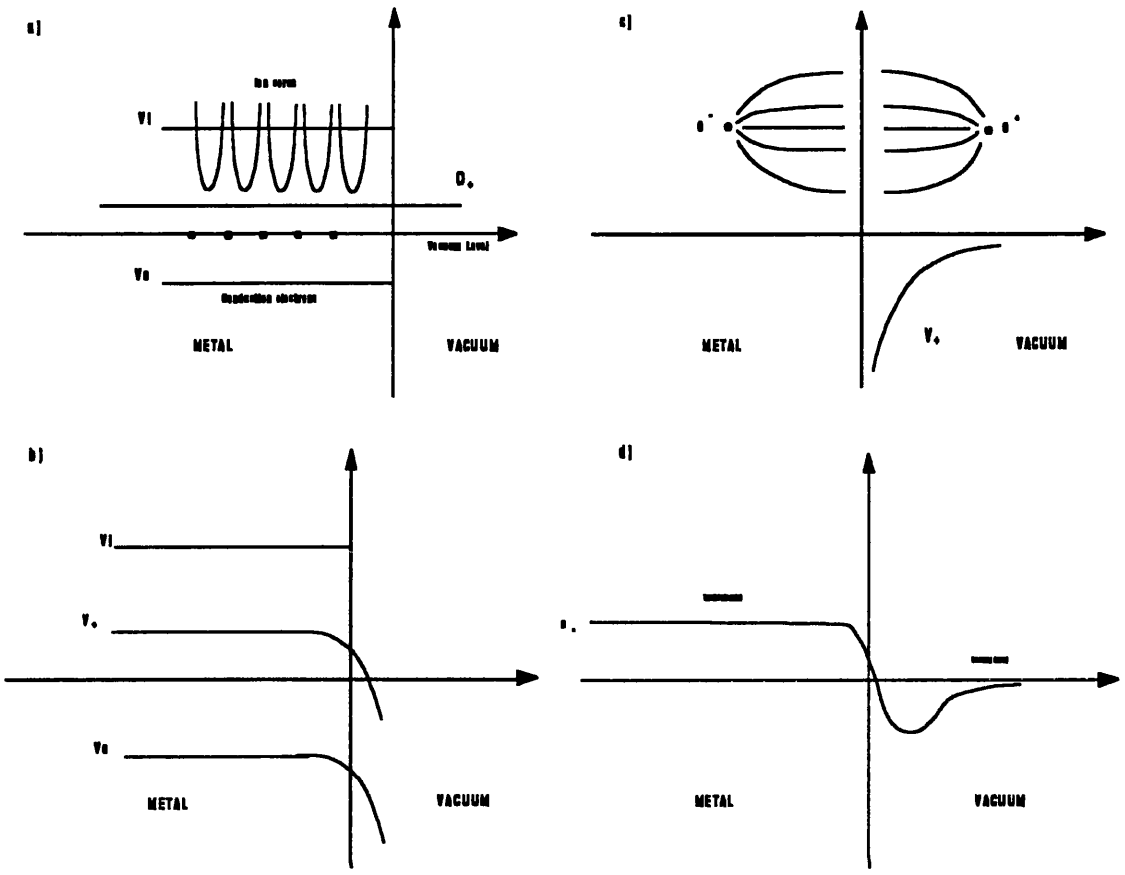

Figure 1.6 e^+ surface potential for a metal; a)bulk potential, b)surface dipole, c)image potential and d)complete potential.

At the surface, assuming the lattice is perfect, the ion density abruptly terminates whereas spillage of the free e^- 'sea' occurs, thus distorting the charge density in this region. An electric dipole is created by the negative charges residing beyond the positive ion surface and the effect of this is to attract e^+s towards the surface (figure 1.6b).

If a e^+ is now considered at a relatively large distance outside the exit surface one may treat the system classically as a charged particle near a conducting surface such that field lines emanating from the e^+ must be terminated perpendicular to the plane of the surface. The effect on the Coulomb field of the e^+ can be conceived by considering the existence of an imaginary mirror charge (of opposite polarity) within the metal, this has the effect of producing a negative so called image potential (figure 1.6c).

Summing these three contributing factors one may produce a complete description of the e^+ potential energy through the surface as shown in figure 1.6d. One notable feature here is the existence of a surface potential well. The same approach may be applied to describe the

potential energy curve for e^-s and here again one gets a bulk chemical potential and an attractive image potential. The surface dipole in the case of e^-s is positive and therefore repels them from the surface thus helping to confine them in the bulk.

The work functions of e^+s and e^-s are considered to be the difference in potential energy of a particle residing in the bulk of the metal, where the effect of the surface dipole is negligble, and a particle which is far enough removed from the surface such that the image potential is insignificant. If the e^+ work function (ϕ_+) is negative then it will gain energy in leaving the surface. This energy is gained perpendicular to the plane of the surface thus creating a forward peaked distribution of emission angles. Assuming that the e^+s being emitted are thermal this will provide an additional component to their momentum as they leave the surface which will broaden their energy and angular distributions. The mean thermal energy possessed by such an emitted e^+ is kT/2 parallel to the surface (energy in one dimension) which in terms of velocity has a magnitude $v_{\parallel}=(kT/m)^{1/2}$. One thus obtains an upper limit to the emission angle of $\theta_{1/2}= \tan^{-1}v_{\parallel}/v_{\perp}$, see figure 1.7, with an upper energy of $-\phi_+$.

If some inelastic process occurs at the surface, say due to a surface contaminant or defect, then an increased emission angle and decreased energy may be observed. Note that increased e^+ emission yield is generally expected as the magnitude of $-\phi_+$ increases. This has been observed for Ni and Cu surfaces (Gullikson et al 1988).

1.3.6c Prompt energetic Ps emission

As has been discussed, the high free e^- density inside metals prevents the formation of Ps in the bulk. Ps however may be emitted from a metal as a result of e^- capture at the surface where the e^- density falls. The concept of a work function for such a process is inappropriate since one is no longer removing a particle from a bulk potential. It is more suitable to consider a formation potential, E_{Ps}, defined by the sum of the e^+ and e^- work functions and the Ps binding energy (equation 1.14). Note that the surface dipole does not affect the energetics of Ps emission since it has a converse effect upon the e^+ and the acquired e^-. The momentum of the e^- may however broaden the angular emission of the Ps.

$$E_{ps} = \phi_+ + \phi_- - 6.8 \quad \text{eV} \qquad 1.14$$

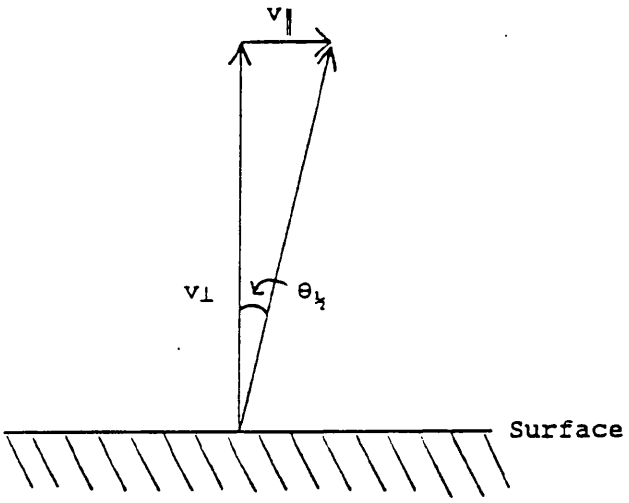

Figure 1.7 Angular emission of work function e^+s from a metal surface.

E_{Ps} is often negative due to the relatively large Ps binding energy and Ps formation can therefore be relatively efficient (Canter et al 1975). The process can, due to its rapidity ($\approx 10^{-16}$s), be non-adiabatic and leave the metal in an excited (electronic) state (Mills et al 1983). This is equivalent to saying that the captured e^- was from below the Fermi surface which has the effect of reducing the energy of the emitted Ps below E_{Ps} such that the Ps kinetic energy spectrum is characteristic of the e^- density of states (Mills 1988).

1.3.6d Thermally desorbed Ps

Referring back to figure 1.6 for the potential energy curve of e^+s at a surface it is clear that they may become trapped in the surface potential well with typical binding energies (E_b) being approximately 2-3 eV. This is well above thermal energies and would not allow a e^+ to escape by phonon scattering. It may however be energetically possible for a e^+ to escape such a trap by the formation and emission of Ps. The activation energy required by the e^+/e^- pair (E_a) in order to be emitted is given by

$$E_a = E_b + \phi_- - R_\infty/2 \qquad 1.15$$

Note that ϕ_- is invariably positive and a few eV thus E_a is normally lower in magnitude than

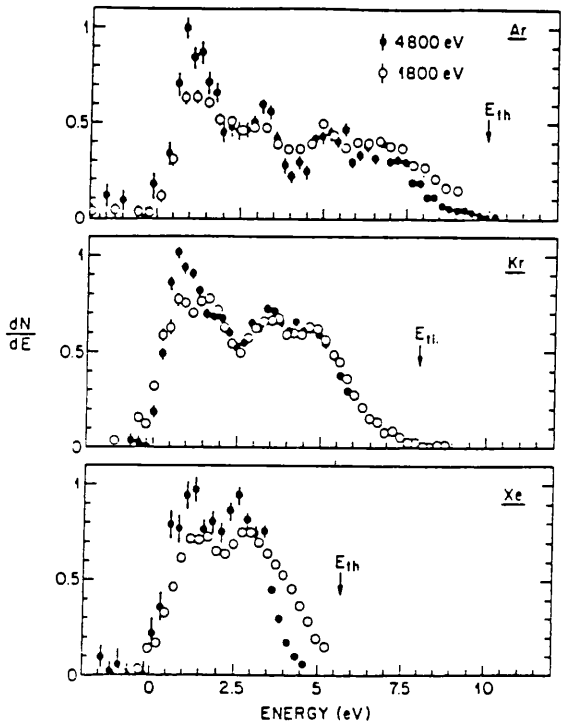

Figure 1.8 Positron emission spectra for solid Ar, Kr and Xe at incident energies of 4800 and 1800eV (Gullikson and Mills 1986).

E_b. If E_a is slightly positive thermal energy fluctuations of the particles within the trap can provide sufficient energy to desorb such e^+ as Ps (Mills and Pfeifer 1979 and 1985, Poulsen et al 1991).

1.3.6e e^+ emission from insulators

The work function mechanism outlined by Tong (1972) for metals does not adequately describe e^+ emission from insulators. This was observed from the re-emission studies performed on various insulating solids by Mills and Crane (1984). Initially this was interpreted as the result of bulk Ps formation followed by diffusion and breakup at the surface with the subsequent release of a free e^+. Later re-emission studies by Gullikson and Mills (1986) on the structurally simpler RGS prompted the development of the 'hot e^+' model described in section 1.3.4. In this case emission occurs at high (epithermal) energies and does not critically depend on the surface electronic structure, in fact measurements indicate that RGS have a positive e^+ work function. As has been mentioned in section 1.3.4 re-emission from RGS is characterised by a broad energy (and angular) distribution compared to metals (see figure 1.8). Figure 1.9 shows the actual e^+ emission spectrum from a neon moderator.

1.3.6f Ps emission from insulators

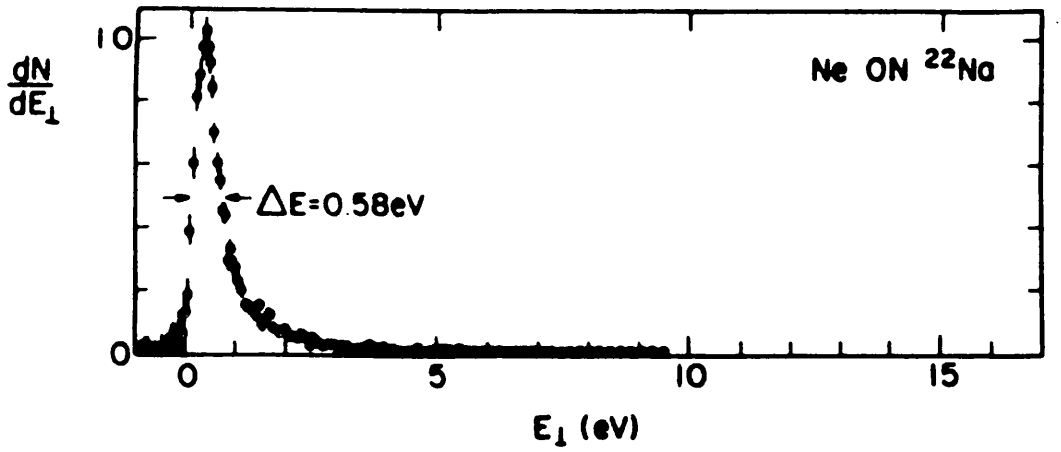

Figure 1.9 Positron energy spectrum from a solid Ne moderator (Mills and Gullikson 1986).

As has been discussed in section 1.3.5 the low free e^- density within insulators can allow the formation of Ps-like (Bloch) states within the bulk. Some insulators may emit such qPs if it is formed close to an exit surface. In this case one may legitimately describe the emission as being characterised by a Ps work function (ϕ_{Ps}) since the diffusing qPs will encounter a potential difference as it travels from the bulk to a vacuum state.

Illustrative work has been performed by Sferlazzo et al (1987) studying Ps emission from quartz (SiO_2) and MgO single crystals. They obtained a value for ϕ_{Ps} for quartz of roughly -3.3eV. No evidence was observed of qPs formation in MgO and it was concluded here that, as with metals, Ps emission resulted from a surface process. Figure 1.10 shows the energy spectra they obtained for the two insulators.

1.3.6g Surface trapping

In section 1.3.6d trapping in the surface potential well was discussed. Similarly e^+s may also become localised at structural imperfections close to the surface such as vacancies or dislocations which could either be intrinsic or the result of the presence of an impurity. As with e^+s localised in the surface potential well the low e^- density may allow Ps-like e^+-e^- correlated pairs to form as bound surface states. Desorption of Ps from surface traps has been observed by Koymen et al (1987) who measured a significant rise in emitted Ps fraction from

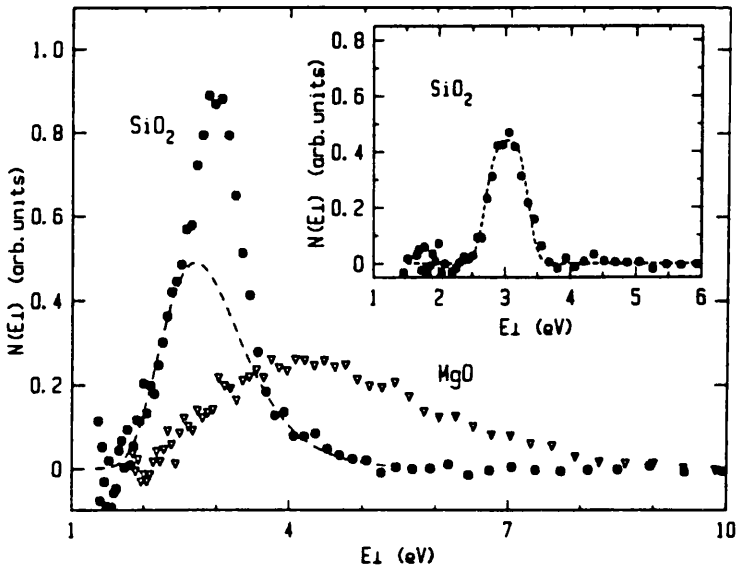

Figure 1.10 Energy spectra of Ps emitted from solid Quartz and MgO (Sferlazzo et al 1987).

a single crystal Ni surface as surface defects were created by further Ni deposition.

Surface trapping of e^-s at radiation induced voids has been used to explain long e^+ lifetimes in irradiated samples (Lynn et al 1984). The high mobility predicted for a delocalised e^+ surface state make them highly sensitive to small amount of surface defects, more so than defects in the bulk.

1.3.7 Secondary e^- emission

It was discussed in section 1.3.3 that during the process of slowing down high energy β^+ particles liberate a considerable number of e^-s by ionisation and some of these may become emitted as secondary e^-s. Compared to e^- or proton impact the production of secondary e^-s by high energy e^-s (β^+) has been little studied. The unpublished (thesis) work by Bodin (1957) presents the most relevant experimental study and constitutes the focus of this discussion on β^+ induced secondary e^- emission.

The experiment performed by Bodin used a magnetic analyser to select certain energy β^+ and β^- particles and measured the secondary e^- yield on impact with a metal target (eg Pt, Cu/Be). The secondary yield was measured using an e^- multiplier and the study aimed to quantify the differences between e^- and e^- impact. As shown in figure 1.11 both e^- and e^+ secondary yields increase rapidly at low impact energy (<100keV). This agrees well with the

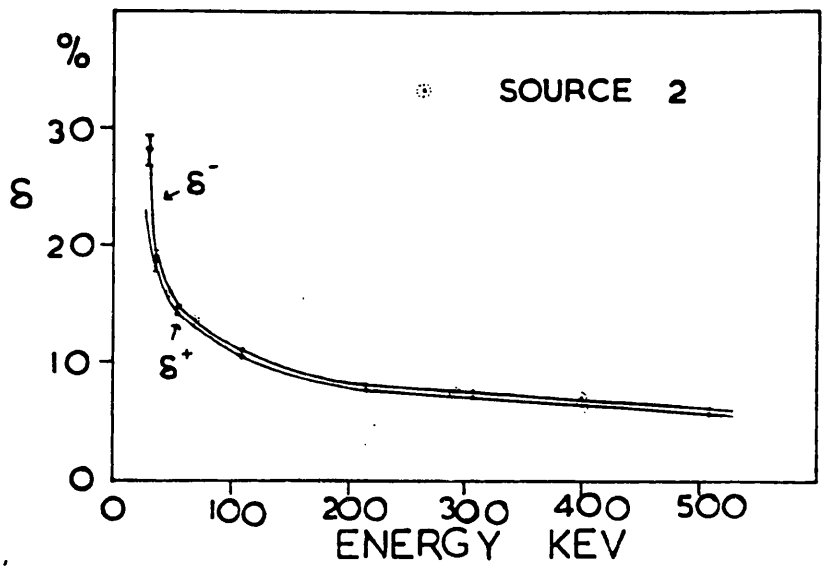

Figure 1.11 Variation of the secondary yield (δ^+, δ^-) as a function of incident e^+ and e^- energy (Bodin 1957).

successful Bethe description of energy loss in solids which may be applied to all charged particles. At lower energies the secondary yield produced by e^-s increased more rapidly than that by e^+s down to the lowest energies of 2keV.

The energy distribution of secondary e^-s emitted from solids is similar for most high energy incident particles since the mechanisms of slowing down, diffusion and emission of the secondaries will be the same. This has been observed for e^- and proton impact as shown in figure 1.12 and which is discussed by Schou (1987). It is also true for x-ray induced emission as demonstrated by Gullikson and Henke (1989), see figure 1.13. Characteristically the secondary e^-s are peaked at very low energies (few eV) and this is generally accepted to be true for e^+s also.

Considerable variation in the absolute magnitude of secondary e^- yield occurs for different materials. The work of Gullikson and Henke indicated that the RGS were (relatively) highly efficient secondary emitters. In fact the authors speculated that these solids could provide the basis for efficient x-ray photocathodes.

1.4 The effect of an externally applied electric field on e^+s in solids

In this section the behaviour of e^+s in solids is examined whilst under the influence of an externally applied electric field. This treatment will mainly concentrate on insulating materials and specifically the RGS. Of particular importance will be the effect on the motion

of slowly diffusing e^+s and the formation of Ps. These two will be considered seperately after a brief discussion of the effect of an electric field on e^+ slowing down.

1.4.1 Implantation and Thermalisation

The effect of an electric field on the β^+ implantaion profile only becomes important for relatively thick samples or at high field strengths (>100kV/mm). This was demonstrated in a study performed by Heinrich (1978) on polyethylene which showed only a few % effect on the implantaion profile.

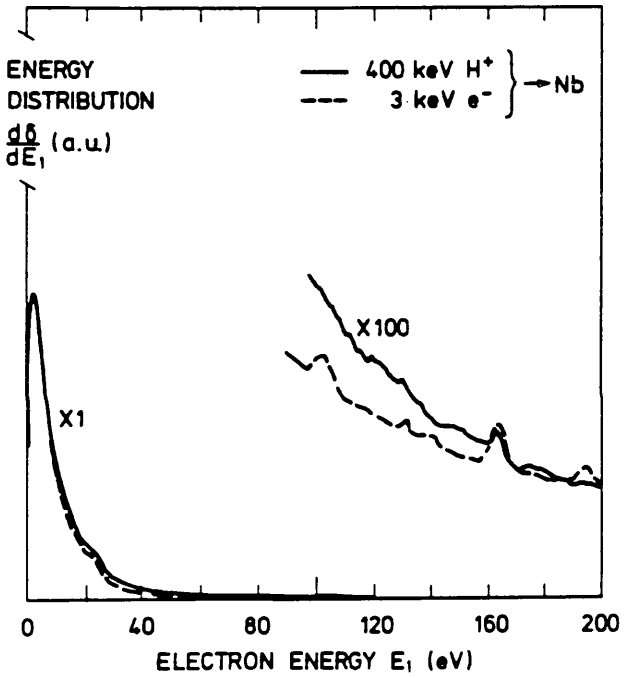

Figure 1.12 Secondary e^- energy spectra from Nb induced by 400keV proton and 3keV electron impact (Musket 1975).

The presence of an electric field would be expected to affect the e^+ thermalisation time within a material. This is generally long in insulators and alteration could be of importance to e^+ diffusion. However, insufficient quantitative work has been carried out to reasonably assess the significance of such effects.

1.4.2 e^+ diffusion

The application of an electric field may be considered to have the effect of drifting a charged particle such as a e^- through a solid. Simplistically, the accelerating field can be said

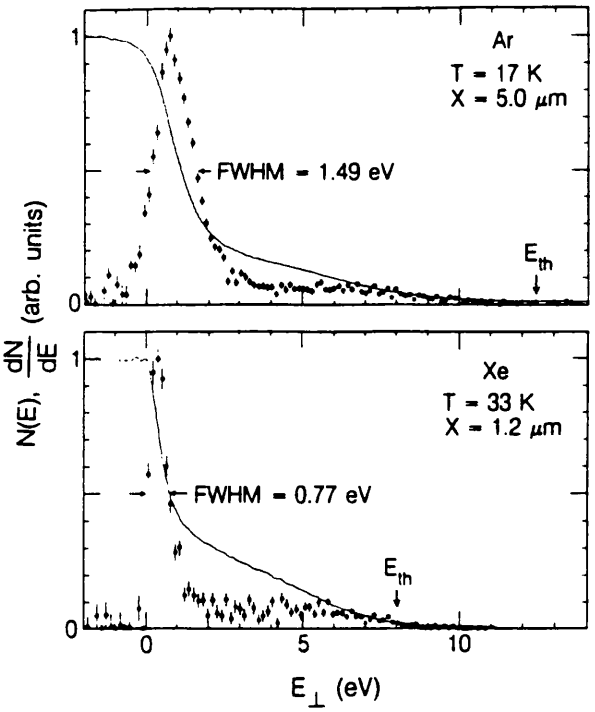

Figure 1.13 X-ray induced secondary electron energy spectra from solid Ar and Xe (Gullikson 1988).

to impart a drift velocity to the diffusing e^+ between scattering events. The drifting of e^-s and holes by such a process has been observed in many insulating and semiconducting materials including the RGS (Spear and LeCombe 1977). The field has been reviewed by Jackobini and Regiani (1979).

As early as 1969 Madey postulated that the application of an electric field (in this case by the application of surface charge) could enhance the emission of e^+s from a moderator. Conceptually this idea is simple and can be theoretically modelled by considering the average time between randomising collisions. During this time the accelerating field will impart a certain (mean) velocity. Hence, superimposed on the random scattering motion an average velocity is applied which can increase the likelihood of a diffusing e^+ reaching the exit surface, see figure 1.14. Finite e^+ mobilities have been observed in several insulating (and semiconducting) materials following the external application of electric fields (McKenzie and Goryachi 1985). Other examples are Si and Ge (Mills and Pfieffer 1977, Corbel et al 1989, Simpson et al 1989), polyethylene (Mills and Gullikson 1986), and diamond (Mills et al 1992). Significant enhancements in moderation efficiency have been predicted (Beling et al 1986) using field induced e^+ drift to an emitting surface and this is discussed in section 1.5.

The acceleration of the e^+s in the electric field may increase their average energy and thereby effectivly 'heat' the e^- distribution. Such heating has been observed for electrons (Spear and LeCombe 1977). A saturation of the e^- drift velocity (mobility) would be

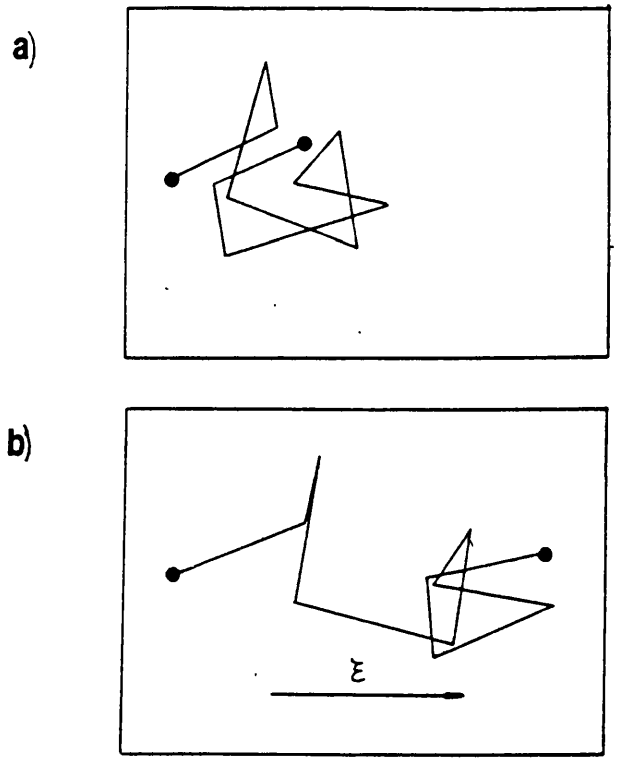

Figure 1.14 Schematic of the motion of a diffusing e^+ a)without and b)with an applied electric field.

expected to occur at high field intensities as a result of heating above the inelastic threshold. (eg exciton formation, ionisation). Possibly a more significant effect could be that of the formation of Ps whichever of the two processes one considers.

1.4.3 Ps formation

There has been little work performed studying the effect of applied electric fields on the formation of Ps in solids and none specifically on the RGS. Much conflict still exists as to the correct interpretation of the experimental results which do exist. This mainly centres on consideration of the process responsible for Ps formation.

This section presents an initial discussion of the field dependence of Ps formation in gases and subsequently considers insulating solids. The reason for discussing gas phase is that in the case of RGS such results could be relevant given the lack of available data. The RGS are structurally the simplest solids and are bonded only by van der Waals attraction which has a relatively small effect on the electronic structure of the constituent atoms. A RGS might be expected to behave similarly to that of the dense rare gas and possibly this may apply to the formation of Ps.

1.4.3a Gas phase

Early work by Marder et al (1956) involved measurement of the Ps formation fraction in dense gases (few atmospheres) under relatively high electric fields (up to 1 kV/mm) and included studying Ar and Ne. Their results consistently showed an increase and eventual levelling off of Ps formation with field strength. Later work by Obenshain and Page (1962) at higher pressures and field strengths showed agreement with these results. This observed increase was consistent with the Ore model of Ps formation which predicted that heating by the field caused low energy (below E_{th}) e^+s to be promoted into the Ore gap and thus increase the Ps yield.

More recent studies of high density molecular gases have shown a decrease in Ps formation at low intensity applied electric fields (eg Charlton and Curry 1985). Jacobsen (1985) considered that this could be explained if Ps formation was occuring by the spur process where the electric field would result in the separation of e^+s and e^-s out of the spur region. Other observations such as the decrease in Ps fraction with the addition of e^- acceptors (eg CCl_4) could also be explained using the spur Ps model (Curry and Charlton 1985).

The conclusion of Charlton and Curry (1985) was that creation of Ps by a combination of the spur and Ore processes could explain their observations of Ps formation in CO_2 under the application of electric fields. It should be noted that the Ore process alone does not adequately describe Ps formation in moderately low density Xe and Kr gases (Charlton 1985). Jacobsen (1983) showed that this cannot be explained in terms of the spur model since this process is unlikely to occur at these rare gas densities.

1.4.3b Solids

The most thoroughly investigated insulator with respect to Ps formation under the influence of electric fields has been polyethylene in a set of experiments by Bisi et al (1981). Since little other conclusive work has been performed this will constitute the focus of the following discussion. These workers measured the Ps yield in a thick (≈0.2mm) polyethylene sample whilst applying electric fields ranging up to 150kV/mm using two electrodes. Polyethylene was chosen since it was the most thoroughly investigated polymer concerning its intrinsic electric field strength. The results are shown in figure 1.15.

As can be seen below ≈10kV/mm there is a significant drop in Ps formation followed at higher fields by a more flat region. Above ≈40kV/mm the Ps fraction begins to rise reaching

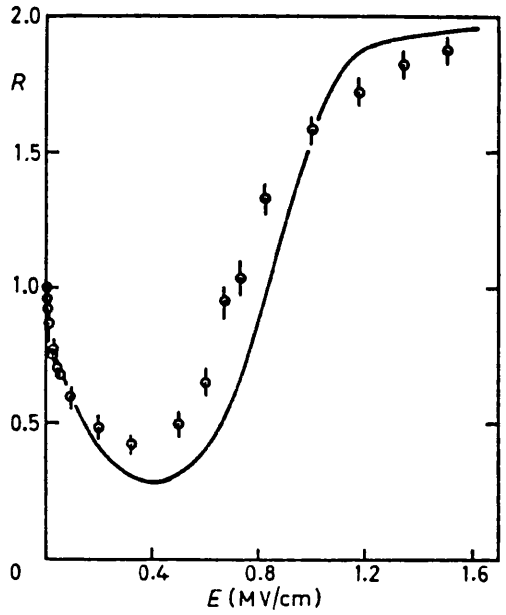

Figure 1.15 Relative Ps yield in polyethylene avrying with electric field (Bisi et al 1981), the solid curve is based on theory (Brandt 1982).

its initial value again at ≈70kV/mm. This increase continues up to the highest fields of around 150kV/mm where a saturation value appears to have been reached with almost a factor of two enhancement in Ps formation fraction.

Two explainations have been proposed for this variation one of which utilises the Ore model and the other the spur model for Ps formation. These will be discussed separately below.

1.4.3bi Spur

It has been mentioned with respect to gases (section 1.4.3a) that at low electric fields a decrease in Ps formation is predicted using the spur model as a result of e^+/e^- extraction out of the spur region. Mogensen (1983) suggested two possible explanations for the subsequent rise in Ps fraction at high (>40kV/mm) electric fields.

Firstly he proposed that bulk/surface charging of the plastic sample could significantly affect the charge density and field strength within the spur region. The results of Bisi et al would in this case be an incorrect measurement of the field dependence of Ps formation.

The second argument put forward by Mogensen was that e^+ trapping at pre-existing sites within the spur region caused a considerable reduction in Ps formation. The application of a large electric field could release e^-s from such traps and thus increase the Ps yield. No subsequent quantitative analysis has been made of these arguments.

1.4.3bii Ore

Brandt and Feibus (1968) considered the effect of an applied electric field to Ps formation in solids with the assumption that the Ore mechanism of formation was dominant. They predicted that as the field strength was increased the Ps fraction initially decreased as a result of e^+ heating out of the Ore gap. For higher intensity fields it was then predicted to pass through a minimum before increasing and asymptotically approaching 100% Ps formation ie all e^+s in the sample form Ps. As described in section 1.4.3a this increase occurs as a result of e^+ heating into the Ore gap from below the threshold.

Brandt (1981) quantitatively applied the Ore model to the experiment performed by Bisi et al. The calculation, having been fitted to the data, provided good agreement as shown in figure 1.15. The author concluded that these results supported the Ore mechanism as the dominant Ps formation process.

There appears to be a large degree of uncertainty as to the correct model to describe Ps formation in either dense gases or insulating solids. This is true of the RGS and it is therefore not possible with any degree of certainty to predict the effect of applying an electric field on the Ps formation fraction. Generally however the arguments appear to be in the case of RGS for the Ore process of Ps formation, given the experimental observations of Tuomisaari (1990) see section 1.3.5.

Source	E endpoint (MeV)	Production	$T_{\frac{1}{2}}$	β^+ fraction (%)	Mean free path λ (g/cm^2)
LINAC	~ 10	$e^- \rightarrow 2e^- + e^+$	—	—	~ 5
^{11}C	0.96	^{11}B(p, n)	20 min	99	0.056
^{22}Na	0.54	^{24}Mg(d, α)	2.6 y	90	0.029
^{58}Co	0.47	^{58}Ni(n, p)	71 d	15	0.025
^{64}Cu	0.65	^{63}Cu+n	12.8 h	19	0.036
^{68}Ge	1.88	^{66}Zn(α, 2n)	275 d	86	0.12

Table 1.1 Some common high energy β^- sources.

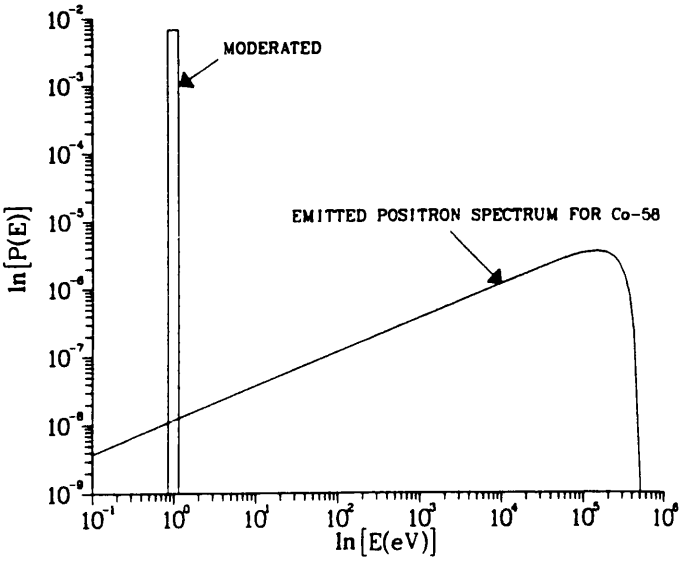

Figure 1.16 Comparison of moderated e^+ spectrum with the β^+ particle energy spectrum for ^{58}Co (normalised).

If extrapolated to the densities of RGS, certain experimental results obtained in the gas phase are in agreement with those for insulating solids. At moderately low intensity electric fields, (order 10kV/mm) a significant decrease in Ps yield occurs prior to an increase up to some high saturation value at fields of order 100kV/mm.

1.5 e^+ moderation and transport

This section is divided into three and considers firstly the process of e^+ production and slowing down (moderation) to produce a mono-energetic beam. Two systems of transport will be discussed namely magnetic and electrostatic confinement though occasionally mixed systems are employed. Lastly, methods of improving the beam quality (resolution) are presented, specifically brightness enhancement using remoderation.

1.5.1 Moderation

Almost all of the e^+s employed in modern beams originate in β^+ radioactive sources. Various different isotopes are commonly used such as those in table 1.1, with ^{22}Na probably the most popular. For high intensity beams e^+s may be liberated in high energy collisions by

(e^--e^+) pair production. This method is, however, rather expensive and requires a device such as an electron linear accelerator (eg Ito et al 1985).

The energy of the β^+ particles emitted by a source such as ^{22}Na is broad, ranging from practically zero up to an endpoint energy which in the case of this isotope is ≈0.54MeV. For beam experiments one ideally requires a collimated mono-energetic distribution. If the e^+s (from a source) which have the required energy are removed by taking a slice out of the distribution the remaining fraction will be extremely small and consitute a low intensity beam. A much more efficient use of the available β^+s was suggested by Madanski and Rasetti (1950) who speculated that implantation into a solid may result in moderation (thermalisation) and re-emission at low energies (see figure 1.16).

As mentioned in section 1.1 the first experimental observation of a moderated e^+ beam was made by Cherry (1958) using a chromium plated piece of mica as the moderating material and a ^{64}Cu source. The unpublished work went largely unnoticed until Madey (1968) revived interest in e^+ moderated beams also using a plastic moderator. Interestingly, this author speculated that surface charging (negatively) of the moderator could enhance the emission of e^+s though his results seemed to be consistent with positive charging of the sample. At this time the moderation efficiencies were comparatively low at a few 10^{-8} ie of 10^8 β^+ created in the source only a few are converted into e^+s in the beam.

An important developement was the MgO powder (smoked) e^+ moderator constructed by Canter et al (1972) which had an efficiency of $\approx 3 \times 10^{-5}$. Following the prediction of work function emission from metals by Tong (1972) and the advent of clean well characterised samples (surfaces) much work was, and continues to be, done in an attempt to understand e^+ dynamics in metals and in their development as efficient moderators.

There are two dominating factors concerning the choice of moderator for a particular beam application. One is the efficiency of the moderator and the other is the energy and angular resolution of the emitted slow e^+s. More discussion will be given on this topic in section 1.5.3.

One method of increasing moderation efficiency, which invariably degrades the emitted e^+ resolution, is the use of more effective source/moderator geometries. Some examples are shown in figure 1.17. Currently the conical geometry (Lynn et al 1989) is considered to be an exemplary design enhancing the moderation efficiency by more than a factor of two above that of the flat plate. A single crystal W cone in the forward re-emission has achieved an

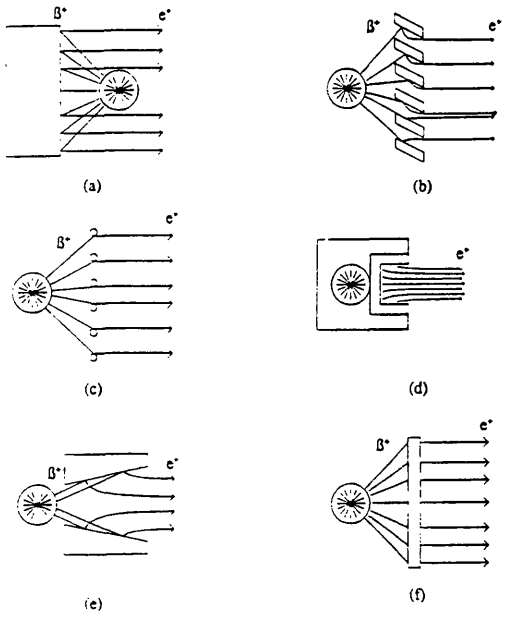

Figure 1.17 Different common source/moderator geometries.

efficiency of 1.5×10^{-3} (Lynn et al 1989). Possibly the most common currently used design is the W multi-mesh moderator with efficiencies between 10^{-4} and 10^{-3} since it appears to be extremely rugged. Note that practically all metal moderators require annealing before use ie heating to a temperature such that dislocations become mobile. This is necessary in order to minimise e^+ trapping at structural defects and may also help to desorb impurities.

Recently, following the re-emission studies of Gullikson and Mills (1986) using the RGS,

	Ne	Ar	Kr	Xe
Efficiency (%)	0.70(2)	0.13(2)	0.14(2)	0.13(2)
ΔE(eV)	0.58(5)	1.7(2)	1.8(2)	3.2(4)

Table 1.2 RGS moderator efficiences and e^+ emission energy widths (Mills and Gullikson 1986)

these solids have been demonstrated to be highly efficient e^+ moderators. In fact the highest currently quoted moderation efficiencies were achieved by Mills and Gullikson (1986), who obtained 0.7% using a neon transmission film (see figure 1.17), and a projected yield of roughly 1.4% was achieved using a conical design (Khatri et al 1990). One drawback with RGS moderators is that the e^+s are emitted with a wide energy and angular spread as summarised in table 1.2. This results from the epithermal nature of the e^+ emission process (section 1.3.6). Lower efficiencies have been observed for the other RGS Ar , Kr and Xe although they are still high in comparison to typical metal moderators (see table 1.3).

Following the suggestion of Lynn and McKee (1979) a considerable amount of work has been performed attempting to develop a so called 'field enhanced' moderator using an externally applied electric field. This work, some of which has been described in section 1.4, initially began with Si and Ge. More recently, work has been performed on diamond involving measurement of the work function (Mills et al 1992), mobility and e^+ lifetime (Brandes et al 1992). This material possesses a large band gap of 5.5eV giving it a long diffusion length and has a large negative work e^+ function (-3.5eV). With field assistance, despite a short bulk lifetime of 97.5±1.5ps (Li et al 1992) this material has a projected moderation efficiency of around 2.8% (Brandes et al 1992). The possibile observation of electri field enhancmnet due to surface charging has also been speculated upon.

1.5.2 Magnetic transport

For magnetic beam confinement typically a ≈100Gauss field is applied axially along the transport direction usually by external (to the vacuum) coils configured in a Helmholtz arrangement. This is a simple system to use since it allows considerable beam adjustment (optimisation) from without. The system is suitable where one is concerned only with the axial momentum component of the e^+ beam since the transverse component manifests itself as rotation (spiralling) around the field lines. Beam focusing may be performed by strengthening the field, thus tightening the radius of the spiral. In experiments where the lateral e^+ momentum component must also be considered, for example in differential scattering measurments, a magnetic system is not generally used.

A device called a Wien filter (eg Hutchins et al 1986) is commonly used in magnetic transport systems in order to prevent fast e^+s (or other radiation) from the source reaching the

Moderator	Experimental Details	Vacuum Conditions (torr)	Efficiency ϵ	Energy Spread ΔE(eV)
Cr[a]	Metal coated mica	$\approx 10^{-7}$	3×10^{-8}	-
Au[b]	"	"	10^{-7}	2
MgO[c]	Coated Au vanes	"	3×10^{-5}	2.3
B[d]	Target bombarded with protons to produce ^{11}C	"	10^{-7}	0.15
Al(100)[e]	Sputtered and annealed *in situ*	$\approx 10^{-10}$	3×10^{-5}	0.1
Cu(111)+S[f]	"	"	9×10^{-4}	0.3
Cu(111)+H_2S[g]	"	"	1.5×10^{-3}	0.6
W[h] (polycrystalline)	Resistively heated *in situ*	$\approx 10^{-7}$	10^{-3}	2.3
W(110)[i]	Heated in O_2 and vacuum	$\approx 10^{-10}$	3×10^{-3}	0.7
W(100)[j] (transmission geometry)	"	"	4×10^{-4}	$\approx$1
Ne[k]	Ne gas condensed onto cooled Cu cylinder (6K)	$\approx 10^{-9}$	7×10^{-3}	.58
W(100)[l]	Annealed in low vacuum	$\approx 10^{-2}$ (annealing) $\approx 10^{-7}$ (beamline)	$\approx 9\times10^{-4}$	$\approx$3eV
Ni(100)[m]	"	"	6.5×10^{-4}	0.3

References

a) Cherry (1958)
b) Costello *et al* (1972b)
c) Canter *et al* (1972)
d) Stein *et al* (1975)
e) Mills *et al* (1978)
f) Mills (1979b)
g) Mills (1980)
h) Dale *et al* (1980)
i) Vehanen *et al* (1983)
j) Lynn *et al* (1985b)
k) Mills and Gullikson (1986)
l) Zafar *et al* (1988)
m) Zafar *et al* (1989)

Table 1.3 Positron moderator characteristics.

interaction region. The principle of this technique is to apply a transverse electric field to the e^+ beam. As the charged particles pass through this field they experience a force perpendicular to both the beam axis and the applied electric field which consequently deflects the beam. Tuning of the magnetic and electric (deflecting) field intensities can select only the e^+ energies required in the beam.

1.5.3 Electrostatic transport

The equipment required for an electrostatically guided beam is usually more complex than

for a magnetic system. It generally requires the construction of several vacuum compatible precision machined lens elements (commonly metal cylinders) most of which must be biased at different voltages. Basically this transport system relies on manipulating the electric field (potential surface) experienced by the beam in order to control the e^+ trajectories and eventually focus the beam at some target.

An electrostatic lens can be constructed by placing two conducting cylinders in close proximity. Since electric fields lines terminate perpendicular to the surface a hemishperical potential surface is created by applying different voltages to these cylinders. This field can act to focus or defocus charged particle beams traversing the curved potential surface.

Central to the discussion of electrostatic transport systems is Liouville's theorem which states that the phase space volume of the e^+s is constant under the action of conservative forces, ie the resolution (spatial, angular and energy) cannot be improved with the use of forces such as those in electrostatic and magnetic fields. This can be expressed quantitatively by equation 1.17 which relates the diameter (d), angular divergance (θ) and energy (E) of the beam;

$$\sin^2\theta \times d^2 \times E = \text{constant} \qquad 1.16$$

It is clear that the resolution of the e^+s emitted from the moderator is then important for the quality of the beam. It can also be important for the efficiency of the tranport system. A beam which is poorly resolved at the point of injection must be accelerated to a higher energy for the same degree of confinement. It would therefore be advantageous to develop methods for improving the resolution of the e^+s leaving the moderator. This is discussed in the next section.

1.5.4 Brightness enhancement

Liouville's theorem, which outlines the limits on the resolution of a beam, only applies for conservative forces. The brightness of a beam may be enhanced in excess of this limit by the application of a non-conservative force. Such a non-conservative (irreversible) process occurs during moderation. A useful quantity for this discussion is the brightness-per-unit energy (R) which relates to the intensity (I) and resolution of the beam as

$$R = I / (\sin^2\theta \times d^2 \times E) \qquad 1.17$$

R may be increased by several orders of magnitude by remoderation of a beam, despite the loss of some intensity (typically 50%). Remoderation was used to great effect by Canter et al (1989) in developing a transmission e^+ microscope. This system employs several stages of remoderation. Figure 1.18 demonstrates the action of remoderation (and subsequent re-acceleration) in R phase space.

Unlike most primary moderators the quality (resolution) of the re-emitted e^+ distribution from a remoderator is of greater importance than the moderation efficiency; increased R being the objective. As discussed in the section 1.5.1 the superior energy and angular resolution of reemitted e^+s from metals currently makes them the best choice. Although higher remoderation efficiencies could be achieved with the use of RGS the brightness (R value) of the beam would undoubtedly be lower.

1.6 **Positron beam timing**

1.6.1 Introduction

In many cases it is beneficial to know at what time e^+s within a beam will reach a particular point in space; examples include e^+ lifetime experiments, time of flight (ToF) measurements and background reduction in the study of rapid processes. There are two different approaches to e^+ beam timing, the first of which relies on detection, or 'tagging', of the individual e^+s constituting the beam which are randomly distributed in time. The second method is more direct involving turning the beam on for only brief periods of time when desired.

For timing of individual slow e^+s a conventional method involves tagging the β^+ particles entering the moderator which may be done either by detection of secondary γ-rays emitted by the source or, more commonly, with the use of a thin plastic scintillator as the particle detector. Alternatively the direct detection of slow e^+s may be performed with the detection of secondary e^-s emitted on entry into a remoderator. Detection of secondary γ-rays is normally an inefficient timing method rarely used for beam work and thus will not be discussed in this chapter.

Pulsed beam systems are often used in association with some form of bunching system

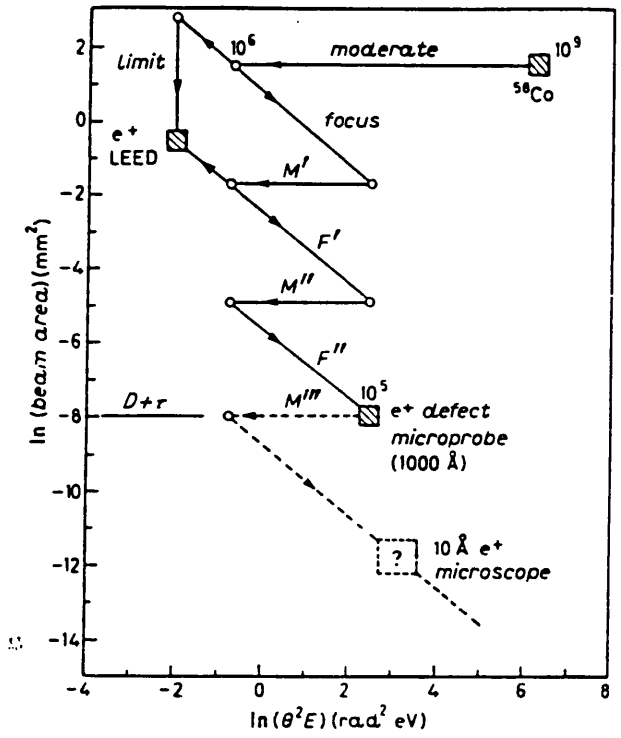

Figure 1.18 Brightness per unit-energy phase space for slow e^+ moderation (Mills 1983).

which sacrifices reduction in energy resolution or enlarged beam spot size for greater time compression.

These techniques will be considered individually in the following sections with some discussion of their respective advantages/disadvantages.

1.6.2 β^+ tagging

The basis of this technique involves placing a thin sheet of plastic scintillator between the source and moderator which allows almost all of the transmitted β^+ particles to be detected. The scintillation photons produced are detected with the use of a photomultiplier tube. A ToF spectrum is usually obtained by reversing the timing signals such that the output from the photomultiplier is delayed and used as a 'stop' signal. The reason for this is that a low 'start' signal count rate is desirable in order to avoid loss of true start signals as a result of electronic 'dead time'.

A high degree of timing efficiency is achieved, tagging practically all of the slow e^+ beam, however a large number of spurious timing signals are produced from incident β^+ particles which do not contribute to the moderated beam. These, in fact, constitute the vast majority of counted β^+. This high background limits the strength of the β^+ source used since saturation

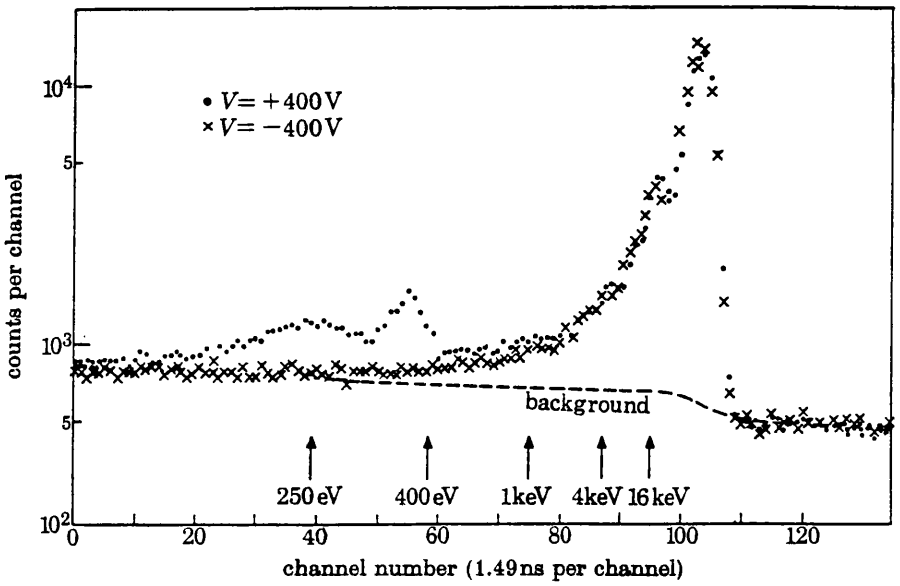

Figure 1.19 Typical raw data using β^+ scintillator technique, Coleman et al (1973)

of the photomultiplier may occur for count rates above roughly $4*10^6 s^{-1}$. Assuming all of the forward transmitted β^+ are detected this corresponds to a source strength of ≈8MBq of ^{22}Na. Reduction in the number of β^+ entering the moderator will be caused by annihilation within the scintillator and this is estimated to be around 50%. Significant reductions in the observed timed slow e^+ yield may also be incurred if, as is common, long (>100ns) times of flight are required or more specifically true signal start-stop time is large. Again this is due to the high background count rate. The reduction is a result of premature conversion of a real 'start' signal by a random 'stop' signal, thus losing a true ToF data point. An exponentially decreasing background will be observed from time zero in the ToF as seen in figure 1.19 which shows typical raw data taken using this technique. Detailed treatment of this and other effects caused by random pulses on ToF spectra is given in Coleman et al (1973) and Coleman (1979).

A useful parameter for simple comparison of timing techniques may be derived by dividing the slow e^+ beam intensity by that of the counted β^+ flux, this signal-to-background (S/B) ratio has a value of $\approx 1.4*10^{-5}$ for this technique. It should be noted, however, that S/B does not correspond to the ratio of signal to background observed in the region of the signal in the ToF spectrum since, in relation to the narrow time width of the slow beam, the background is spread over all time.

1.6.3 Secondary e^- tagging at a remoderator

Secondary e^- tagging at a remoderator is also an efficient method of slow e^+ beam timing, with commonly ≈50% of the remoderated beam being tagged. It does not incur the same spurious background count rate as with β^+ tagging since only the slow beam is analysed and S/B values around 10^{-1}-10^{-2} may be achieved. This method involves transport of a moderated slow e^+ beam through a hole bored centrally in a CEMA detector and subsequent implantation into a remoderator, commonly a thin metal foil. Secondary e^-s emitted from the rear of the remoderator are extracted and detected at the CEMA while the transmitted beam may be re-accelerated for transport.

A large fraction of the beam intensity is lost during remoderation since even the current most efficient thin foil transmisson remoderators which use laser annealing (Jacobsen et al 1989) only have a re-emission fraction of 40%. Such remoderators are generally difficult to handle, requiring careful preparation and the use of ultra high vacuum systems in order to obtain optimum efficiencies.

Some improvement in beam quality however may be gained using the technique of brightness enhancement at the remoderation stage.

1.6.4 Pulsed/bunched beams from radioactive sources

This technique commonly uses some form of periodic pulsing device in order to switch the slow e^+ beam on only at brief pre-determined times. Two immediately obvious benefits of a pulsed beam system are that one has control over when the next e^+ is to be transported and secondly the restrictions on timing resolution incurred using the previous two techniques by the detector response are not applicable and ideally the only limit on resolution is the electronic switching time.

A serious drawback may be seen if one considers a slow e^+ beam intensity of say $10^6 s^{-1}$ to which a pulse gate of 10ns width is applied. There will only be a 1% likelihood of a e^+ being in the beam within such a timing pulse. Here a technique may be employed in which manipulation of beam voltages are used in order to increase the linear density of the beam so as to form a compressed bunch of e^+s, hence the term 'bunching'. Since this technique

increases the effective beam strength within a certain time interval pulsing of the beam in coincidence with bunching should increase the number of e^+s per pulse and raise the efficiency of this timing technique.

One method of bunching involves applying a decelerating potential to the leading e^+ swarm components and an accelerating potential to the trailing components of the beam such that all particles arrive at the same time at a particular point in space (along the beam line). As has been mentioned before this method thus increases the density of the e^+ swarm in real space by reducing it in momentum space (ie increasing the momentum spread). These considerations are applications of Liouville's theorem (see section 1.5.3).

There are several ways to implement a bunching system in practice. One possibility is, when a beam pulse reaches the buncher, to switch on a potential that varies quadratically with distance (z) along the beam line. An example of such a potential function could be,

$$V(z) = k \times z^2/2 \qquad 1.18$$

where k is a constant. After a time equal to $2\pi /(m/k)^{1/2}$, m being the e^+ mass, all of the e^+s should arrive at the point z=0 at the same time.

As well as sacrificing energy resolution methods may also be devised in order to decrease the lateral spatial density (spot size) of the beam in order to increase the longitudinal e^+ density.

It should be noted that bunching is a technique not restricted to pulsed e^+ beam systems but may also be employed to enhance the timing resolution of tagged beams such as those discussed earlier in this section.

1.6.5 Conclusion

There are many aspects to consider when comparing the timing techniques described such as efficiency, resolution, beam intensity and experimental complexity. The suitability of a particular system will depend on the desired application. For low intensity e^+ beam experiments (using small sources; <200μCi) β^+ tagging would probably at present be the wisest choice since it is straightforward and efficient.

Moderate beam intensities (10^2-$10^5 s^{-1}$) may warrant the use of a remoderator for secondary e^- timing. This would provide an efficient, fairly high resolution system with a 'clean' (low background) signal.

Pulsed systems are somewhat restricted to rather high intensity, precision experiments since they require sophisticated experimental equipment.

1.7 **Motivation for present work**

Many techniques are employed in e^+ research in order to surmount the problems caused by the scarcity of this anti particle. Historically this has concentrated on the developement of better quality primary moderators with the aim of producing more intense well characterised beams from the available sources of β^+. A number of sophisticated mechanisms have also been developed in order to increase the effective beam intensity such as bunching, timing or brightness enhancement. Intense high resolution beams have allowed e^+s to be used in many areas of physics (eg solid state, atomic physics) as a unique probe to complement other more conventional projectiles such as e^-s or ions.

Significant improvements in moderation efficiency have recently been achieved with the use of RGS which for the first time are of the order of one percent. They represent a departure from the current conventional metal based moderator and possess different benefits and disadvantages. In chapter 3 solid Ar, Kr and Xe are studied in various geometries and using both magnetic and electrostatic transport with the aim of assessing their comparative merits over those of conventional moderators.

The process of e^+ moderation is generally well understood and involves the slowing down (moderation) and random diffusion to an exit surface. One method for significant improvement in the efficiency of this process would be the active extraction of e^+s with the application of an electric field to a suitable material. Considerable research has been performed attempting to develop this so called field assisted moderator. Chapter 4 of this thesis describes work which attempted to observe field assisted e^+ extraction/emission using the RGS with the aim of significantly enhancing their moderation efficiency.

A technique employed in e^+ beam work for improving the quality of measurements (signal to background) taken at the low count rates typically encountered in this research field is single particle timing. Using this method one can reduce the background on an acquired

signal by resolving the interaction in time. The development of more efficient and/or easily used methods for such timing is the motivation for the work presented in chapter 2. The technique investigated in this chapter is the timing of e^+s by detection of secondary e^-s liberated on β^+ impact of the moderator. Justification for the possible success of this technique is that the efficiency for both moderation and secondary emission processes are high for a similar set of (low energy) implanted β^+.

The work presented in this thesis can be categorised as the improvement in current e^+ beam technology and focuses on increasing both the intensity and quality of the beam.

CHAPTER 2

SECONDARY ELECTRON TIMING AT THE PRIMARY MODERATOR

2.1 Introduction

The work presented in this chapter is an attempt to develop a new slow e^+ timing method based on detection of secondary e^-s liberated at the moderator by the impact of the incident β^+ particles. As has been discussed in section 1.3.7 secondary e^- emission by e^+ impact is highly energy dependent, with the major contribution coming from lower energy incident particles. Similarly for metal foil and mesh moderators β^+s of moderate to low energy entering the bulk are likely to be those which slow down and diffuse to a surface to be emitted as part of the slow beam (see section 1.5). Thus it would seem likely that, since both processes are sensitive to β^+s within a similar energy range, e^+ tagging using moderator emitted secondary e^-s may provide an efficient timing technique which would not affect the slow e^+ beam intensity or have very high background count rates. If this were the case it would constitute an attractive alternative to current timing methods such as β^+ tagging using thin plastic scintillator or secondary e^- detection at a remoderation stage (see section 1.6).

The following sections present a description of the apparatus used for this investigation, followed by an outline of the experimental procedure and a discussion of the results obtained. Finally, some brief concluding remarks will be made.

2.2 Experimental arrangement

A magnetic field of 60 Gauss was employed in order to axially confine the slow e^+ beam during transport, this field was achieved with the use of five coils placed in the Helmholtz arrangement (see figure 2.1). The sample moderator was held between two brass plates behind which was placed a pin mounted uncovered 30μCi ^{22}Na source. The source was approximately 1mmx2mm in size and was clamped axially behind the 1cm diameter moderator, both of which were held at +25V when the beam was on. A high transmission grid behind the pin source was held at +65V and accelerated the β^+ induced secondary e^-s

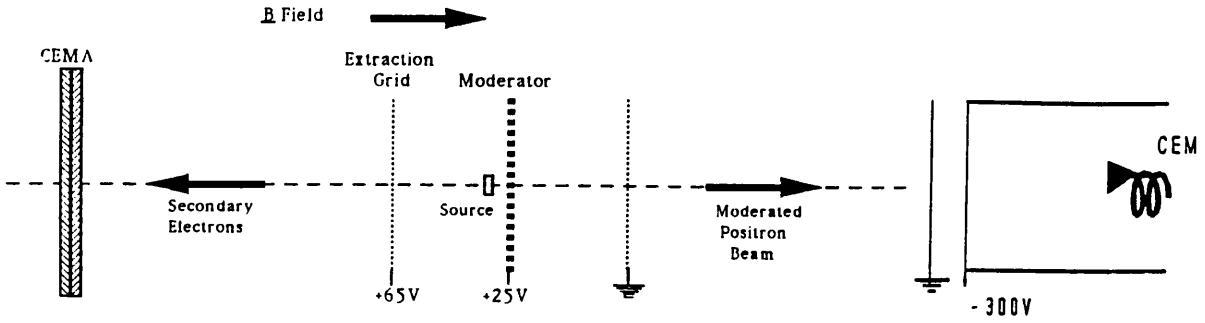

Figure 2.1 Schematic of the magnetically guided slow e^+ beam employed in these experiments.

emitted by the moderator to a channel electron multiplier array (CEMA) detector. Another high transmission grid was grounded and placed in front of the moderator in order to extract the slow e^+s emitted. After traversing an ≈1.5m long flight tube the slow e^+s were passed through two high transmission grids. The first was grounded and the second was held at -300V and was attached to a short metal tube. Mounted in this tube was the cone of a channel electron multiplier (CEM) at which the e^+s were detected.

The vacuum system which housed this arrangement employed two diffusion pumps and two Edwards rotary pumps. Pressure in the vacuum chamber was monitored using a Penning gauge. Typically a pressure of $\approx 10^{-6}$Torr was achieved.

Annealing of the metal moderator samples was performed in a seperate vacuum rig following the work of N.Zafar and G.Laricchia (Zafar 1990). A Speedivac rotary pump evacuated the system to a pressure of $\approx 10^{-3}$Torr as measured by an Edwards Pirani gauge. A small oven was constructed from two pieces of foil ≈25μm thick, made from the same metal as the moderator which was clamped between thick metal electrodes as shown in figure 2.2. A high current supply provided the power to heat the two sides of the oven which was required to achieve annealing temperatures.

When obtaining data various electronic devices were used to process the signals produced by the two detectors. The detected e^+ signal from the back of the CEM, after being de-coupled from the high voltage bias, was passed to a pre-amplifier (x10) and subsequently a

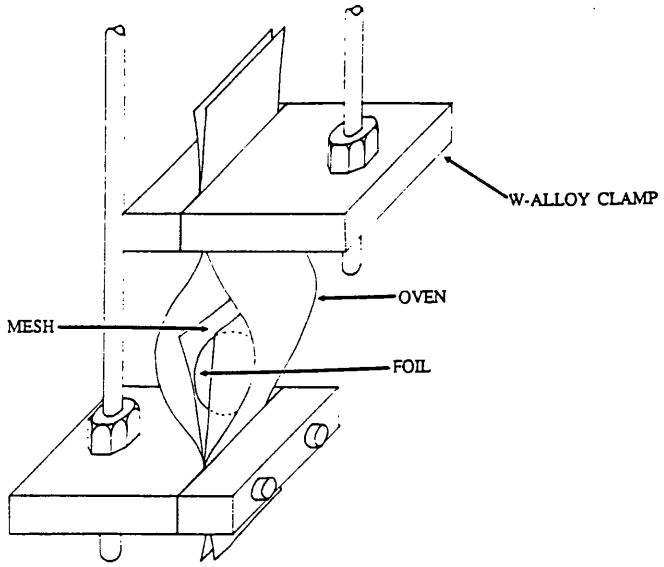

Figure 2.2 Vacuum rig used for the annealing of the metal moderators.

(x4.5) Ortec fast amplifier. This amplified signal was then able to trigger a discriminator the output of which was fed into the 'START' of a time to amplitude converter (TAC). Similarly the signal from the secondary e^- CEMA detector was also passed through a pre-amplifier and amplifier arrangement after which it was delayed by several hundred nanoseconds with the use of long shielded cables. This delayed signal then triggered a discriminator which subsequently provided the 'STOP' input to the TAC. The output from the TAC was fed to a multi channel analyser (MCA) where the inverted ToF spectrum could be viewed, a schematic of the electronics is shown in figure 2.3. Once a spectrum had been accumulated it could be stored on floppy disc and passed to a BBC micro computer where a BASIC plotting program had been written which enabled the spectrum to be analysed in more detail and for a printed copy to be produced.

2.3 **Experimental procedure**

In the case of the thin metal foil moderators studied, sample preparation would begin by removal of the epitaxially grown film from its substrate. In the case of nickel this was a thick NaCl crystal cleaved along the (100) plane. Removal entailed immersion in distilled water such that the foil was left floating on the surface. A 25μm thick metal ring mount was then used to lift the foil from the liquid such that a free standing circular film was produced.

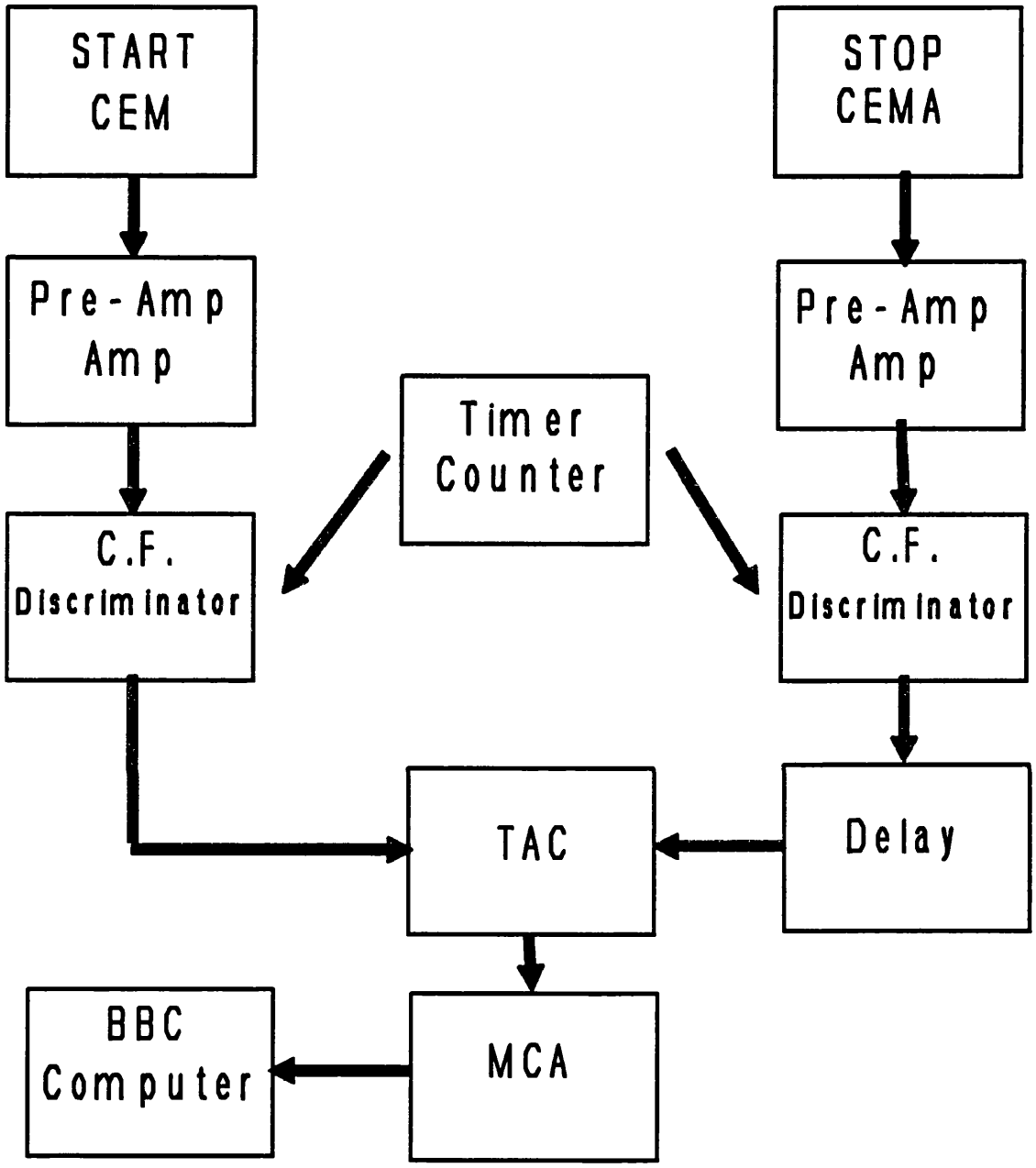

Figure 2.3 Schematic of the electronics employed for the e^+ time of flight measurements.

Tungsten and molybdenum foils were epitaxially grown on an MgO substrate which was removed by immersion in a heated (to about 90°C) Chloric acid solution ($HClO_3$), followed by washing in distilled water after which the same procedure as that for nickel would be performed (Zafar 1990). After construction of the oven, as in section 2.2, the moderator would be annealed by heating to about 2000°C in the case of tungsten, 650°C for nickel or

1500°C for molybdenum. Temperature was monitored by an optical pyrometer. Heating would last about 10 seconds and, after allowing the foil to cool, was repeated several times. A tungsten mesh moderator was prepared simply by cutting squares of $\approx 1 cm^2$ and annealing as with the foils. The manufacture of an MgO moderator involved the burning of magnesium ribbon in air such that the fumes (MgO powder) collected on two tungsten meshes placed above the flame thus forming a thick coating.

Generally after maximising the e^+ beam intensity by slight adjustment of the magnetic coils a stable beam was obtained. Positron and electron count rates were recorded (over 100 seconds) with both beam on and beam off. The beam off measurements were performed by biasing the source and moderator at -25V and the extraction grid behind the source at -65V thus preventing slow e^+s from reaching the CEM detector or slow e^-s from reaching the CEMA detector. Typically a 1000 second long ToF spectrum would then be obtained while the e^+s in the beam were being counted. The e^+ and e^- beam on/off measurements were then repeated in order to account for any drift during the ToF acquisition.

Variation of the energy of the e^+ beam was performed by altering the voltage applied to the source/moderator mount. The voltages on the e^- extraction grid and the CEMA plates were similarly altered such that the e^- transport properties were not affected.

Retardation of the secondary e^-s emitted by the moderator could be carried out by simply varying the voltage on the e^- extraction grid whilst maintaining all other potentials.

2.4 **Results**

Figure 2.4 shows a typical ToF spectrum taken using this arrangement with a moderator consisting of four annealed tungsten meshes. As can be seen the fast and slow e^+ beam components may be easily resolved, with the background being insignificant in the region of the latter. The fast component was thought to be due to either high energy e^+s, e^-s or γ-rays.

A brief test was performed firstly in order to obtain some information on the energy distribution of secondary e^-s emitted by the moderator, but also to observe the variation of slow e^- timing efficiency as a function of secondary e^- energy. The retarding spectrum shown in figure 2.5 reveals that the majority of the secondary e^-s are confined to a narrow energy band, with what appears to be an almost flat higher energy tail extending beyond 30eV. In

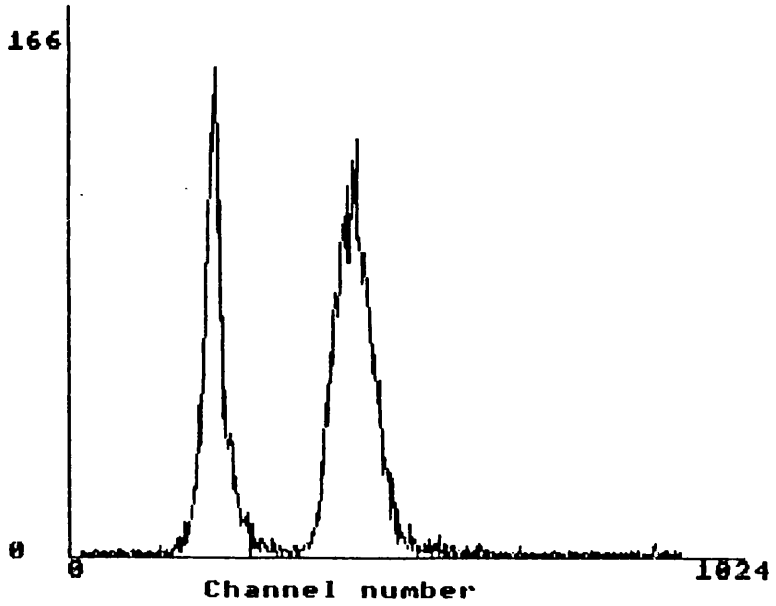

Figure 2.4 Typical raw data time of flight spectrum recorded over 1000secs using this apparatus with four W mesh moderators.

fact positive extraction had to be applied in order for the low energy electrons to be transported, this may indicate that most of the secondary e⁻s emitted by this four mesh moderator were at large angles to the beam direction and were re-absorbed if no accelerating potential was applied. The presence of the pin source on the beam axis was also likely to have hindered secondary e^- transport under low extraction fields.

Although the TAC and MCA arrangement should in principle have provided a linear relationship between channel number in the observed ToF spectrum and the detector start-stop time, it is known that offsets and non-linearities can occur. A series of measurements were therefore made in order to obtain the time calibration for the electronics and also a value for the absolute time zero position. This will not correspond to that of the fast e^- peak due to their finite ToF. These measurements involved varying the slow e^+ beam energy from 7eV to 40eV while recording the channel number separation of the centroids (T) for the fast and slow e^+ peaks in the ToF spectra. The assumption was made that the small changes in acceleration potential should not have significantly affected the flight time of the keV energy fast e^+ beam component. From the relation between beam energy (E) and flight time (t) quoted in equation 2.1, and assuming the measured quantity T is linearly dependent on t then T should also be linearly related to $E^{-1/2}$ as expressed in equation 2.2.

$$t = d\,(\,2E / m\,)^{-1/2} \qquad 2.1$$

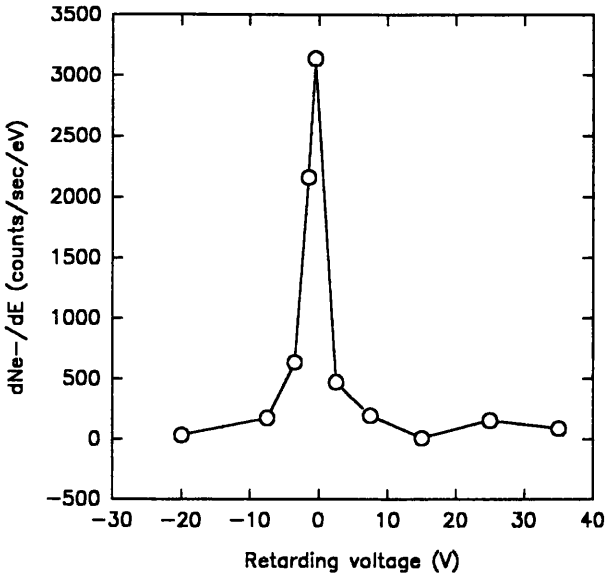

Figure 2.5 Secondary e^- energy spectrum obtained by retardation using this apparatus.

$$E^{-1/2} = a + b\,T \qquad 2.2$$

Plotting T as a function of $E^{-1/2}$ should thus produce a straight line curve from which the values of a and b quoted in equation 2.2 may be obtained. Such a plot is displayed in figure 2.6, this was consistent with values of $a = 3.0 \pm 0.5 \times 10^{-2}\,eV^{1/2}$ and $b = 5.8 \pm 0.6 \times 10^{-4}\,eV^{1/2}\,channel^{-1}$. These may then be used to obtain beam energy spectra from ToF measurements (channel seperation) obtained using this beam arrangement.

At energies below 10eV significant broadening began to occur to the slow e^+ peak in the ToF spectra, probably due to the increased significance of the finite slow e^+ energy distribution. Determination of the slow e^+ peak centroid thus became difficult below about 7eV. The beam intensity did not begin to decrease significantly (more than 5%) until the energy was lowered to 5eV.

The good linearity shown in figure 2.6 over such a broad energy range indicated that the ToF system was essentially functioning correctly. The simplistic time calibration obtained above does, however require certain corrections. Consideration of the flight time of the secondary e^-s will introduce some time-zero offset though this should be small compared to the e^+ ToF. As has been mentioned earlier in this section the narrow energy spread of the secondary e^-s emitted should have introduced no significant effect on the timing resolution.

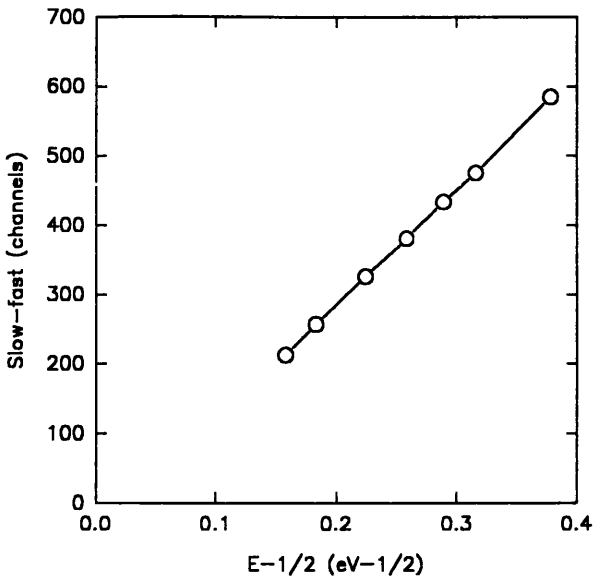

Figure 2.6 Calibrating the ToF system by varying the slow e^+ energy and measuring the fast-slow e^+ component separation

Some unavoidable reduction in timing resolution will have been introduced however within the electronic and detection system. This should be small compared to the major factor affecting timing resolution in this experiment which is the longitudinal (axial) energy

Table 1.1 Parameters of timed beam using different numbers of annealed meshes in the moderator.

Number of meshes	Positron yield s^{-1}	Timing efficiency %	Secondary e^- count rate
3	33.8±0.6	27.6±1.0	18829
4	39.3±0.6	24.7±0.7	19457
5	44.3±0.7	24.3±0.7	19850
6	46.3±0.7	22.2±0.7	19218
7	49.7±0.7	22.5±0.7	19832
8	48.0±0.7	20.7±0.6	19863
9	46.6±0.7	20.6±0.6	20823
10	43.5±0.7	19.7±0.6	19967
11	38.5±0.6	19.3±0.6	20206
0	-2.8±0.2		12000

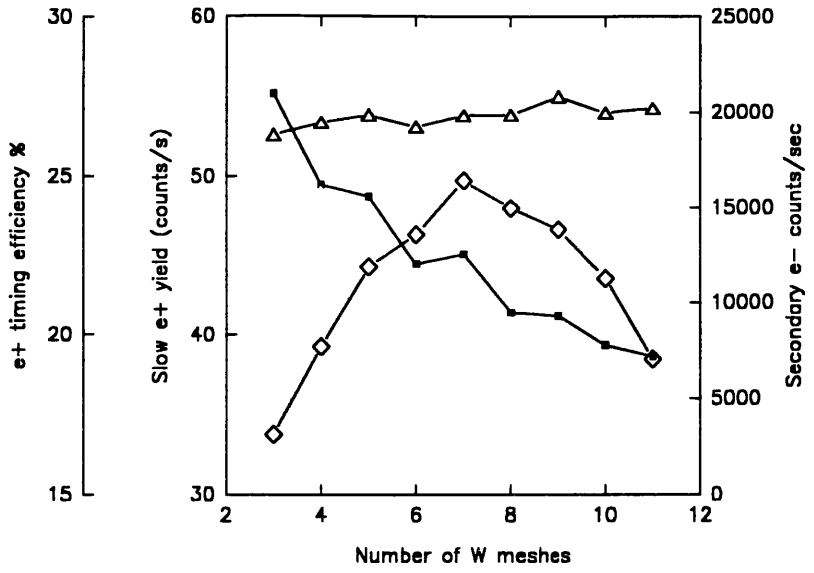

Figure 2.7 Number of W moderator meshes vs △ secondary e^-, □ slow e^+ yield and • e^+ timing efficiency

distribution of the slow e^+ beam. This has components from both the spread in absolute energy and variation in angle of emission from the moderator.

A systematic study was performed by using various numbers (3-11) of annealed tungsten meshes in the moderator and recording the slow e^+ yield, secondary e^- intensity and slow e^+ timing efficiency achieved. Table 2.1 and figure 2.7 show the results obtained, the secondary e^- yield varied little; from $\approx 19000 s^{-1}$ to $21000 s^{-1}$ but showing some tendency to increase with the number of meshes. A peak value of $\approx 50 s^{-1}$ for the slow e^+ yield was obtained with the use of 7 meshes, the yield decreased for both higher or lower numbers. The optimum number of timed e^+s was also obtained using 7 meshes which gave a count rate of $\approx 11 s^{-1}$, thus producing a timing efficiency (ε_t) of ≈22%. Slow e^+ timing efficiency appeared to fall gradually with increasing numbers of meshes in the moderator from a value of over 27% to about 19%. This variation may be understood as an effective decrease in the efficiency of secondary e^- extraction per moderator mesh as their numbers are increased due to attenuation by the meshes already present. It should be noted here that a significant fraction of the slow secondary e^-s counted may not have arisen due to e^- impact on the moderator, but rather from surronding supports or grids. The secondary e^- yield taken without the presence of a moderator fell only by roughly a factor of two. This value however may have been enhanced by the decreased attenuation of β^+s from the source due to the removal of the moderator. The explaination for the variation in secondary e^- yield with number of meshes in the moderator

is probably rather complex, involving several factors.

Using the time calibration previously carried out, a measurement of the width of the slow e^+ timed peak was performed with the beam at 25eV, this consistently gave a value of ≈20ns (FWHM). If this were solely due to energy spread in the slow e^+ beam it would correspond to ≈1.8eV.

Neither the investigations using metal foils or MgO powder achieved the magnitude of slow e^- yield or timed beam obtained with the tungsten meshes, as sumarised in table 2.2. Consideration of timing resolution for the various materials is also an important factor when comparing these moderators since this directly affects the signal-background ratio in the region of the signal. MgO was slightly broader than Mo or W which in turn were significantly broader (by nearly a factor of two) in resolution than the Ni foils which were measured to have a FWHM of ≈12ns (for a beam of 25eV) and would correspond to an energy spread of ≈1.1eV. Some qualitative agreement was made here with the studies carried out by Zafar et al (1989) using similar experimental procedures where retardation spectra of e^-s emitted from nickel foil moderators were observed to be ≈5 times narrower than those from W. It would also seem likely that broadening due to angular spread and epithermal effects in emission should be larger for the MgO powder moderator.

The large timing efficiency (≈63%) observed for the MgO moderator was significantly greater, by more than a factor of two, over the metal samples analysed. This may easily be understood given the roughly two fold enhancement in secondary e^- yield observed for this moderator, indicating a much higher probability of β^+ induced secondary e^- production from an MgO surface over that of a metal (see section 1.3).

A significant inaccuracy in determination of slow e^- yield, and thus also slow e^+ timing efficiency, should be considered at this point. When determining the background count rate at the CEM, reversal of the +25V applied to source/moderator may not only retard slow e^-s but could also accelerate secondary e^-s of moderately high energy (few hundred eV) such that some, otherwise undetected, particles could thus be counted if they gained enough additional energy to strike the CEM. This would increase the measured background and thus reduce the slow e^+ yield recorded. This argument was somewhat supported by an observation which was made whilst no moderator was present, the beam off count rate was higher (by ≈$3s^{-1}$) than that recorded when the slow e^- beam was supposedly being transported. For moderators producing large (>$10s^{-1}$) slow e^- beams this would represent a small (fractional) correction.

Table 2.2 Timed beam parameters for different moderator materials.

Moderator	Positron yield	Timing efficiency	Resolution
Ni 2000Å	6.9±0.3	31±3	12±4
Ni 5000Å	4.1±0.2	18±2	
Ni 5000Å	1.8±0.1	23±3	
Mo 5000Å	17.2±0.4	10.6±0.5	20±6
Mo 2000Å	13.2±0.4	12.8±0.8	20±6
W 5000Å	18.7±0.4	9.9±0.4	20±6
W mesh 7of	49.7±0.7	22.5±0.7	20±6
MgO smoked	4.1±0.2	63±6	25±6

For lower intensity beams however it could be highly significant since any reduction in the measured slow e^+ yield would proportionally increase the stated timing efficiency. The samples which would have been most affected were nickel and MgO. The correction, if assumed to be equal to a reduction of $\approx 3s^{-1}$ in the measured slow e^+ beam, would still leave MgO with timing efficiency of ≈30% but bring the two nickel foil measurements more in line with the other metal foils at ≈10% and ≈20%.

A brief test was performed on the transport and detection system entailing detection of secondary e^-s at the CEM detector with the source/moderator biased to +65V, the CEM cone held at +300V and a +600V increase to the extraction voltage at the back of the CEM in order to maintain the potential applied across the device. Similarly the e^- extraction grid was biased to -25V and the front of the channel plates lowered to -200V with a similar reduction to the back extraction electrode of the CEMA which now collected the e^+ beam signal. A two fold enhancement in the e^+ count rate and a corresponding two fold decrease in the number of secondary e^-s counted was observed. This was consistent with twice the detection efficiency being achieved at the CEMA as that of the CEM detector. This may have been due to poor transport or reduced CEM detection efficiency. Since the timing efficiency is independent of absolute e^+ beam intensity such factors should not have affected the nature of the results obtained in this study.

Good secondary e^- transport and detection efficiency is of great importance to the efficiency

of this timing system. One factor which was considered as a possible loss mechanism for secondary e⁻s was obscuration by the pin source. Several geometries were thus tried with the source mounted to one side of the moderator and positioned at various angles. Maximum e^+ and secondary e^- yields were obtained with the source placed axially behind the moderator and parallel to it so as to face its centre. No further significant secondary e^- yield increase could be obtained by holding the source at a different bias to that of the moderator or by increasing the secondary e^- extraction voltage up to a value of ≈+150V.

2.5 **Discussion**

Taking the values obtained using the most efficient of the moderators tested, being that constructed from seven tungsten meshes, the highest S/B ratio achieved using this method of slow e^+ beam timing was $\approx 5*10^{-4}$. This is a factor of about 30 higher than that recorded using the thin scintillator β^+ tagging method developed by Coleman et al (1972). This would allow correspondingly larger source strengths to be used, of up to 40MBq, before detector saturation occurs. Timed fluxes of order 10^2-$10^3 s^{-1}$ could be obtained. This limitation arises since with the use of high source strengths and using long ToF the large number of random events causes signal degradation by premature conversion of start pulses.

This timing technique involved no complex experimental equipment or sample preparation and was operated for long periods at only moderately high vacuum ($\approx 10^{-6}$Torr). It would thus appear to represent a rather robust, easily constructed method for low intensity slow e^+ beam timing. There are some geometrical considerations with the use of this technique owing to the necessity of secondary e^- extraction, for example a pin mounted source was used in this investigation. The ease of manufacturing ^{22}Na sources in unusual geometries is of considerable benefit in this respect.

Further developement of this technique could come from the use of moderators with increased β^+ moderation efficiency and/or larger secondary e^- yield per incident particle. One such material may have been found with the rare gas solids (RGS). They are currently quoted with the highest achieved β^+ moderation efficiency (for neon) of ≈1.4% (Khatri et al 1990) and as discussed in section 1.3.7 these solids should also liberate large numbers of secondary e⁻s. They are currently being studied as possibly a new type of efficient x-ray photocathode (Gullikson and Henke 1989). The RGS are considered in more depth in chapter 3.

CHAPTER 3

RARE GAS SOLID MODERATORS

As discussed earlier (section 1.5) experiments performed on the rare gas solids (RGS) have demonstrated their potential to provide substantial improvement on existing e^+ moderation efficiency. This chapter describes work performed using solid Ar, Kr and Xe films investigating their moderation efficiencies under various conditions.

Two different arrangements were employed in this series of experiments. The first of these utilised a magnetic beam transport in the study of solid argon frozen onto a cryogenically cooled copper cup source and also investigated the effects of varying the pressure and time of gas exposure during deposition. The second involved an electrostatically guided e^+ beam and studied the moderation efficiencies of all three RGS using a conical and a flat shaped geometry as well as the cup source.

Some comparison to theory is made by performing a crude calculation in order to predict the transmission moderation efficiency of a solid argon film implanted with β^+ particles. Details of this calculation are presented in the first section.

3.1 Theoretical treatment

From a knowledge of the β^+ stopping profile and e^+ diffusion characteristics in solid argon it would in principle be possible to predict the transmission moderation efficiency of a condensed Ar film and also its variation with film depth. In practice this can be done by solving the diffusion equation.

As described in chapter 1.3.2 an exponential function can provide a sufficiently good approximation to the β^+ implantation profile. The diffusion of e^+s in the RGS has been discussed in section 1.3.4 and from the work of Gullikson and Mills (1986) an estimate for the energy averaged diffusion length of low energy e^+s (up to a few eV) in Ar was made of $\approx$5000Å. As described by Vehanen and Mäkinen (1985), after making the assumption that the incident and emission surfaces are fully absorbing, the fraction of implanted β^+ that are stopped and transmitted can be expressed as a function of film depth (d) by;

$$J(d) = 1/\sinh(d/L_+)\int_0^d \sinh(z/L_+)P(z)dz \qquad 3.1$$

where L_+ is the e^+ diffusion length.

Assuming all of the β^+ produced by a source are implanted into the moderator this expression should thus provide an estimate of the slow e^+ moderation efficiency defined as the number of slow e^+s per β^+ emitted by the source. In order to evaluate equation 3.1 it was re-expressed in a more convenient form. This was done partly by making the substitution of $a=d/L_+$, $b=\alpha d$ and also by solution of the integral, this expression is given in equation 3.2.

$$J(d) = b/(a^2-b^2)[e^{-b}(a \times \coth(a) + b - a/\sinh(a)] \qquad 3.2$$

A short Fortran program was written in order to evaluate equation 3.2 for various values of argon film thickness. Figure 3.1 shows the results of this calculation which predicted a maximum moderation efficiency of 0.144% for an Ar film thickness of 3.6μm assuming a e^+ branching ratio of unity at the surface.

If the value taken for the diffusion length of epithermal slow e^+s within the solid Ar was in error this would have affected the validity of this calculation. Further calculations were performed in order to test the sensitivity of equation 3.2 to changes in the value of the diffusion length and thus the variable a. Increasing L_+ by 20% to 6000Å caused a similar increase in the slow e^+ yield to 0.172% at an optimal film depth of 4.2μm, decreasing L_+ by 25% to 4000Å reduced the predicted moderating efficiency also by 25% to 0.115% with the maximum yield achieved at a depth of 3.0μm.

3.2 **Experimental arrangements**

The two sets of experiments involving magnetic and electrostatic beam transport were performed at the University of Aarhus, Denmark. The studies were undertaken approximately one year apart.

3.2.1 Magnetic beam

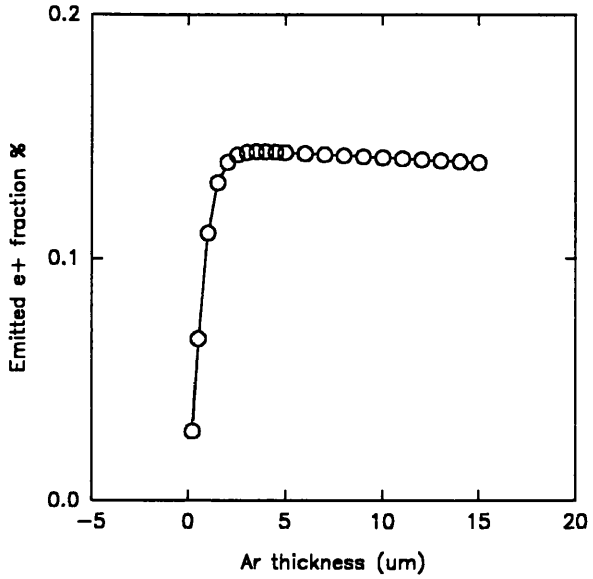

Figure 3.1 Calculated solid Ar moderation efficiency as a function of film thickness using a diffusion equation.

The β^+ source used in the first series of e^+ moderator efficiency measurements was 5.7μCi of ^{22}Na deposited on a copper cup with an aspect ratio of 2 as shown in figure 3.2. This source was mounted on the second stage of a CTC cryogenics cold head from which it was electrically isolated by a thin (≈0.1mm) Mylar sheet. A platinum resistance thermometer was mounted on one side of the cup in order to monitor the temperature at the source which was typically around 28K.

A polished copper shield surrounded the second stage of the cold head in which a 10mm diameter mesh-covered hole was bored allowing the extraction of e^+s or secondary e^-s from the source. This radiation shield was mounted on the first stage of the cold head, which typically reached about 70K. The cold head arrangement was mounted within a vacuum chamber which typically achieved a base pressure of $\approx 8*10^{-8}$Torr. The vacuum was provided by a turbomolecular pump and a backing rotary pump. The pressure was monitored using a model IGC26 ion gauge which was also used during the controlled admittance of argon gas into the chamber. The gas was admitted from a 99.99% pure, 10Bar flask of argon and controlled through a needle valve attached by a gas line to the chamber.

Four coils mounted in Helmholtz configuration surrounded the chamber and provided the ≈60 Gauss magnetic field which confined the slow e^+ or secondary e^- beam. After passing through the earthed grid on the radiation shield the beam was transported roughly 1 metre to a second high transmission earthed grid after which it underwent acceleration through to a

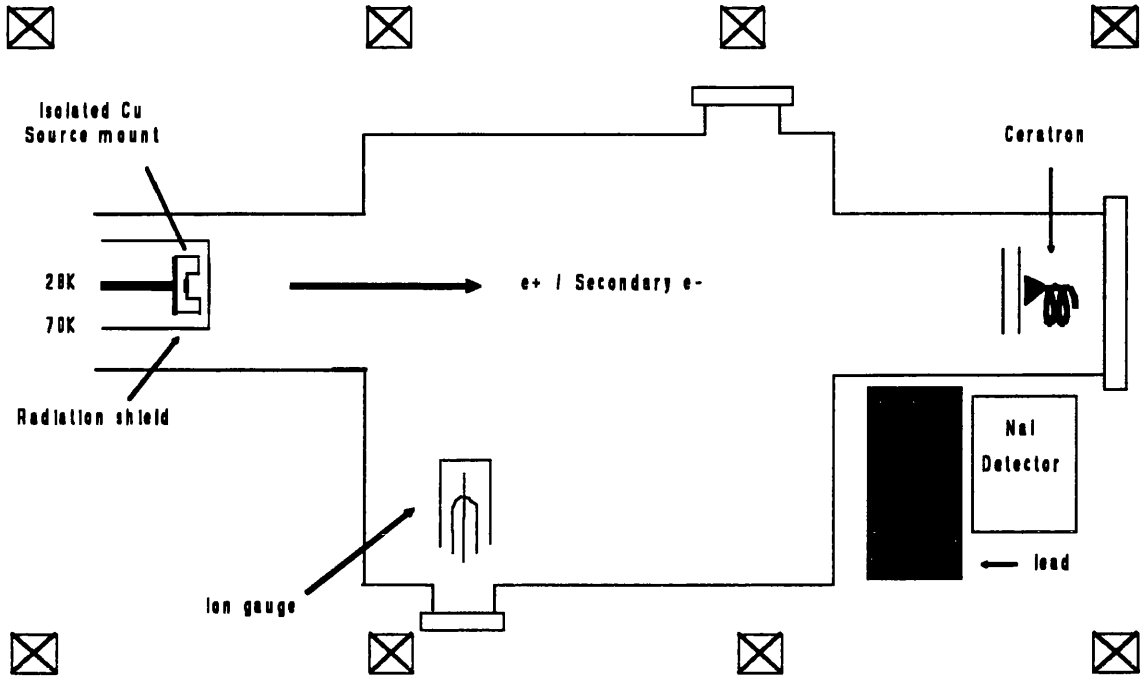

Figure 3.2 Schematic of the magnetically guided slow e^+ beam

third grid before detection at a ceratron. A NaI detector was placed close to the ceratron (outside the chamber) in order to intercept γ-rays emitted on e^+ annihilation. This enabled coincidence measurements using the two devices to be performed and thus the absolute e^+ beam intensity to be determined.

The electronics used was standard for such coincidence measurements involving amplification of the signals provided by the ceratron and NaI detectors by Ortec model 454 amplifiers. The two signals were then fed to two Ortec model 584 constant fraction discriminators after which the γ-ray output, being at a higher count rate than that of the ceratron, was delayed by about 200ns and used as the 'stop' signal for a TAC. The discriminator levels for the NaI signal were set so as to detect only γ-rays less than 511keV. This was done in order to minimise the number of detected secondary 1274keV γ-rays emitted from the source. The 'start' signal was provided by the ceratron detector and the resulting coincidence spectrum was observed using an IBM compatible 286 computer on which an MCA card provided interfacing to the TAC. A schematic of the electronics used is shown in figure 3.3.

3.2.2 Electrostatic beam

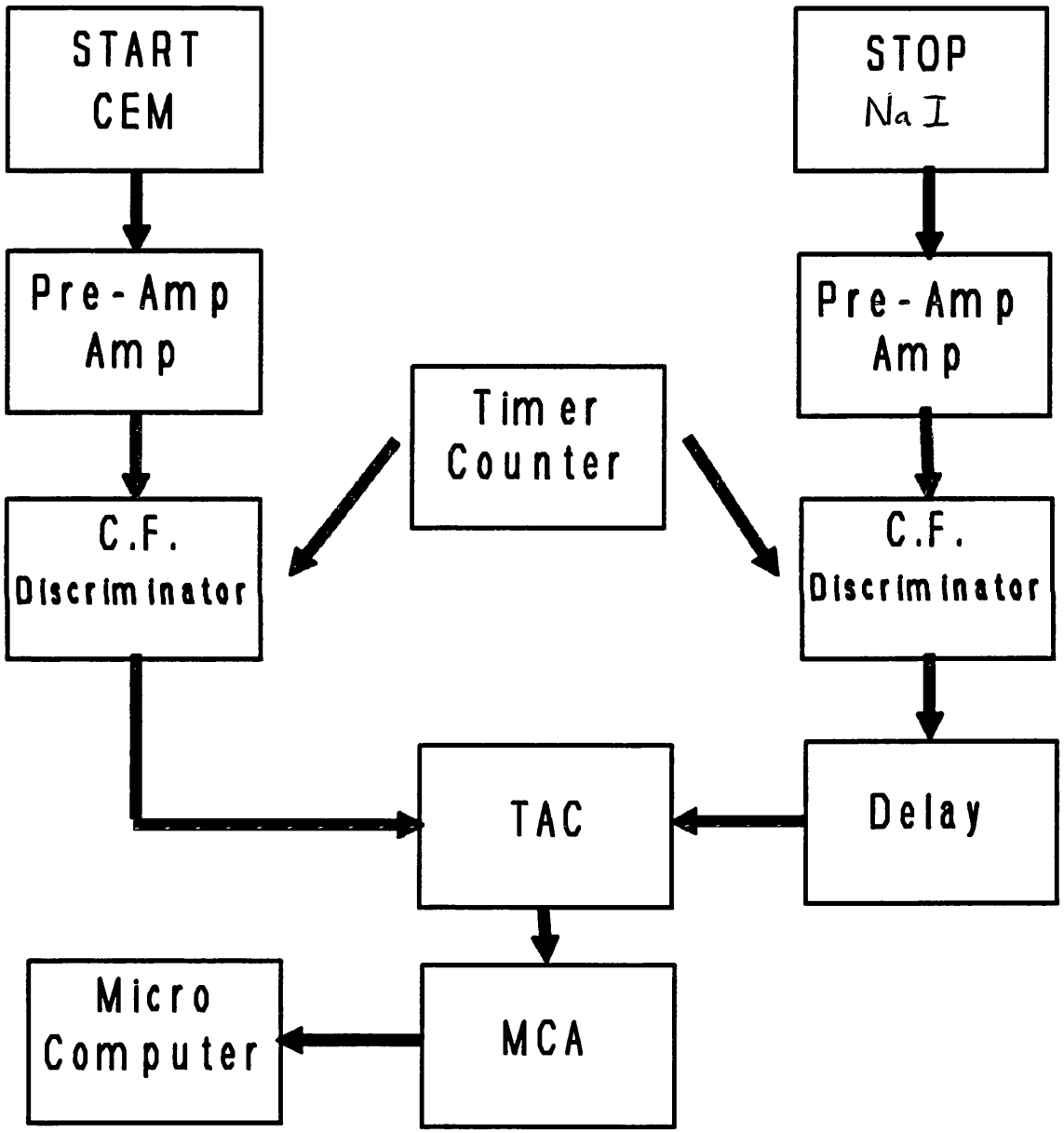

Figure 3.3 Schematic of the electronic employed for the coincidence measurments.

Three copper source mounts were constructed in addition to the cup described earlier all containing 6.0μCi ^{22}Na β^+ activity deposited as a spot as shown in figure 3.4. The first geometry was identical to that of the old cup except that it had a thicker base whilst the second was a conical design with the same proportions as that used in the studies reported by Khatri et al (1990). The third design was essentially a flat plate except for a shallow (1mm) circular recess cut in the middle of the front face of about 1cm width. At the centre of this recess the ^{22}Na was deposited.

Calibration of the ^{22}Na sources deposited on their copper mounts was performed both prior and subsequent to carrying out this set of experiments. This calibration utilised a NaI γ-ray detector and signal counting electronics adjusted in order to detect only the 1274KeV secondary γ-rays (photopeak) emitted on β^+ formation. Calibration of this detection system was performed with the use of a standard ^{22}Na source.

An APD cryogenics model H-2 cryopump system was used in this set of experiments which, as shown in figure 3.4, had a different cold head and radiation shield geometry to the system used with magnetic beam transport. This was the reason for the construction of the first of the source mount designs which was the same as the old cup source except that the accelerating grid on the radiation shield was closer to the top of the cup. This allowed better extraction fields to be applied.

The first source orientation used the old cup source which was clamped directly onto the second stage of the cold head while the polished copper radiation shield was attached. This radiation shield was electrically isolated from the first cooling stage by a thin (0.1mm) mylar sheet. As before the temperature was monitored by a platinum resistance thermometer. The cryopump achieved lower temperatures than those measured using the previous device. Temperatures of <50K were observed at the first cooling stage (the radiation shield) and <15K at the second stage (source). When using the three other source mount designs no temperature monitoring device was attached, although some indication of temperature could be obtained from a device internal to the cryogenic cold head. Stable temperatures (presumably of ≈15K as before) were usually obtained after about 1-2hrs of cooling.

The copper radiation shield had a 10mm diameter aperture covered by a high (90%) transmission copper mesh through which the e^+ or secondary e^- beam was accelerated. The electrostatic transport consisted of seven electrically isolated stainless steel lens elements as

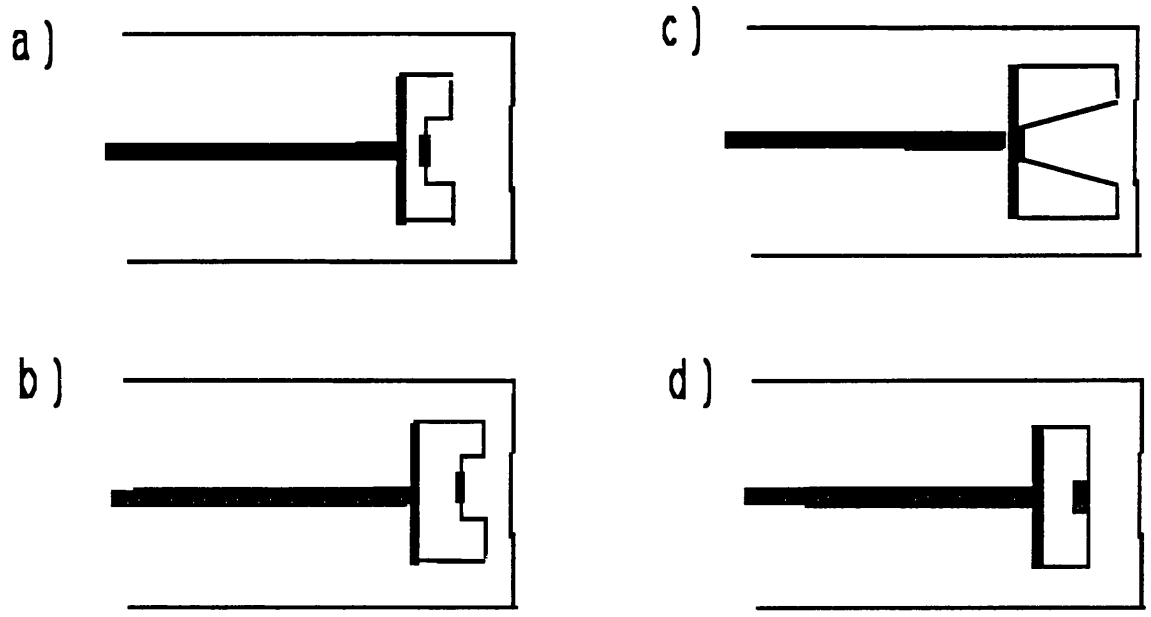

Figure 3.4 Source mount and cold head designs for RGS moderators; a)cup1, b)cup2, c)cone and d)flat plate.

shown in figure 3.5. The beam, having left the radiation shield, passed through another mesh (tungsten) covering the entrance to the first of the lenses. The beam was transported about 30cm and brought to focus upon a 1cm wide mesh covered aperture at the end of the last lens. The beam was subsequently accelerated through another mesh and detected at a ceratron. Detection of coincident e^+ annihilation γ-rays was performed by a lead shielded NaI detector as seen in figure 3.5. As before this enabled the absolute e^+ beam intensity to be measured.

The focusing properties of the lens system and the resultant transport efficiency of this electrostatic beam was simulated using the SIMION PC/AT computer software package (Dahl and Delmore, 1987). Figure 3.6 shows a schematic of the lens transport modelled by SIMION with the typical operational voltages, also shown are the flight trajectories for 2eV e^+s emitted at an angle of 20° to the moderator surface. The simulation indicated that a transport efficiency of practically unity should be achieved. Significant losses only occurred for e^+s emitted at large angles (>30° to the beam axis) with high energies (>3eV). Referring back to section 1.3.6e (figure 1.9) it can be seen that this should be a small fraction of the total emitted slow e^+s. Particles emitted from the sides of the cup may also be lost although this was not quantitatively investigated.

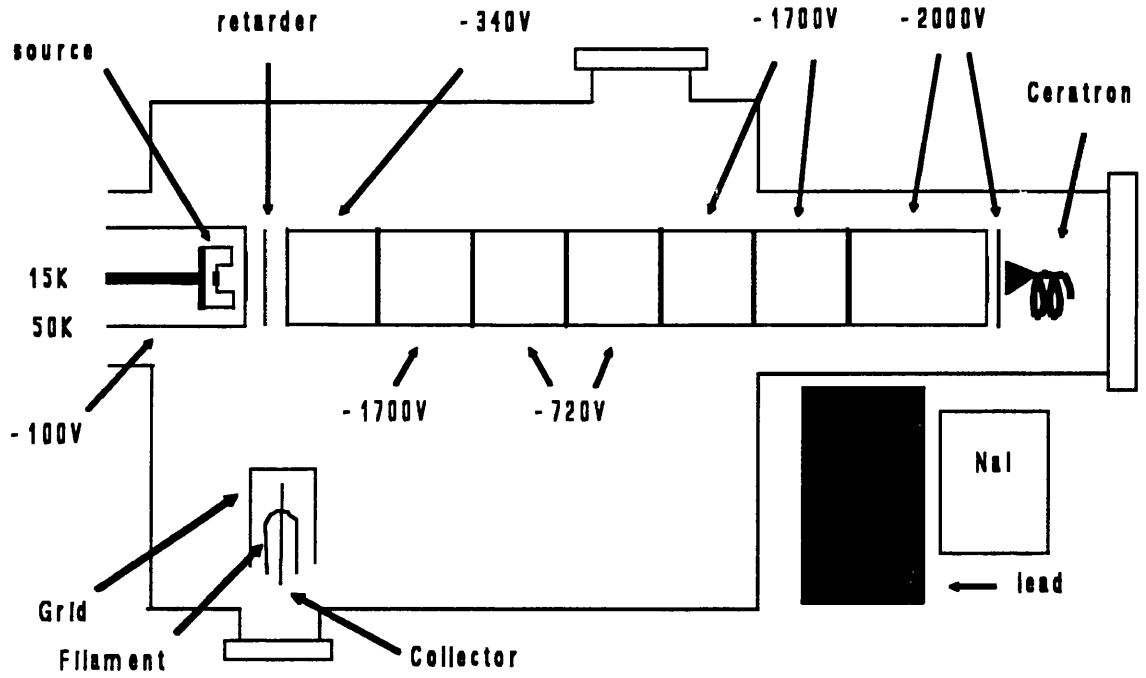

Figure 3.5 Electrostatic guided slow e^+ beam arrangement.

Two pairs of Helmholtz configured coils were placed around the chamber in order to annul unwanted magnetic fields (eg that from the earth) perpendicular to the beam direction. An Oersted meter was used in order to monitor this field while adjustment of the coil currents was being made.

Base pressure in the vacuum chamber during operation was typically $\approx 4*10^{-9}$Torr as measured by a model IGC26 ion gauge. The same system of rare gas admittance into the chamber was used as before ie with a needle valve attached to a gas line which is adjusted while monitoring the ion gauge reading.

An almost identical electronic arrangment was used to process the detector signals as that employed earlier (figure 3.3). After amplification and discrimination the γ-ray signal was delayed by $\approx$500ns before being used to 'stop' the TAC. The 'start' originated at the ceratron

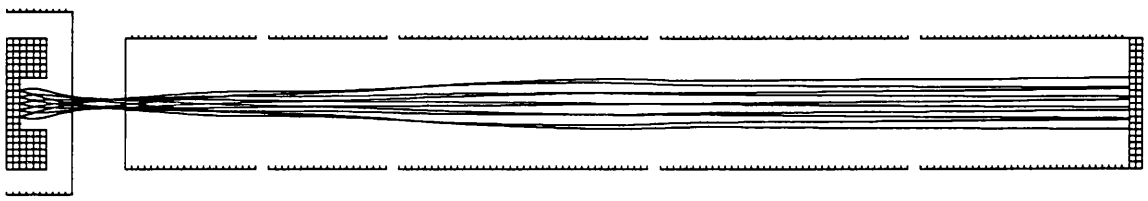

Figure 3.6 SIMION simulation program of the electrostatic beam optics for 2eV e^+s emitted at $\pm 20^\circ$ from the cup source.

detector. In the preliminary experiments the computer controlled MCA was used to determine the coincidence count rate (by integrating over the 'prompt' peak). Normally however a gating signal was taken directly from the TAC and passed to an Ortec counter/timer which in effect performed integration over the whole 1μsec time scale of the TAC.

3.3 **Experimental procedure**

3.3.1 Magnetic transport

Using the first cup source and the magnetic beam transport described, several solid argon moderators were constructed. Once the source temperature had stabalised argon was leaked into the chamber such that a constant pre-determined pressure was registered at the ion gauge of between $5*10^{-4}$ and $5*10^{-6}$Torr. The ion gauge would then be switched off and the beam and ceratron voltages applied. Slow e^+ beam on and beam off count rates would be monitored over time as the solid argon was deposited. The beam voltages would be switched off occassionally in order to check that a stable gas pressure was being maintained. Once sufficient argon had been condensed the gas leak valve would be closed and the e^+ and secondary e^- beam count rates would be monitored over time. In the case of the preliminary moderators adjustment of the coils would then take place in order to assure maximisation the slow e^+ beam transport. Moderated e^+ yield was monitored for several hours (over 12) in order to determine any loss of efficiency over time. Removal of a moderator simply involved turning off the cryopump for several minutes (around 10). During this time pressure measurements would show an increase usually up to a value of $\approx 10^{-4}$Torr followed by a sharp decrease back to the base vacuum pressure. Moderator evaporation would occur at a source temperature of roughly 40K measured with the platinum resistance thermometer.

Determination of the ceratron detection efficiency (and thus the absolute e^+ beam intensity) was performed towards the end of this series of measurements. Following the deposition of a solid argon moderator this entailed recording the NaI γ-ray counts and the number of coincidence events recorded on the computer MCA over an ≈4000 second period with both slow e^+ beam on and off. Ceratron count rates were measured with both beam on and off (over 100s) before and after such a 4000s γ-ray/coincidence measurement was taken.

3.3.2 Electrostatic transport

The same cup source was used initially with the electrostatic transport system in order to maintain some consistency with previous measurements. Having adjusted the Helmholtz coil current settings such that the magnetic field registered by the Oersted meter was minimised perpendicular to the beam direction some initial tests on the lens optics of the transport were performed using secondary e^-s emitted from the β^+ source. The cryopump achieved a temperature of less than 20K after about 30mins. Accurate measurement below this temperature was not possible using the platinum resistance thermometer. As before deposition of a RGS moderator involved leaking the gas into the chamber at some pressure monitored by the ion gauge. The beam was not active during deposition due to high pressure effects observed at the ceratron detector. It was noted that even when using argon, which has the lowest freezing temperature of the gases studied, some condensation would occur on parts of the cold head other than the source and its support (eg. the base of the first cooling stage). Since these parts were slightly warmer than the source such condensation would be characterised by a high chamber pressure after the rare gas inlet had been closed. This may be understood given the high and strongly temperature dependent vapour pressure of these RGS at temperatures close to freezing point. In order to alleviate this problem after deposition of the RGS the cryopump would be turned off for a brief period of time such that heating of the coldhead evaporated any such deposits. During this process as the temperature rose, a steady increase in pressure would be observed over several minutes which in the case of Xe reached a maximum pressure in excess of 10^{-3}Torr. A rapid decrease would then follow before settling at the base pressure.

Kr and Xe were not studied in great depth using this source, but several argon moderators were deposited in order to test their consistency. The approximate time and presure settings required in order to obtain deposition of an argon moderator with optimal moderation efficiency was determined by constructing the RGS film using consecutive condensed gas overlayers and measuring the slow e^+ beam intensity after each added layer.

For determination of slow e^+ yield, during all further studies, coincidence measurements would be performed in order that any variation in detection efficiency either of the ceratron or NaI counter would not affect the results. Lengthy tests were performed in which lens voltages were systematically varied in order that slow e^+ beam optimisation was achieved.

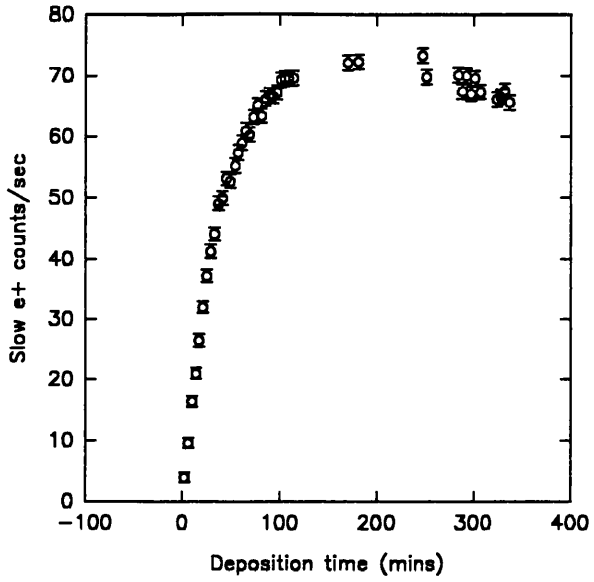

Figure 3.7 Slow e^+ yield from a cup mounted Ar moderator as a function of time at a pressure of $5x10^{-5}$Torr.

Variation of the Helmholtz coil currents was also carried out in order to test that effective cancellation of unwanted magnetic fields was achieved.

After taking several Ar moderator efficiency measurements using the computer controlled MCA, where the shape of the coincidence peak could be studied, measurements were taken just using a counter/timer. In this case ceratron, NaI and coincidence pulses would be counted for 100 seconds with both beam on and beam off. This would generally be repeated 4 or 6 times in order to obtain good statistics.

Following the brief study using the old cup, more systematic tests were performed on the second cup, the cone and flat plate geometries. The same procedure was carried out for each which involved a brief check of the slow e^+ transport by variation of the lens voltages, followed by slow e^+ beam intensity measurements as a function of RGS moderator 'depth'. The latter paramter was controlled by depositon time at a fixed gas pressure. This was done for solid Ar, Kr and Xe on all three geometries. In order to obtain secondary e^- yields from these moderators beam voltages would be reversed and the back of the ceratron raised to +6kV.

3.4 Results and discussion

3.4.1 Magnetic beam

Figure 3.7 shows the variation of slow e^+ yield as a function of the argon deposition time (in hours) at a pressure of $5*10^{-5}$Torr measured in the chamber. The general features are a rapid rise followed by a broad peak which precedes a gradual decrease. It would not seem an unreasonable assumption that moderator thickness be a linear function of pressure and time, in which case figure 3.7 represents the variation of e^+ moderation efficiency with depth for solid argon in this transmission geometry.

If comparison is made between these experimental results and the predicted function of moderation efficiency with argon thickness shown in figure 3.1 the same general features can be seen. A slightly more rapid decrease in slow e^+ yield appears in the experimental curve, this could be due to a number of effects including impurity/defect trapping in the bulk reducing the effective diffusion length, or possibly a geometrical effect resulting from the use of a cup geometry. This same profile was observed at different deposition pressures with, as expected, the time scale roughly varying inversely with the gas pressure. This is demonstrated in figure 3.8 which shows the slow e^+ yield as a function of pressure*time at two different values of gas pressure, specifically $2*10^{-5}$ and 10^{-4}Torr. Some small offset was observed between these two curves which would seem to indicate an inaccuracy in the time or pressure determination. Although small this offset is larger than would be expected as a result of error incurred in the recording of these parameters, a likely explaination could be that the pressure and/or time of exposure was different at the source than near the ion gauge where the pressure was measured. The gas flow into and pumping speed out of the source region would be expected to differ from that of the ion gauge and such a difference could well be pressure dependent.

A determination of absolute slow e^+ yield, or rather beam intensity, was made which involved calculation of the ceratron detection efficiency using measurements taken of the γ-ray, ceratron and coincidence count rates labelled here N_γ, N_c and N_I respectively. Assuming the absolute slow e^+ beam intensity to be N_{e+} and the detection efficiencies to be ε_γ for the NaI (including the solid angle of acceptance) and ε_c for the ceratron detector then three relations may be constructed;

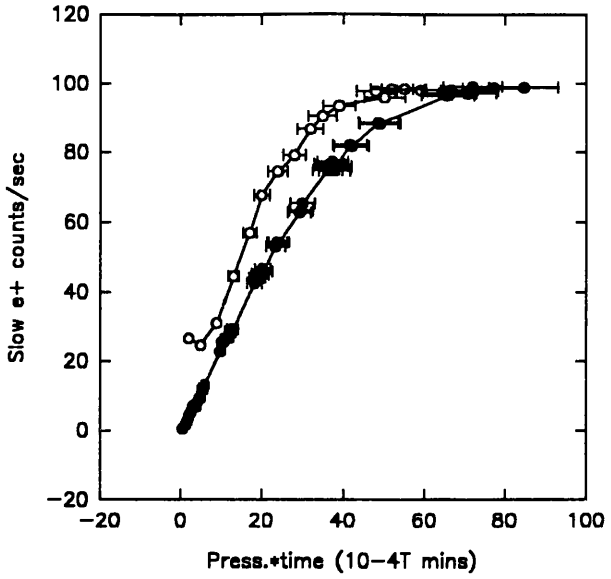

Figure 3.8 Slow e^+ yield as a function of pressure×time for Ar moderator deposition at ● 2×10^{-5} and ○ 10^{-4} Torr.

$$N_\gamma = \varepsilon_\gamma \times N_{e+}$$
$$N_c = \varepsilon_c \times N_{e+} \qquad 3.3$$
$$N_I = \varepsilon_c \times \varepsilon_\gamma \times N_{e+}$$

From these, using simple algebra, both detector efficiencies and also the absolute slow e^+ beam intensity may be obtained in terms of the three measured quantities;

$$N_{e+} = N_\gamma \times N_c / N_I$$
$$\varepsilon_c = N_I / N_\gamma \qquad 3.4$$
$$\varepsilon_\gamma = N_I / N_c$$

A value for the ceratron detection efficiency of 23(4)% was obtained which gave a typical peak moderator efficiency of 0.22(0.04)% for this solid argon coated cup geometry. The error quoted here on the moderator efficiency was determined by evaluating the statistical accuracy (within one standard deviation) of each of the three measured quantities (N_γ, N_c and N_I) from which calculation of the upper and lower bounds to the determination of the ceratron detection efficiency could be made and thus the bounds on the absolute slow e^+ moderation efficiency. The low value obtained for the ceratron detection efficiency was not solely due to the detector itself but also to the presence of two grids (for beam acceleration) close to the cone of the

detector (see figure 3.5). Positrons annihilating on these metal meshes would be detected with practically equal efficiency by the NaI γ-ray counter as would e^+s striking the ceratron and would therefore be included in the calculated detector efficiency (ε_c).

No direct comparison can be made between the maximum moderation efficiency calculated in section 3.1 (0.14%) and the value measured above since no consideration of the geometry of the source mount was included in the calculation (Mills and Gullikson 1986). Discussion of the theoretical and experimentally obtained efficiencies will be made later in this section when analysing the results obtained using the flat source.

Secondary e^- count rates in excess of $100{,}000s^{-1}$ were measured for an argon moderator giving optimal slow e^+ yield. This corresponds to around one secondary e^- emitted for every implanted β^+. It should be noted that no adjustment of the magnetic coils was made for this measurement and it is possible that maximum transport efficiency for electrons had not been achieved. Background, beam off, secondary e^- count rates were $<40s^{-1}$. Although no measurement of slow secondary e^-s emitted by retarding grids was made this was not thought to be a significant factor given the small intensity of the radioactive source used.

3.4.2 Electrostatic beam

The same cup source was used in the initial stages setting up the electrostatic beam transport in order that direct comparison of moderator efficiency determined using the two systems could be made. Since this study took place some time ($\approx$1yr) after the earlier magnetic beam experiment the source had decayed to $\approx$4.4μCi. Optimum deposition of argon, in terms of slow e^+ yield, was found to occur with a pressure of $\approx 4.5*10^{-4}$Torr for an exposure time of about 20 minutes. This was determined very roughly by noting the ceratron count rate for a few consecutive gas exposures. Accuracy was not thought to be critical since the peak yield was seen to be a broad function of moderator 'depth' (figure 3.7). Absolute slow e^+ yield was calculated using equation 3.4a from the measurements made on eight different argon moderators constructed using these exposure conditions. An average value (over 11 separate measurements) for the maximum solid argon moderator efficiency was obtained of 0.21(+0.04, -0.03)% using this cup. This value is in good agreement with the previous maximum efficiency determined for this moderator using the magnetic transport. Again error here has been calculated from the statistical accuracy of the measured quantities. The ceratron

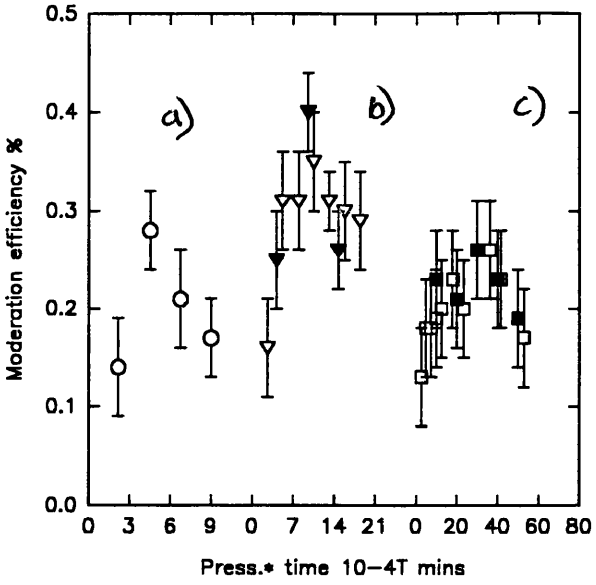

Figure 3.9 Slow e^+ yield from cup 2 as a function of ○ Xe, ▾▽ Kr and □■ Ar deposition time.

efficiency determined from equation 3.4c was ≈12%, almost a factor of two lower than the value quoted earlier during the magnetic beam experiment. This was thought to have been partly a consequence of the higher e^+ impact energy at the ceratron (≈2keV) which was well above the recomended value for optimum efficiency of ≈500eV. Such a decrease in the efficiency of the ceratron should have had no effect on the results quoted in this study since the coincidence measurments are independent of this quantity. The same experimental procedure was employed with the use of Kr and Xe RGS using this source, although fewer measurements were made thus reducing their accuracy. The optimal efficiency for Xe was obtained at a pressure of $4*10^{-4}$Torr and exposure for 30mins, for Kr it was 20mins at $5*10^{-4}$Torr. Table 3.1 shows the values obtained as well as all other maximal efficiency measurements made. Secondary e^- emission from argon deposited on this source, at peak e^+ moderation efficiency, was measured to have an intensity of $91{,}000s^{-1}$.

A more systematic approach was taken determining the slow e^+ moderation efficiency using the second cup design (where the extraction optics were improved) and also the conical geometry. Here absolute e^+ yields were measured as functions of RGS 'depth' for all of the gases Xe, Kr and Ar. Plots of the results are shown in figure 3.9a,b,c and 3.10a,b,c for the cup and cone source geometries respectively, the so called 'depth' parameter used as the x-axis for these plots was simply the product of deposition pressure and time given in units of 10^{-4}Torr for 1 minute. Accuracy of the moderator 'depth' quoted is somewhat misleading in the

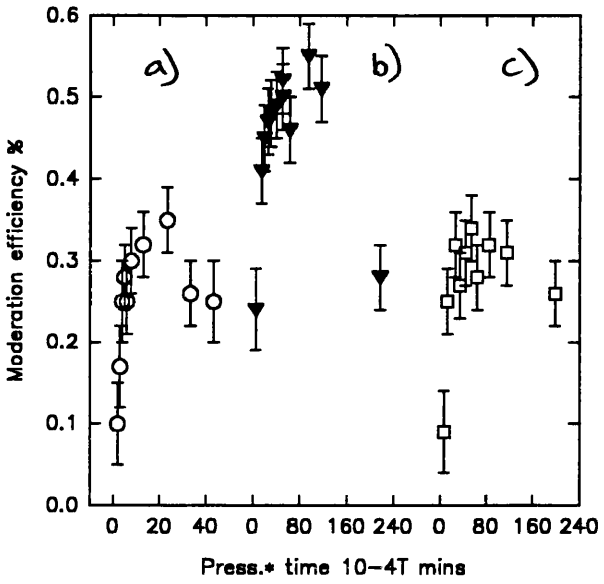

Figure 3.10 Slow e^+ yield from a conical source as a function of ○ Xe, ▾ Kr and □ Ar deposition time.

case of Kr and especially Xe due to the neccessity for evaporation of condensed RGS from warmer parts of the cold head which as described in section 3.3 caused very high vapour pressures for several minutes this undoubtedly caused significant further deposition upon the source. This effect may not have invalidated the pressure/time measurements since they were empirical in nature and this phenomenon might be expected have had a systematic effect ie enhanced the effective pressure/time for each deposition.

The optimal efficiencies quoted in table 3.1 for Ar deposited on the cup source and Kr and Ar on the cone were obtained by averaging over the approximate peak regions in figures 3.9a, 3.10a and 3.10b respectively and was done in order that greater accuracy could be obtained. This was thought especially important in the case of the conical geometry given the high efficiencies quoted for all of the RGSs studied using this source. It should be noted that the peak efficiency measured for the conical geometry using Kr, shown in figure 3.10b, was 0.55(+0.05, -0.04)% which was in agreement with the average value of 0.51(±0.02)% quoted in table 3.1, the lower bound however indicated a value (statistically) in excess of 0.5%.

In this experiment no account was made for e^+ beam attenuation incurred due to the presence of two extraction grids in the transport system near the source end. The quoted efficiency was calculated by dividing the slow e^+ beam intensity by the number of β^+ particles emitted by the source and thus did not account for β^+ loss due to the low backscattering coefficient of the copper source mount (roughly 30%).

Table 3.1 Summary of the maximum RGS moderator efficiencies determined for different copper source designs and RGS samples.

Source geometry	RGS	Moderation efficiency %	+ error	- error
cup1 (B field)	Ar	0.22	0.03	0.04
cup1 (E field)	Ar	0.21	0.04	0.03
cup1	Kr	0.34	0.05	0.04
cup1	Xe	0.19	0.08	0.06
cup2	Ar	0.22	0.02	0.02
cup2	Kr	0.40	0.05	0.04
cup2	Xe	0.28	0.05	0.04
cone	Ar	0.31	0.02	0.01
cone	Kr	0.51	0.02	0.02
cone	Xe	0.35	0.05	0.04
plate	Ar	0.18	0.06	0.05
plate	Kr	0.32	0.05	0.04

It was noted that over the roughly three month period of operation during the latter part of these experiments the detection efficiency of the ceratron fell by approximately a factor of two (from around 12%). No change in NaI detection efficiency was observed and the derived moderation efficiency for a particular moderator arrangement did not vary with time. As with the magnetic transport the low value for the ceratron detection efficiency was attributed partly to grid attenuation close to the detector, as measured in section 3.4.1, but also to the high incident e^- beam energy (2KeV). This energy is about an order of magnitude higher than that recommended by the manufacturer for optimal operation of this detector. The reason for the drift in detection efficiency of the ceratron was not clear, but may have been due to accumulation of surface contaminents.

Measurements performed using the flat plate source were made in the same manner as the first cup using the electrostatic transport. Crude determination of optimum efficiency was performed using only Ar and Kr. Consistently lower efficiencies were observed using this compared with the other sources. Even given the poor statistical accuracy of these

measurments the maximum yields were significantly below those obtained using the conical geometry. For comparison of the predicted moderation efficiency calculated in section 3.1 (0.143%) some corrections must be applied in order to account for experimental conditions under which measurments were taken. These corrections include β^+ losses due to absorption in the source mount (35%), attenuation during beam transport (metal grids 15%) and e^+ emission losses due to the presumed positive work function of the solid Ar (Gullikson and Mills 1986). The maximum experimentally obtained moderation efficiency for solid argon (table 3.1) was >0.12%, this is higher than the theoretically predicted value of 0.08% obtained after having made correction for grid attenuation and source mount absorption. This discrepancy could be due to some experimental effect, such as surface charging which will be discussed in some depth in chapter 4, but is more likely to be a consequence of the simplicity of the theoretical treatment and crudity of the estimated (average) diffusion length.

3.4 Conclusions

The maximum e^+ moderation efficiency of solid argon deposited on a cup shaped source mount was determined under two very different conditions such that the important experimental components which could have systematic effects on the measured moderation efficiency were all changed. These changes included the transport, detector and electronics systems with first a magnetic and later an electrostatic beam guidance. A third set of measurments was also carried out using a different source of the same cup geometry using the electrostatic transport. The good agreement obtained for all three values, of 0.22(0.02)%, is indicative that a high transport efficiency, expected using the magnetic guidance, was also obtained using the electrostatic arrangement. Such consistency, despite radical changes in experimental design, is also supportive of the validity of these results. The Kr and Xe moderation efficiencies measured were also consistent when using the two cup sources although generally slightly lower values (within statistical variation) were obtained for the first cup (see table 3.1). Some small beam loss would be expected in this case since, owing to the use of a different cryopump design, the extraction optics were poorer.

It should be noted that all of the efficiencies quoted here for the cup source are considerably higher than those published by Mills and Gullikson (1986) of 0.14% for Kr and 0.13% for both Xe and Ar where a similar source geometry was used. The most significant contributing

factor here was probably the use of a sealed (^{22}Na) source which was encapsulated by 10μm of plastic in the Mills and Gullikson experiment. The highest moderation efficiency obtained in this study for the cup source design was given by solid Kr which achieved a value of 0.40 (+0.05, -0.04)%. A study performed by Khatri etal (1990) investigated improvement of RGS moderator efficiency by deposition on a conical source geometry, an enhancement by a factor of 2.7(±0.2) was obtained over the cup geometry. The conical source used in the present investigation was of the same design as that used in the experiment mentioned above (see figure 3.4). Although moderation efficiencies for all of the RGS studied showed enhancement using the cone over those using the cup this enhancement was considerably less than that obtained by Khatri etal (1990) and was less than 70%. The most accurate determination of this enhancement was obtained for Ar with an increase of 41(+24, -16)%.

The highest e^+ moderation efficiency observed in this series of experiments was that obtained for solid Kr deposited on the conical geometry which attained a value of 0.51(0.02)%. The highest currently quoted moderator efficiency is 1.4(0.2)% which was obtained by Khatri et al (1990) using solid neon deposited upon an encapsulated ^{22}Na source with the same conical geometry as used in this investigation. This efficiency was obtained only after certain corrections (eg for source encapsulation) which involved multipilcation by a factor of 3.1(0.5). The highest measured moderation efficiency previous to this was quoted by Mills and Gullikson (1986) as 0.70(0.02)%. In obtaining this value the only correction made was for detection efficiency.

The only correction performed in order to obtain the efficiencies quoted in this investigation was that for the ceratron detection efficiency using the γ-ray coincidence arrangment. The highest efficiency observed in this study (quoted above) is more than an order of magnitude greater than those obtained using metal foil or mesh moderators (Zafar et al 1990). Conversely however sophisticated cryogenic equipement is required for this moderation technique and ultra high vacuum is desirable for extending the moderators useful life span. Also possible surface charging effects may occur for RGS with significant overlayers of impurity (see chapter 4). An added benefit with the use of RGS moderators is the ease and speed with which a new moderator may be manufactured (less than 1hr) without the need to open the vacuum system. Such moderators may also be fabricated into unusual geometries which could prove experimentally advantageous. This study has shown the RGS (especially Kr) to be a viable alternative to conventional slow e^+ moderator materials. Further improve-

ment could probably also be made given additional development.

The moderation efficiencies obtained for solid Xe deposited on a conical source were only about 30% lower than the highest values observed in this investigation (for solid Kr). Xe has the lowest condensation temperature of the RGS investigated, at ≈164K this is well above liquid nitrogen temperatures, the boiling point of Xe is ≈77K. Unfortunately the vapour pressure of Xe does not fall to the 10^{-6}Torr level (a reasonable vacuum pressure) until ≈60K. This is still not an unattainbly low temperature to be achieved using liquid nitrogen cryogenic methods which would be far less expensive than the cryopump used in these experiments. Solid Xe could provide a cheap highly efficient (≈0.35%) slow e^+ moderator for low intensity (small source strength) beams.

Secondary e^- yields from both cup and cone sources (6μCi ^{22}Na) were consistently greater than $10^5 s^{-1}$ when overlayered by solid Ar or Kr moderators which is approaching one e^- for every incident β^+. Such high yields would indicate that secondary e^- tagging using these RGS moderators should be a highly efficient timing technique. High background count rate problems could arise, however, similar to those seen using the thin plastic scintillator β^+ tagging technique (see chapter 2) which would exclude the use of high intensity sources.

CHAPTER 4

SURFACE CHARGING AND FIELD ASSISTED MODERATION USING RARE GAS SOLIDS

4.1 Introduction

The observation of an enhancement in the slow e^- yield from a solid argon moderator following the degassing of an ion gauge prompted the initiation of an investigation to study what appeared to be a surface charging effect. It was discovered that the effect relied upon the presence of an adsorbed impurity (initially air) which was able to capture low energy electrons incident on the surface. This chapter outlines the results of this study essentially chronologically, important developments in the experimental technique included the controlled adsorption of known impurities (oxygen and air), quantified low energy electron bombardment and importantly the measurement of slow e^+ and β^+ induced secondary e^- energy spectra from which a determination of the surface potential was made.

Following this introduction the second section of this chapter is devoted to a brief summary of the work previously performed on surface charging and will cover charging of dielectric materials, electron stimulated desorption from RGS and mechanisms for charge trapping at RGS surfaces. After a short description of the experimental arrangement in section three, the fourth section gives a description of the work carried out in this study and the results obtained. This fourth section is subdivided into six parts. The first two describe a series of tests measuring e^+ and secondary e^- yields under various conditions of RGS moderator, contaminant overlayer and using different charging mechanisms. The third sub-section presents crude e^+ and secondary e^- retardation spectra and uses oxygen as the adsorbate. In the final three parts of this section a significantly more precise system for obtaining retarding spectra was developed allowing some relation between surface potential and e^+/e^- yield to be made. Results are also presented of attempts to observe field assisted extraction using a biased metal grid.

In section five there is discussion of the possible physical processes responsible for the observations presented in this chapter. Detailed consideration is given to field assisted e^-/e^- extraction. Finally in a concluding section the significance of the work presented is discussed

and its relevance to other research.

4.2 Surface charging

The secondary e^- current emitted by an irradiated surface is highly dependent on the energy of the incident e^-s. Figure 4.1 shows the variation of secondary yield (including backscattered primaries) as a function of e^- beam energy striking a Teflon (PTFE) sample, a curve of this type is typical for all materials. The secondary yield is expressed as a fraction of the incident intensity. The number of secondary (plus backscattered) e^-s becomes equal to the number of primaries at two energies called the first and second cross overs. Between these energies (0.1keV and 1.6keV) the number of emitted e^-s exceeds that of the incident beam, holes are thus generated in the surface region which can cause positive charging. Outside this energy region e^-s may be accumulated at the surface and can cause negative charging (Seggern et al 1985). Gross et al (1984) observed both positive and negative charging of a thin (≈25μm) Teflon sample by treating the insulator as a simple capacitor and measuring the effective surface potential with a rear mounted electrode.

The bombardment of a dielectric material by positive ions, unlike e^- bombardment, may cause positive charging of the surface whether the secondary e^- emission yield (per incident particle) is greater than unity or not. This was demonstrated by Koshida and Yoshida (1978) in an experiment which measured the enhancment in secondary e^- emission of a compound powder (MgO, $MgCO_3$, Ag paste) under positive ion bombardment. The surface electric charge caused field dependent e^- emission (see chapter 1.3, Jacobs 1955).

One research area using the RGS within which much work has been performed is that of electron stimulated desorption (ESD). Commonly this involves the low energy (0-30eV) e^- impact of multilayer RGS either containing or having a thin overlayer of a molecular impurity (eg O_2, N_2, H_2O, etc). The observation and study of desorbed species from the RGS surface can be made. These often include anions and anion complexes (ie anions attached to one or more rare gas atoms).

One process for anion production from e^- bombardment of molecules, observed in the gas phase by Tate and Smith (1932), occurs as a result of resonance e^- capture with the production of a transient excited anion. This anion is unstable to auto-ionisation and in order to stabilise it must de-excite before this occurs. One way in which energy loss can occur is as a result

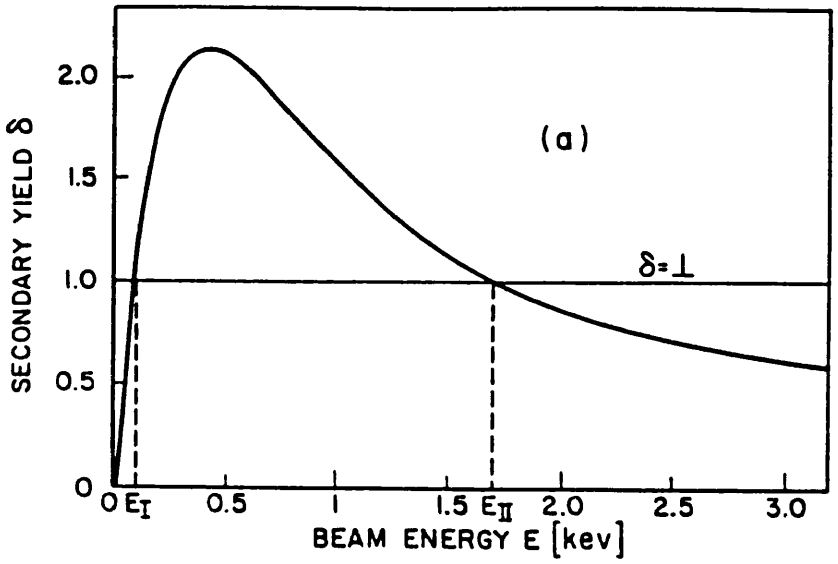

Figure 4.1 Secondary electron emission curve from Teflon (PTFE) as a function of incident energy.

of dissociation. This dissociative attachment (DA) process has been observed resulting from e^- impact of various different targets ranging from isolated molecules to molecular complexes, some containing RGS (Echt 1986).

Another process for energy loss which may leed to stabilisation of a transient anion was observed to occur in complexes. In this case vibrational modes of the surrounding molecular/atomic structure are excited (Märk et al 1986). This so called resonance stabilisation invariably causes some evaporation from the cluster.

It has been shown that both of these processes of anion production occur for condensed molecular species and may be observed using ESD. A detailed study was performed by Sanche et al (1989) on O_2 coated and O_2 doped RGS where ESD of various anions was observed (eg O^-, O_2^-, O_3^-, etc). Other molecular species which have been studied are N_2 (Michaud and Sanche 1990), N_2O, Cl_2 (Sanche and Paranteau 1989), H_2O (Rountree et al 1991), and various hydrocarbons (Rountree et al 1992). The field of low energy e^- scattering from molecules on surfaces is an active one, involving researchers from atomic and solid state physics/chemistry (see eg Sanche (1990) and Palmer and Rous (1992)).

Following the work performed on e^- scattering experiments using RGS the technique of low energy e^- transmission (LEET) spectroscopy was employed in order to investigate charge trapping in these dielectric materials (Marsolais et al 1989). In this technique a condensed layer of dielectric material is deposited on a metal substrate. Through this film a

monoenergetic e^- beam is guided in order to strike the metal electrode (substrate). The current being transmitted is measured as a function of e^- beam energy. A plot of this is known as an injection curve (IC). This technique is sensitive to accumulated surface charge which manifests itself as an offset in the IC. It arises as a result of the incoming e^-s requiring acceleration over the negative potential barrier in order to become implanted. One experiment of this type which has some relevance to the work presented in this thesis used a 0-10eV e^- beam to study surface charge trapping of a partially O_2 coated (0.1 monolayer) thin Kr film (20 monolayers). Long exposure to the beam was used in order to produce the charging, see figure 4.2, (Sanche and Deschenes 1988).

The shift (ΔV) in the IC may be related to the surface charge density (σ) by treating the dielectric film as a charged capacitor ;

$$\Delta V = \sigma \times h / \varepsilon \qquad 4.1$$

where ε is the permittivity and h is the thickness of the dielectric. The electric field strength (E) within the film can then be related to ΔV;

$$E = \sigma / \varepsilon = h^{-1} \times \Delta V \qquad 4.2$$

If bulk charging of the film occurs then a factor of 1/2 is included in equation 4.1 ($\Delta V = \sigma \times h/2\ \varepsilon$). This could occur if an impurity dopant was deposited in the bulk of the RGS instead of the surface, as in a matrix.

The rate of surface charging with time ($d\Delta V/dt$) is called the charging coefficient (A_s) and as a function of e^- beam energy this can be directly related to the energy variation of the e^- capture cross section (Sanche and Deschenes 1988). An example of such a measurment is shown in figure 4.3 for an oxygen overlayered (0.1 monolayer) krypton film.

As discussed above in the case of O_2 two major channels for charge trapping occur in the 0-10eV energy range. Below 2eV this is due to resonance stabilisation resulting in the production of an O_2^- ion whereas in the 4-10eV region dissociative attachment occurs with the production of a stable O^- ion. Knowledge of the geometry of the sample/beam arrangment allows absolute cross sections for e^- capture (trapping) to be calculated. The process of DA is discussed by Sambe et al (1990). Similar surface trapping processes have been observed

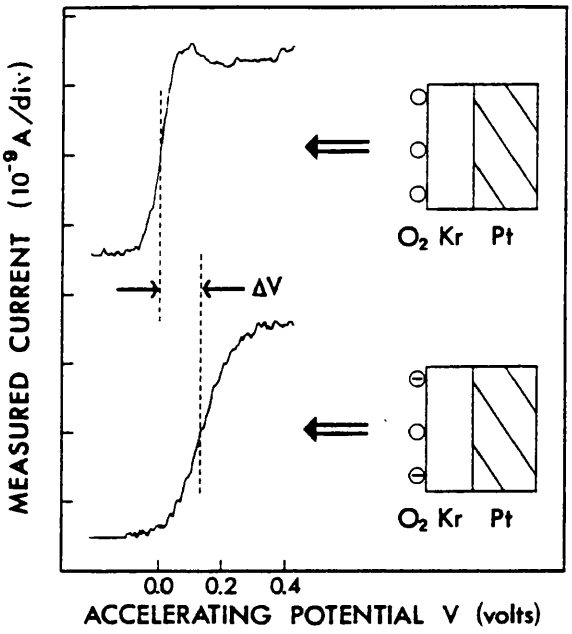

Figure 4.2 Current transmitted by an uncharged (top) and charged (bottom) $Kr+O_2$ film with e^- beam energy (Sanche and Deschenes 1988)

to occur for H_2O adsorbed on Kr and Xe films using the LEET technique (Bass and Sanche 1991).

4.3 Experimental arrangement

The bulk of the experimental investigations described in this chapter were carried out using the electrostatic e^- beam apparatus described in chapter 3.2 using the first ^{22}Na cup source. Initially the ion gauge was used for surface charging of the RGS and was positioned as in figure 3.5. Operation of an ion gauge relies on electrons emitted by a heated filament ionising the surrounding gas with the production of positive ions, these are then accelerated and detected at a cathode (the collector). During degassing the grid and collector of the ion gauge are biased at +650V with the heated tungsten filament being grounded. Electrons emitted by the filament will be accelerated towards the grid and may cause ionisation. The resultant positive ions would then be repelled by the grid and accelerated by a possible maximum of 650V.

A heated tungsten filament, capable of being biased to -150V, was subsequently used in order to produce energetic electrons, as shown in figure 4.4. Heating of the filament was performed using a 0-250V a.c. regulator which was electrically isolated on the output side

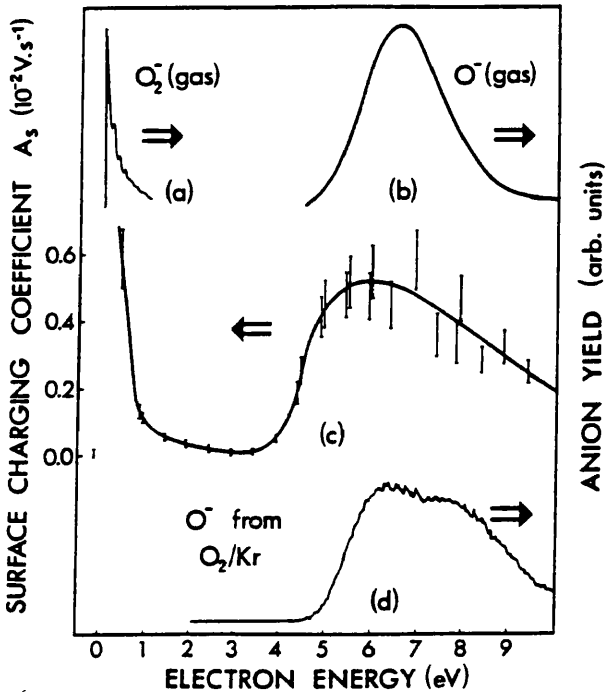

Figure 4.3 Electron energy dependence of the surface charging coefficient A_S for a 0.1-L-O_2/Kr film.

such that the filament could be biased.

Additional gas inlets were attached to the chamber described in chapter 3.2 which allowed the admission of other gases than air, specifically oxygen and SF_6. An electrically isolated high transmission retarding grid was attached to the inside of the copper radiation shield such that energy spectra of the e^+s and secondary e^-s emitted from the RGS surface could be obtained. At a later stage of this investigation the flat plate source was used, as shown in figure 4.4, to replace the old cup source. At this stage the retarder was placed on the outside of the radiation shield, close to the first lens element as also shown in figure 4.4.

Following the surface charging experiments the flat source was isolated from the cold head and attached to a pico-ammeter in order to measure the current striking the moderator whilst the tungsten filament was being heated. The source could be held at -100V by electrically biasing the pico-ammeter with the use of a d.c. power supply.

The final experimental arrangement consisted of the plate source mounted directly onto the cold head upon which an isolated high transmission copper grid was mounted at some 0.7mm separation. This grid could be electrically biased up to -3kV using a Brandenburg H.T. power supply (figure 4.4).

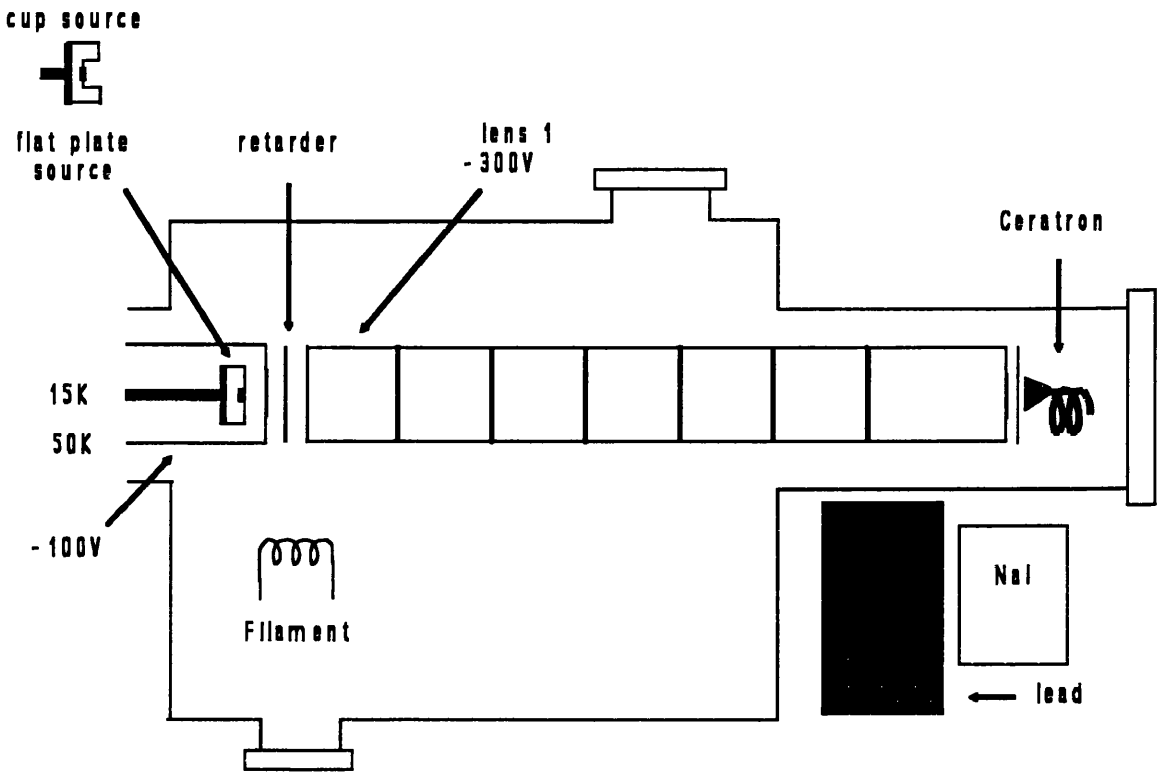

Figure 4.4 Modified electrostatic beam arrangement employing an e^- filament.

4.4 Results

4.4.1 Observation of e^+ enhancement and preliminary tests

The first observation of enhanced e^+ emission was made using a solid argon moderator deposited at a pressure of $5*10^{-4}$Torr for 20 minutes. The absolute slow e^+ yield was measured using the procedure outlined in chapter 3.2 in which the NaI, ceratron and coincident count rates were all recorded. A beam strength of $250\pm100s^{-1}$ was thus determined which corresponded to a moderation efficiency of $0.17\pm0.06\%$. The β^+ induced secondary e^- count rate measured at the ceratron was $90{,}000s^{-1}$. About 42 hours after depositing this moderator, at a base pressure in the chamber of $1.5*10^{-8}$Torr, the ion gauge was degassed with a filament power of 20Watts for around 30 seconds. The slow e^+ beam intensity was observed to rise by almost a factor of three to $635\pm100s^{-1}$ corresponding to a moderation efficiency of $0.42\pm0.06\%$, this increase was observed in the NaI, Ceratron and coincidence count rates.

The slow e^+ beam intensity was subsequently monitored for nearly an hour and seen to fall to $430\pm100s^{-1}$. A repeated activation of the ion gauge, again at 20Watts for roughly 30 seconds, produced a further enhancement in the slow e^+ yield reaching a value of $980\pm100s^{-1}$ (a moderation efficiency of $0.65\pm0.07\%$). The e^+ beam intensity was monitored again for a little over an hour by which time it had fallen to $430\pm100s^{-1}$. During the next roughly 90 minutes the beam intensity was maintained at between 500 and $700s^{-1}$ by activating the ion gauge at regular intervals, some 7 times in all.

Figure 4.5 shows a plot of the slow e^+ yield from this moderator as a function of time during this experiment. As well as the relatively steep decay of the enhancement after activating, the fall in peak yield attainable following the second activation should be noted.

After the first activation of the ion gauge an average enhancement in the slow e^+ yield was maintained in excess of a factor of two for approximately 4 hours. During this time a total loss of beam time of about 15 minutes was incurred whilst performing further activation.

Deposition of a second ('clean') solid argon moderator for the same time and at the same pressure resulted in practically the same unenhanced slow e^+ yield of $290\pm100s^{-1}$. Activation of the ion gauge at 20Watts for 30 seconds had no observable (<10%) effect on the slow e^+ yield. Further activation for longer times (2 minutes) or higher power (40Watts) also had no effect on the RGS moderation efficiency.

A third solid argon moderator was constructed using the same time and pressure as before for the deposition and achieved again roughly the same slow e^+ yield of $200\pm100s^{-1}$ corresponding to a moderation efficiency of $0.14\pm0.06\%$. This time air was admitted into the chamber at a pressure of 10^{-7}Torr. After 30 minutes of exposure ion gauge activation at 40Watts was performed for 30 seconds which resulted in the slow e^+ yield increasing to $850\pm100s^{-1}$ at a moderation efficiency of $0.57\pm0.06\%$.

These results showed that exposure of the moderator to air (or some contaminent) was required in combination with activation of the ion gauge in order to achieve the observed slow e^+ enhancement. This indicated that some surface related process was occuring which involved a condensated overlayer upon the RGS and emission from the ion gauge.

Shortly after this latest ion gauge activation the β^+ induced secondary e^- yield was measured from the 'enhanced' argon moderator. A value of approximately $12{,}000s^{-1}$ was obtained which was a factor of over 7 less than that measured for an unenhanced solid argon moderator. Having subsequently allowed the slow e^+ yield to decay to $500\pm100s^{-1}$ a further activation was

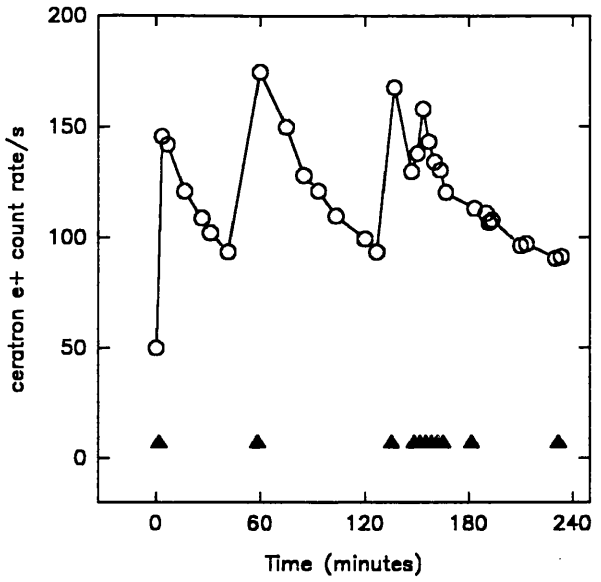

Figure 4.5 Slow e^+ yield from an Ar/air moderator with time during which e^- irradiation (▲ filament activation) is performed.

performed during which the first lens element was biased at +1kV and all other electrodes were grounded (see figure 3.5). The activation was performed for 40 seconds at 40Watts and resulted in a practically complete elimination of the slow e^+ yield. The beam intensity was too small to be determined in the usual manner. The slow e^+ count rate at the ceratron was $5.5\pm0.6s^{-1}$ which, given the 20±2% efficiency of the detector determined at this time, corresponded to an absolute beam intensity of $25\pm9s^{-1}$. Conversely the secondary e^- yield had been greatly enhanced to a count rate of roughly $370{,}000s^{-1}$ which is over a factor of four higher than an untreated moderator. From these results, summarised in table 4.1, and having some knowledge of the degassing process (activation) of an ion gauge, a reasonable description of the nature of these charging effects was formulated.

In section 4.2 the possibility of producing energetic positive ions during ion gauge degassing was mentioned. With the radiation shield and the first lens element grounded no direct path to the moderator surface was possible for positive ions produced at the ion gauge. These ions would be likely to strike the inside of the radiation shield or possibly one of the two beam accelerating grids close to the source. Secondary e^-s liberated by such impact could strike the moderator surface and, if trapped by some impurity overlayer (eg air), cause negative charging. Negative surface charging would be expected to affect the e^+/e^- diffusion/emission process and concievably produce the slow e^+ yield enhancment and β^+ induced secondary e^- reduction.

Table 4.1 Positron/secondary e^- yield from an air coated Ar moderator after various surface activation processes

Activation process	Positron yield s^{-1}	Moderation efficiency %	Secondary e^- yield s^{-1}
Positive ion bombardment	25±9	1.7±0.6 $x10^{-2}$	370,000
No treatment	200±100	0.13±0.07	90,000
Elelctron bombardment	850±100	0.57±0.07	12,000

Holding the first lens element at +1kV, whilst grounding the radiation shield and source, was thought to have sufficiently deflected the positive ions emitted by the ion gauge that they were able to strike the moderator surface. Such impact may not only directly charge the surface, but could liberate secondary e-s which would also produce positive charging (see section 4.2). This argument agrees with the observation of the simultaneous enhancment of β^+ induced secondary e^- emission and almost total reduction in slow e^+ yield; these being the converse effects of negative surface charging.

4.4.2 Other RGS/Overlayers and charge application

A krypton moderator was deposited at a pressure of $5*10^{-4}$Torr for about 15 minutes and a slow e^+ yield of $360\pm70s^{-1}$ was obtained. After exposure to $6*10^{-7}$Torr of air for about 5 minutes activation of the ion gauge at a power of 50Watts for 30 seconds increased this yield to $830\pm100s^{-1}$. A repetition of this activation further enhanced the yield to $910\pm100s^{-1}$ giving a moderation efficiency of 0.60±0.07%.

Having determined that this effect was not restricted to solid argon, deposition of a pure gas overlayer, rather than air, was attempted as a method of charge capture. The first pure gas adsorbate to be tested was SF_6. The reason for this choice of chemical for the condensate was its relatively strong electro-negative nature. It was expected to be comparatively efficient at capturing e-s and therefore effective at surface charging.

Four consecutive solid argon moderators were constructed all by deposition at $5*10^{-4}$Torr for 20 minutes. Different exposures of SF_6 were performed ranging from 1.5 minutes at a pressure of 10^{-7}Torr to 15 minutes at $2*10^{-7}$Torr and including 5 and 10 minutes at 10^{-7}Torr.

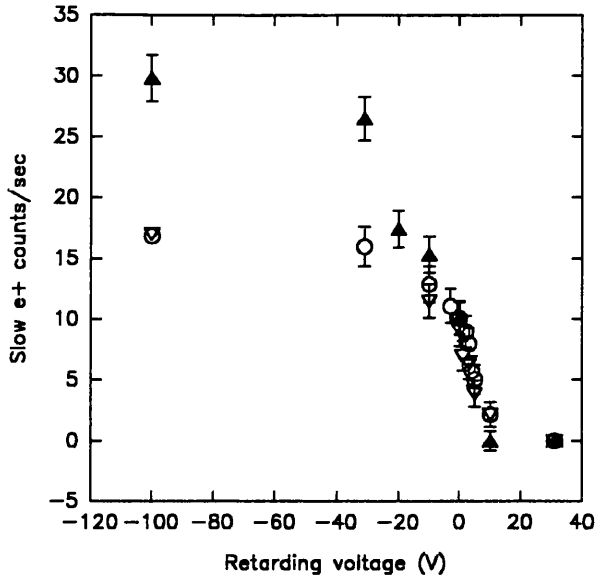

Figure 4.6 Slow e^+ retarding spectra from an ○ Ar, ▽ $Ar+O_2$ and ▲ $Ar+O_2$ after e^- irradiation.

The slow e^+ yield was typically around $250\pm100s^{-1}$ for such a moderator and was not observed to vary (<50%) for any of the samples following ion gauge activation which was usually performed at 40Watts for 20-30 seconds.

Following these failed attempts to achieve enhancment using condensed SF_6 a solid argon moderator was deposited at $5*10^{-4}$Torr for 30 minutes and subsequently exposed to air for 5 minutes at a pressure of $6*10^{-7}$Torr. The slow e^+ yield produced was $200\pm100s^{-1}$ (a moderation efficiency of $0.13\pm0.07\%$) which rose to $980\pm100s^{-1}$ (a moderation efficiency of $0.65\pm0.07\%$) after ion gauge activation at 50Watts for 30 seconds. The β^+ induced secondary e^- count rate was measured to have fallen from $80,000s^{-1}$ to $20,000s^{-1}$. This procedure was carried out in order to determine that no systematic effect had occured which might have prevented the observation of e^+ yield enhancement using SF_6.

An alternative and somewhat more straightforward method of passing charge to the RGS surface was developed using a biased, heated tungsten filament (see figure 4.4). This crude electron gun was intended to liberate low energy secondary e^-s in a similar manner to those emitted on positive ion bombardment during ion gauge degassing. A solid argon moderator was constructed at a pressure of $5*10^{-4}$Torr for 20 minutes and a slow e^+ yield of $290\pm100s^{-1}$ was obtained which did not alter after 5 minutes of exposure to 10^{-7}Torr pressure of air. Heating of the tungsten filament was carried out for 20 seconds by application of a 200V a.c. voltage whilst it was being biased at -10V. This had no observable effect on the measured

Table 4.2 Positron yield and moderation efficiency as a function of RGS depth (deposition time × pressure)

RGS	Depth (Pxt) 10^{-4}Torr min	Surface coating	Depth (Pxt) 10^{-7}Torr min	e^+ yield s^{-1} Before e⁻s Ion gauge	moderator efficiency % before	e^+ yield s^{-1} After e⁻s Ion gauge	moderator efficiency % After
Ar	100±10	air	250±130	250±100	0.17±0.07	980±100	0.65±0.07
Ar	100±10	none		290±100	0.19±0.07	317±100	0.21±0.07
Ar	100±10	air	30±10	200±100	0.13±0.07	850±100	0.57±0.07
Kr	75±8	air	35±10	360±100	0.24±0.07	910±100	0.61±0.07
Ar	80±10	SF_6	1.5±0.5	310±100	0.21±0.07	240±100	0.16±0.07
Ar	100±10	SF_6	5.0±1.0	230±100	0.15±0.07	240±100	0.16±0.07
Ar	100±10	SF_6	10±2	240±100	0.16±0.07	280±100	0.19±0.07
Ar	120±10	SF_6	30±5	180±100	0.12±0.07	220±100	0.15±0.07
Ar	150±15	air	5.0±0.5	200±100	0.13±0.07	980±100	0.65±0.07
Ar	150±15	air	5.0±0.5	Secondary e⁻s 80,000		20,000	
Ar	100±10	air	5.0±0.5	290±100	0.19±0.07	FILAMENT 790±100	0.53±0.07

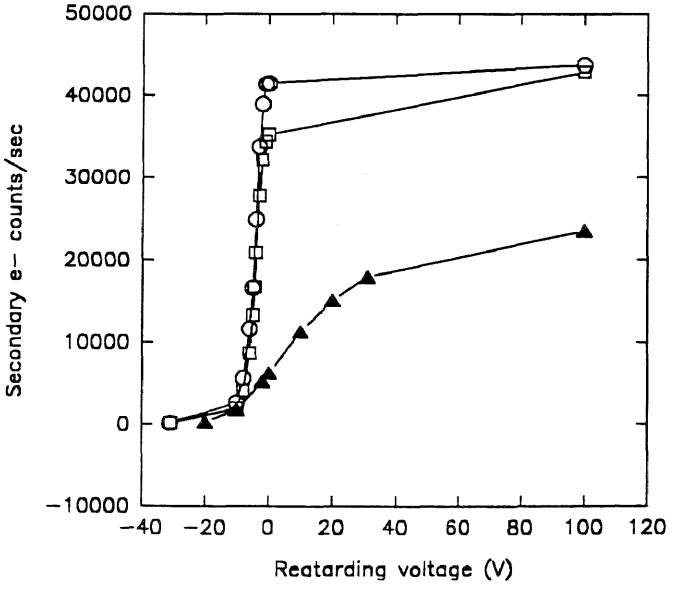

Figure 4.7 β^+ induced secondary e⁻ spectra from ○ Ar, □ $Ar+O_2$ and ▲ $Ar+O_2$ after e⁻ irradiation

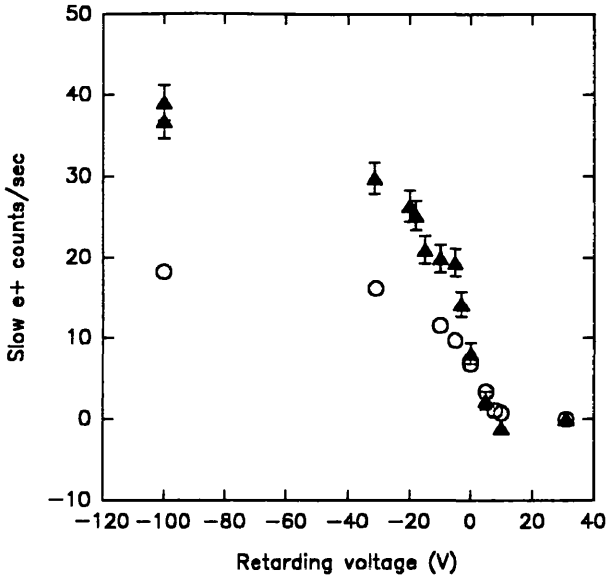

Figure 4.8 Slow e^+ retarding spectra taken ○ before and ▲ after e^- irradiation.

slow e^+ yield (<30%). Similarly biasing the filament to -50V while heating had no effect. With the filament held at -100V, however such heating (again for 20 seconds) raised the slow e^+ beam intensity to $790\pm100s^{-1}$. Having allowed the enhanced yield to fall to $450\pm100s^{-1}$ a repeated heating of the filament (at -100V) partially regained the flux to give $630\pm100s^{-1}$.

4.4.3 Preliminary retarding spectra

The installation of a grid, as shown in figure 4.4, enabled retardation of e^+s and β^+ induced secondary e^-s to be performed. Such measurements were expected to be sensitive to charging of the moderator surface if this was of the order of a few volts potential. An argon moderator was deposited at a pressure of $5*10^{-4}$Torr for 20 minutes after which the absolute slow e^+ yield was measured to be $170\pm100s^{-1}$ and the secondary e^- count rate to be about $43{,}000s^{-1}$. A retarding spectrum taken, using only the ceratron detector, showed a broadly distributed slow componenet (figure 4.6 .) which extended to high 'negative' energy. This was indicative of poor optics within the cup source which necessitated the application of high voltages to the accelerating grid in order for extraction of some components of the slow beam (see figure 3.6).

The secondary e^- energy distribution was not as broad, but also had a significant component which required a high extraction voltage (see figure 4.7). An oxygen overlayer was

deposited at a pressure of 10^{-7}Torr for 5 minutes and both yield measurements and retarding spectra were again obtained. The absolute slow e^+ yield was measured five times giving an average value of $130\pm40s^{-1}$. This was consistent with the uncoated yield, as was the retarding spectrum shown in figure 4.6 which showed no significant change. The β^+ induced secondary e^- yield had risen slightly to around $45,000s^{-1}$ and the retarding spectrum, shown in figure 4.7 , appeared to have shifted by a small degree to higher extraction voltages.

With the filament biased at -100V heating was provided by an a.c. supply at 230V for 20 seconds. The slow e^+ yield subsequently rose to $270\pm80s^{-1}$ whereas the β^+ induced secondary e^- count rate fell to about $23,000s^{-1}$. Both e^+ and secondary e^- energy distributions, seen in the retarding spectra of figures 4.6 and 4.7 respectively, appeared to have broadened with the increased slow e^+ component apparently consisting of particles requiring large extraction voltages. No clear shift in cut-off energy was observed for either the e^+s or e^-s and little accuracy was possible owing to the poor energy resolution of these measurements.

A second solid argon moderator was constructed at a pressure of $5*10^{-4}$Torr for 25 minutes and exposed to oxygen for 2 minutes at 10^{-7}Torr. The slow e^+ yield was measured to be $175\pm50s^{-1}$, corresponding to a moderation efficiency of $0.12\pm0.03\%$ whilst the secondary e^- count rate was recorded as $38,000s^{-1}$. Retarding spectra were taken for both e^+s and e^-s and again the e^+ distribution was broader than that of the e^-s with both being poorly resolved. The tungsten filament was heated by applying 240V for 30 seconds at a bias of -137V. The slow e^+ yield then rose to $780\pm100s^{-1}$, at a moderation efficiency of $0.52\pm0.07\%$, while the secondary e^- count rate fell to $19,000s^{-1}$. Figures 4.8 and 4.9 show respectively the e^+ and e^- retarding spectra both before and after filament heating. The same features observed previously appear, specifically energy broadening of both e^+ and e^- distributions with the additional slow e^+ component occuring only under high extraction voltages. The two values of e^+ count rate shown at a retarding voltage of -100V in figure 4.8 represent measurements taken before and after those taken at other voltages in the spectrum. This was done in order that any drift in yield over this time might be quantified. The small difference observed was indicative, as described earlier, of the decrease in magnitude of the enhancement effect with time. Forty minutes after the filament had been heated the slow e^+ yield was measured to be $260\pm60s^{-1}$. This was a significantly more rapid decay than that observed for an 'enhanced' air coated argon moderator since the enhancement had fallen to half its value in only 20 minutes.

As with the previous moderator no convincing shifts in the retarding spectra was observed.

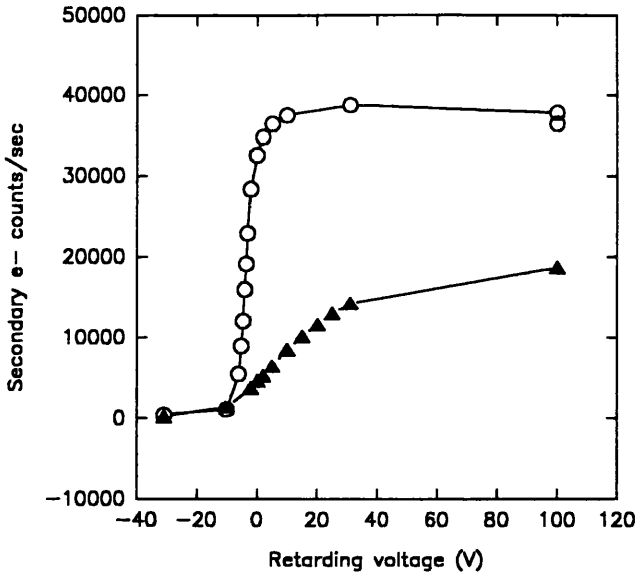

Figure 4.9 β^+ induced secondary e^- retarding spectra taken O before and ▲ after e^- irradiation.

Contributing factors, other than the optics within the cup source, could have been the effect of either non-uniform argon/oxygen deposition, non-uniform e^- exposure (charging current) or more probably both. In this situation the moderator surface potential would vary in magnitude within the cup thus causing broadening rather than a discrete shift in the retarding spectra. Such complex electrostatic fields would also probably hinder extraction of both e^+s and e^-s.

A krypton moderator was deposited at a pressure of $5*10^{-4}$Torr for 20 minutes. The slow e^+ yield was measured to be $280\pm70s^{-1}$ and the secondary e^- count rate was recorded as $49{,}000s^{-1}$. Retarding spectra taken of e^+s and secondary e^-s are shown in figures 4.10 and 4.11 respectively. Approximately 30 minutes after moderator deposition the secondary e^- yield had risen slightly (13%) to $56{,}000s^{-1}$. This was not considered of great significance and thought to be due to variation in ceratron detection efficiency or possibly some moderator surface contamination. This moderator was exposed to $7*10^{-7}$Torr of oxygen for 5 minutes after which the slow e^+ yield was determined as $370\pm50s^{-1}$. Note that the e^+ count rate at the ceratron had not significantly altered (<3%) as a result of oxygen exposure. A e^+ retarding spectrum taken at this time and shown in figure 4.10 also showed no significant change.

When the beam voltages were reversed in order to detect secondary e^-s the count rate at the ceratron was lower than expected at $28{,}000s^{-1}$ and appeared unstable. The secondary e^- yield was observed to be steadily rising and figure 4.12 shows the detected beam intensity as a

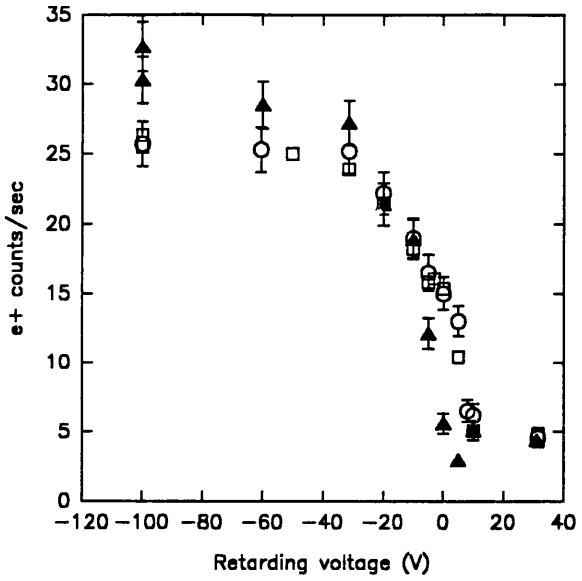

Figure 4.10 e^+ retarding spectra from ○ Kr, □ Kr+O and ▲ $Kr+O_2$ after e^- irradiation.

function of time. This variation was too rapid to be explained by surface contamination and since the positron count rate was not similarly affected by this phenomena it did not seem indicative of variation in the efficiency of the ceratron or beam transport. The intensity seemed to be stabilising with time and after about 160 seconds reaching a value of $37{,}000s^{-1}$ which was significantly (37%) higher than that initially recorded. At this time a retarding spectrum could be taken with little variation in peak secondary e^- yield. Figure 4.11 shows such a retarding spectrum which indicated that the fall in secondary e^- yield was due to loss within the high energy (>5eV) component of the beam. Resolution was poor and as described previously the optics in this arrangement gave some ambiguity to retarding measurements in terms of emission angle and energy.

A possible explaination for these observations is that while running the e^+ beam β^+ induced secondary e^-s liberated from the moderator (or nearby surfaces) would necessarily be returned to the RGS surface after emission and could act in a similar manner to the e^-s applied using the tungsten filament. The observed gradual increase in secondary e^- yield would be caused in this case by the decay of this surface charge with the removal of negative particles emitted by the moderator while e^-s were transported. Although the charging produced may have been too small to be observed as an enhancement in the slow e^+ yield it could possibly have caused reduction in low energy secondary e^- emission by inhibiting their transport to the exit surface.

With the filament biased at -137V heating was carried out for 50 seconds using an applied

voltage of 240V. The slow e^- count rate rose by about 50% with the absolute intensity measured as $500\pm90s^{-1}$ whilst the secondary e^- count rate fell to $11{,}000s^{-1}$. As before, following such treatment, the secondary e^- retarding spectrum (figure 4.11) was broadened to higher extraction voltages. The slow e^+ retarding spectrum (figure 4.10) showed a significant shift in cut-off energy, despite some similar broadening. The shift was approximately 10eV in magnitude and thus indicated an effective negative surface potential of -10V. More accurate determination of this shift would involve making assumptions about the intrinsic enhanced e^+ energy/angular emission profile which might easily have altered. Note that any such alteration could not account for the observed shift in the retarding spectrum.

The reason for the clear shift observed using this oxygen coated krypton moderator, where none had been seen using argon, was not entirely understood. Factors such as the moderator thickness, oxygen layer depth and charging distribution could have had effect. Note that this moderator showed only a small degree of slow e^+ enhancement, when compared to that of previous air coated Kr samples.

Table 4.3 summarises the e^+/secondary e^- yield measurements obtained for the oxygen coated Kr and Ar samples studied in this sub-section. These results may be compared to those previously obtained for air and SF_6 coated RGS (table 4.2).

4.4.4 Precision retarding spectra

The major factor limiting the accuracy of the surface charge measurements performed using the previous experimental arrangement was the poor resolution obtained from retarding spectra taken using the cup source geometry. These last three sub-sections describe results obtained

Table 4.3 Positron and secondary e^- yields from (clean) RGS moderators and following O_2 coating and surface activation.

RGS	Depth 10^{-4}Tmin	e^+ yield s^{-1}	e^- yield s^{-1}	over-layer	Depth 10^{-7}Tmin	$e^+ s^{-1}$ Before	$\varepsilon_f e^+$ % Before	$e^- s^{-1}$ Before	$e^+ s^{-1}$ After	$\varepsilon_f e^+$ % After	$e^- s^{-1}$ After
Ar	100±10	170±100	43000	O_2	5±1	130±40	0.09±0.03	45000	270±80	0.18±0.05	23000
Ar	125±10			O_2	2±1	175±50	0.12±0.03	38000	780±100	0.52±0.07	19000
Kr	100±10	280±70	56000	O_2	4±1	370±50	0.25±0.03	37000	500±90	0.33±0.06	11000

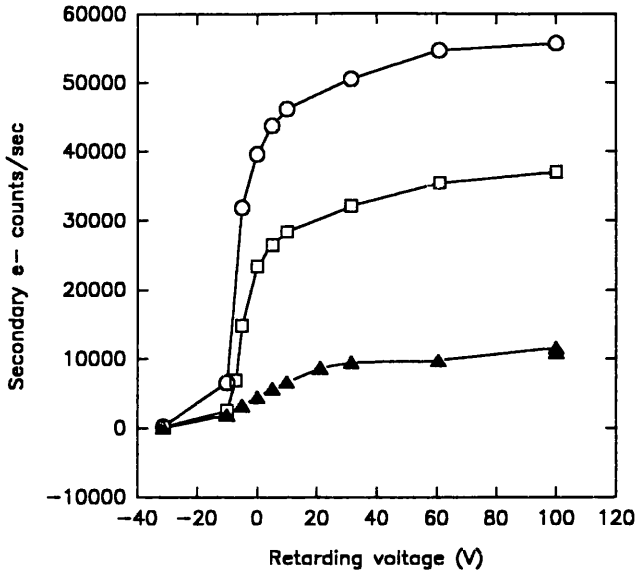

Figure 4.11 β^+ induced secondary e^- retarding spectra from ○ Kr, □ $Kr+O_2$ and ▲ $Kr+O_2$ after e^- irradiation.

using a flat source, see figure 3.4. This first sub-section describes the measurements performed using a krypton moderator which was initially constructed in order to test the optics of the new arrangement. Kr was chosen since it generally gave greater beam intensity when compared with Ar.

The Kr was deposited for 18 minutes at a pressure of $5*10^{-4}$Torr after which a slow e^+ beam intensity of $100\pm50s^{-1}$ was recorded, this corresponded to a count rate at the ceratron of $13.6\pm0.7s^{-1}$. Note that the ion gauge had been moved and the geometry had been altered thus preventing comparison of pressure/time measurements to those taken previously. The beam intensity was lower than previous quoted values partly as a result of the reduced efficiency of the flat geometry compared to the cup, but probably also because optimal Kr film thickness had not been achieved. The Ceratron detection efficiency had fallen from its earlier value presumably, as was discussed in section 3.4.2, as a result of contamination. Note that this does not affect the absolute determination of slow e^+ yield using the coincidence system or the relative intensity measurements taken during the acquisition of e^+/e^- retarding spectra.

A retarding spectrum was taken of the emitted e^+s and is shown in figure 4.13a. From this the median energy of the slow component could be determined, this is equal to the voltage (V_e) at which the slow yield falls to half its maximum value ($Y_{1/2}$). The measured maximum (Y_{max}) and minimum (Y_{min}) e^+ yield values relate to $Y_{1/2}$ simply;

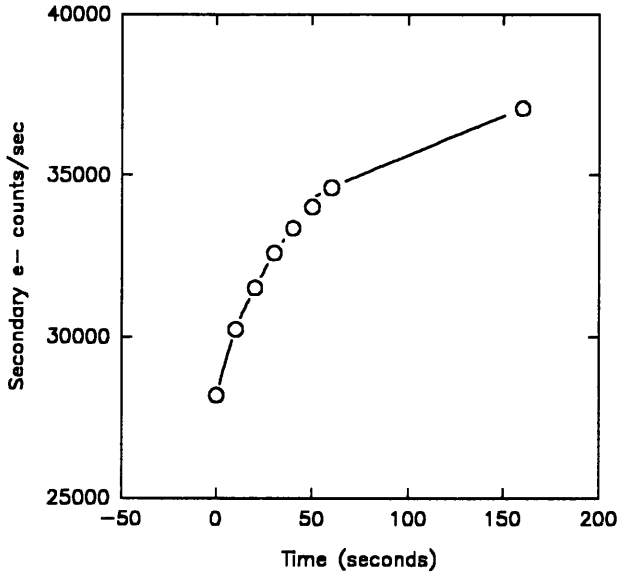

Figure 4.12 β^+ induced secondary e^- yield from a Kr moderator as a function of time.

$$Y_{1/2} = Y_{min} + (Y_{max} - Y_{min})/2 \qquad 4.2$$

This value of $Y_{1/2}$ will invariably lie between two measured yield values, say Y_{v1} and Y_{v2}, taken at two different retarding voltages V_1 and V_2 respectively. The gradient of the retarding spectrum, (dy/dv), between these two values may be calculated;

$$dy/dv = (Y_{v2} - Y_{v1})/(v_2 - v_1) \qquad 4.3$$

The reciprocal of this gradient can then be used in order to extrapolate a value for the median slow e^+ energy as

$$v_e = (Y_{1/2} - Y_1)/(dy/dv) \qquad 4.4$$

The error on this value can be obtained by summing the statistical uncertainties of the measured quantities of $Y_{1/2}$, Y_{min} and Y_{max} which will impose upper and lower bounds on V_e within one standard deviation. A value for the median slow e^+ energy of 1.6±0.6eV was thus derived for this krypton moderator.

The secondary e^- yield was taken about 30 minutes after deposition of the moderator, with the base pressure at $5*10^{-9}$Torr, it was unstable initially (as noted previously), increasing after

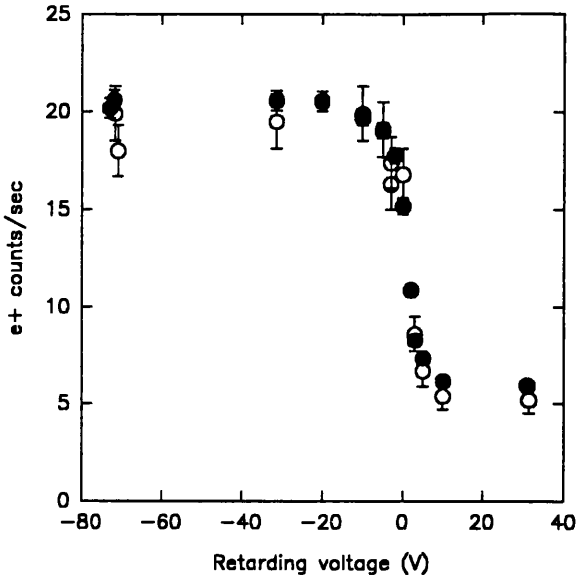

Figure 4.13 e^+ retarding spectra taken ○ before and ● after O_2 exposure of a Kr film.

a few minutes from approximately $2000s^{-1}$ to a value of $47,000s^{-1}$ at which time the retarding spectrum shown in figure 4.14 was taken. The median secondary e^- energy obtained, as above, from this spectrum was 0.18±0.07eV.

An oxygen overlayer, deposited at a pressure of $2*10^{-7}$Torr for 5 minutes, was constructed following which the slow e^+ count rate was unaltered at $13.9\pm0.3s^{-1}$. Figure 4.13 shows also that the e^+ retarding spectrum had not significantly changed and the median slow e^+ energy was determined to be 1.0(0.3)eV. The secondary e^- count rate had fallen to $24,000s^{-1}$, although as seen in figure 4.14 the shape of the retarding spectrum had not altered and the median energy was consistent with that determined before oxygen deposition at a value of 0.23±0.02eV. No significant ($<1000s^{-1}$) drift in the secondary e^- count rate was observed. It was concluded that the reduction in secondary e^- yield after oxygen exposure was not as a result of a charging effect but more likely to be a consequence of direct interaction between the escaping e^-s and the molecular overlayer, possibly involving a trapping or energy loss mechanism preventing escape.

If, as proposed, the instability previously observed in the secondary e^- yield was caused by negative charging of the RGS surface then, from e^+ retarding spectra taken at the time, it would seem to have been due to a negative potential of less than 0.3 Volts. This would indicate a very strong dependence of secondary e^- yield on surface potential. The possibility of bulk charging of the RGS moderator causing or contributing to this effect was considered.

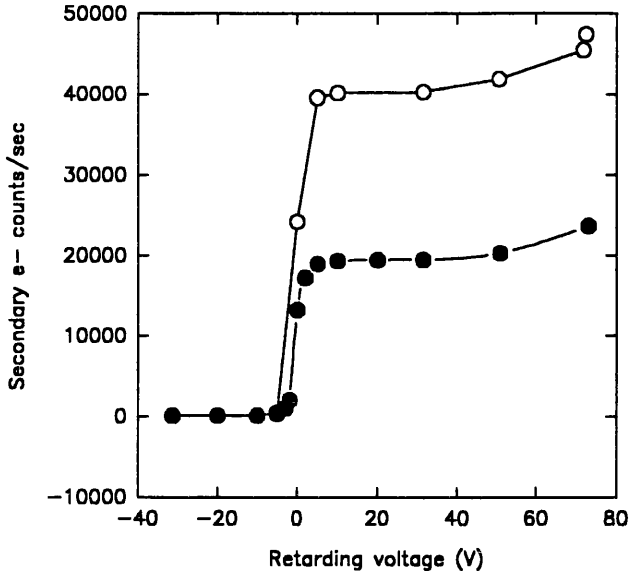

Figure 4.14 β^+ induced secondary e^- retarding spectra taken ○ before and ● after O_2 coverage of a Kr film.

Impurities within the solid could concievably trap significant amounts of charge and such a process would be expected to halve (see section 4.2) the observed surface potential for a given number of trapped charges. It is not entirely clear, however, how this could explain the notable lack of observed emission energy shift and significant yield reduction.

Figures 4.15 and 4.16 show energy spectra for emitted e^+s and secondary e^-s obtained by performing crude differentiation of the retarding spectra taken after oxygen exposure. This differentiation consisted of evaluating equation 4.3 between successive retarding voltages, the error being the uncertainty on the yield values. The resolution has contributions from the intrinsic variation in forward emission energy and also the resolution of the apparatus (ie the variation in transport efficiency with angle and energy). Values for the FWHM energy of transmitted e^+s from a ^{22}Na Ar moderator (Gullikson and Mills 1986) and X-ray induced secondary e^- from Ar (Gullikson and Henke 1989) are 1.8eV and 1.5eV respectively. The e^+ and β^+ induced secondary e^- energy FWHM in this study, taken from figures 4.15 and 4.16, were 5±1eV and 3±1eV respectively. If the preliminary observation of a surface potential of magnitude 10V is correct, then this experimental arrangement should be sufficiently sensitive in order to study the surface charging associated with these enhancement phenomena.

4.4.5 Precision charging measurements under controlled conditions

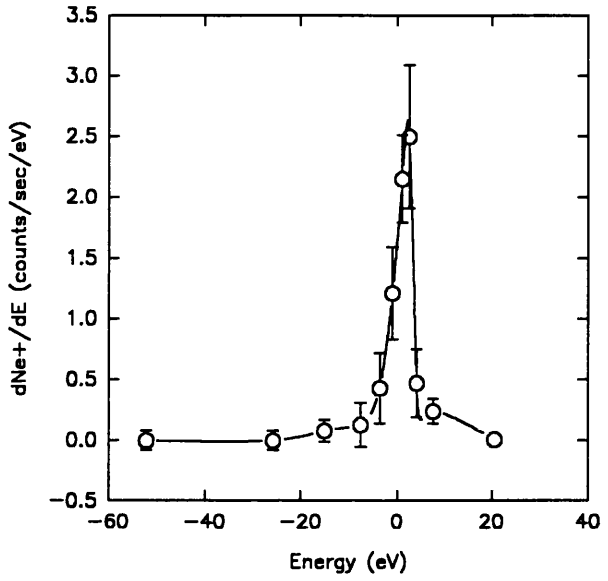

Figure 4.15 e^+ energy spectra emitted from a Kr film derived from a retarding spectrum.

The construction of a solid argon moderator was performed in two stages, the first being the admission of gas at a pressure of 10^{-4}Torr for 5 minutes and the second at the same pressure for 10 minutes. After the first deposition the slow e^+ count rate was measured at the ceratron to be $8.2\pm0.6s^{-1}$ and after the second layer this rose to $12.2\pm0.5s^{-1}$. Determination of the absolute slow e^+ yield was inaccurate owing to the low beam intensity, this gave poor statistical accuracy when counting using the NaI detector. After the second deposition the absolute slow e^+ beam intensity was $90\pm190s^{-1}$.

Assuming the solid argon moderation efficiency curve predicted in section 3.1 (figure 3.1) to be correct and also that the moderator depth is proportional to pressure and time of deposition. Fitting of the two slow e^+ yield measurements to this function could be used to obtain a value for the thickness of the solid argon moderator after the second deposition, this value was $2.4\pm0.5\mu m$. Oxygen was deposited over this argon layer at a pressure of $1.7*10^{-7}$Torr for 2 minutes. This may be compared to the pressure and time for the solid argon layer deposition and assuming a sticking coefficient identical to that of argon atoms an O_2 layer of thickness 5.5 ± 2.6Å would be expected to have been produced. The inaccuracy of this estimate was difficult to ascertain given the number of assumptions made in order to obtain it. The error quoted was taken purely on the grounds of the inaccuracy in determining the argon thickness (curve fitting) and the relative pressure and time for deposition of the O_2 and Ar layers. Taking an approximate value for the O_2 molecular bond length of 1.3Å the depth

of the overlayer given above would correspond to 2±1 monolayers of coverage.

The slow e^+ count rate appeared to fall slightly to $10.7\pm0.7s^{-1}$ after oxygen coverage. Figure 4.17 shows a e^+ retarding spectrum taken at this time from which the median slow e^+ energy was determined to be 1.0±0.5eV. Measurement of the secondary e^- yield showed a low initial value of $2900s^{-1}$. Subsequent recordings showed a similar behaviour to that observed previously with a gradual increase up to an effectively stable value, in this case of $14{,}000s^{-1}$. Figure 4.19 shows the variation of secondary e^- count rate over time. Unlike a similar variation observed using an oxygen coated krypton moderator and the cup source (figure 4.12) this variation appeared to be linear. A retarding spectrum was taken of the secondary e^-s emitted by the moderator after this yield had been left to stabilise and this is shown in figure 4.18. The median slow secondary e^- energy was determined to be 0.50±0.05eV. The error quoted here was mostly caused by some small residual drift in secondary e^- count rate observed while taking the measurements.

Heating of the filament was carried out for 15 seconds by applying a voltage of 240V a.c. during which time it was biased at -100V. Following this treatment the slow e^+ count rate, at the ceratron, rose to $28.3\pm1.0s^{-1}$ which is a factor of 2.6±0.2 higher than before. The absolute slow e^+ yield was found to be $420\pm120s^{-1}$. Figure 4.17 shows a e^+ retarding spectrum taken at this time which shows, in addition to the enhanced yield, that a clear shift in the energy of the slow component had occured. A large negative extraction field was now required in order to transport the e^+ beam away from the RGS surface. The median slow e^+ energy was determined to be -18.4±1.0eV, this value was consistent with an effective surface potential of -19.4±1.5 Volts taking the previous determination of the uncharged median slow e^+ energy.

The secondary e^- yield had fallen to $3700s^{-1}$, as measured about 15 minutes after filament heating, a retarding spectrum was taken which is shown in figure 4.18 and as with the e^+ retarding spectrum a significant shift was observed. The median slow secondary e^- energy was determined to be 12.5±0.9eV, this was consistent with an effective surface potential of -12.0±1.00Volts. This value is less than would have been expected at the time of acquisition from the results of e^+ retarding spectra taken before and after this measurement. This will be discussed later in this section. It should be noted that in order to obtain the values quoted here for the surface potential it was necessary to assume that the intrinsic energy distribution of the emitted electrons (and positrons) remained the same after charging, despite the gross

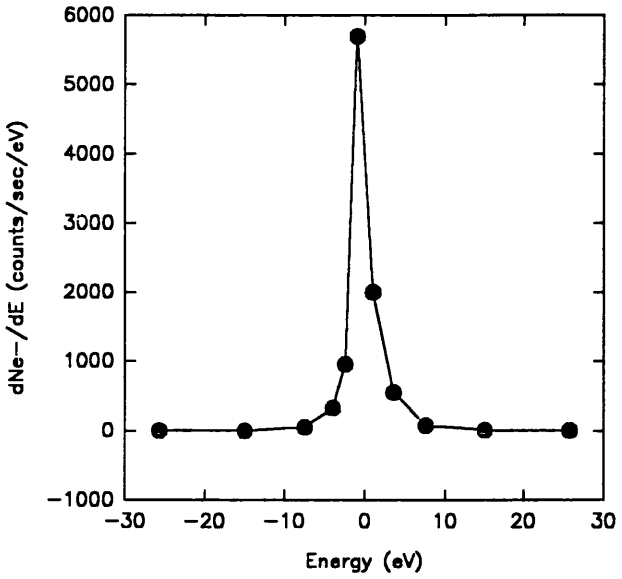

Figure 4.16 β^+ induced secondary e^- energy spectra emitted from a Kr film derived from retarding spectra.

reduction (enhancement) in intensity. Positron retarding spectra were taken regularly for about three hours following heating of the filament during which time both the slow e^+ enhancment and the effective surface potential (shift in median slow e^+ energy) were observed to decay. Figure 4.20 shows the variation of median slow e^+ energy with time, the decay appears to be of exponential form.

In the description of the dynamics involved in this slow e^+ enhancement effect probably the most significant set of results which were obtained from this data are displayed in figure 4.21 which shows the variation of slow e^+ yield as a function of median slow e^+ energy. This should reflect the dependence of moderation efficiency on the effective surface potential and as can be seen this is not consistent with a linear relationship since the slow e^+ enhancement apparently saturates for a surface potential greater than about -13V. Treating the dielectric film as a charged capacitor allows equation 4.2 (section 4.1) to be applied. Taking the value for the film thickness determined above this equation indicates an electric field strength of 5.4±0.9kV/mm within the RGS moderator at the saturation potential.

Two additional secondary e^- retarding spectra (and yield measurments) were also taken during this three hour period (see figure 4.22). The median slow component energies were consistent with surface potentials of -5.3±0.5V and -2.7±0.8V and the respective beam intensities were 2895±35s^{-1} and 2966±40s^{-1}. The errors here reflect some small variation in count rate during data aquisition. These values are significantly (>700s^{-1}) smaller than the

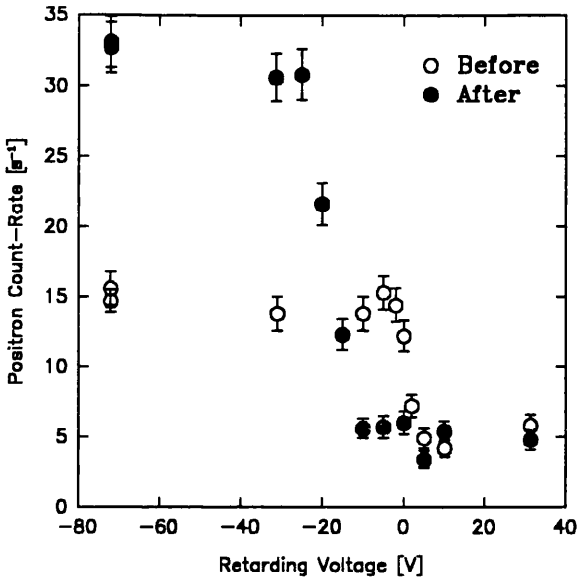

Figure 4.17 e^+ retarding spectrum taken before and after low enrgy e^- bombardment of an Ar/O_2 moderator film

count rate quoted previously which had been taken at an earlier stage. Work previously performed on molecular (and ionic) desorption from RGS surfaces could provide an explanation for this observation (see section 4.1).

Given that electron bombardment of an oxygen coated solid argon surface can cause the liberation of negative ions (O^- and O_2^-) it would be reasonable to assume that desorption of such ions could also occur as a result of β^+ implantation since considerable numbers of high energy particles (including β^+ induced secondary e^-s) subsequently pass through the exit surface and might easily detach the weakly bound anions. Negative ions emitted by the moderator could undoubtedly be transported and detected (at the ceratron) in a similar manner to slow secondary e^-s. If the exponential decay of the surface potential measured previously (figure 4.15) is correct then the majority of this ion emission would occur soon after surface activation thus giving, as observed, an enhanced initial secondary e^- count rate. This explaination is consistent with that given for the drift in secondary e^- yield in which the moderator may surface charge itself by the return of secondary e^-s during slow e^+ transport, but 'desorbs' this charge when secondary e^-s/negative ions are transported. This may also be the reason for the low effective surface potential determined from secondary e^- as opposed to e^+ energy spectra.

Following this set of measurments an experiment was performed in order to determine the current being passed to the moderator during the process of filament activation (electron

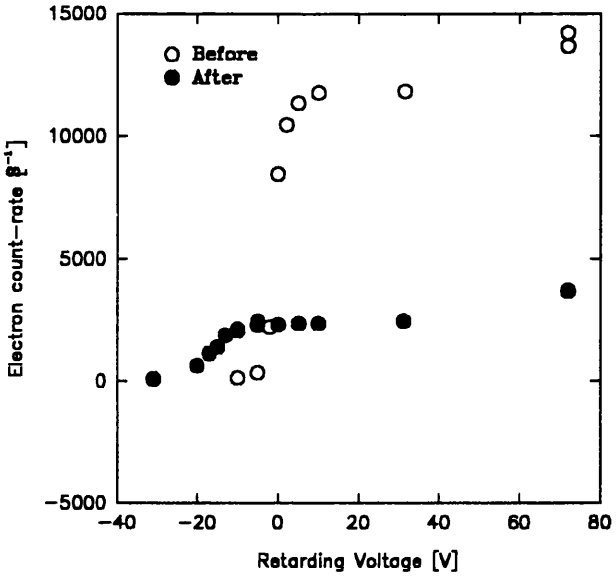

Figure 4.18 β^+ induced secondary e^- spectra taken before and after low energy e^- bombardment of an Ar/O_2 moderator

emission). The source was electrically isolated from the cold head and connected through a pico-ammeter to a biasing voltage supply. Using this arrangement (figure 4.4) the flow of negative charge (assumed to be electrons) was monitored as a function of source retarding voltage. These measurments, shown in figure 4.23, indicated that over 90% of the secondary e⁻s hitting the moderator surface possessed energies between 0 and 10eV and 97% were below 15eV. The electron surface trapping cross section for condensed oxygen (on a krypton film, see figure 4.3) has two maxima within the 0-10eV energy region which result in the production of O^- and O_2^- surface ionic states. The cross section for these channels falls off at higher energies. Since the oxygen overlayer interacts very little with the RGS substrate the same behaviour would be predicted for an argon film as for krypton. The processes responsible for the ion production would be expected to also be the same, namely resonant O_2^- stabilisation (0-2eV) and dissociative attachment resulting in the production of O^- (4-10eV). Many complicating factors preclude the use of these energy dependent cross sections in order to quantitatively relate the measurments made of the current striking the source to the moderator surface charging. One such factor is that the charging of the surface will affect the electron impact energy since incident e⁻s must overcome the surface potential. Accumulation of a -10V surface potential would produce a -10eV offset in the incident e^- energy spectrum (figure 4.17). Another problem is that of assessing the area of RGS over which this negative current is flowing. From a geometrical argument one would expect a non-uniform charging

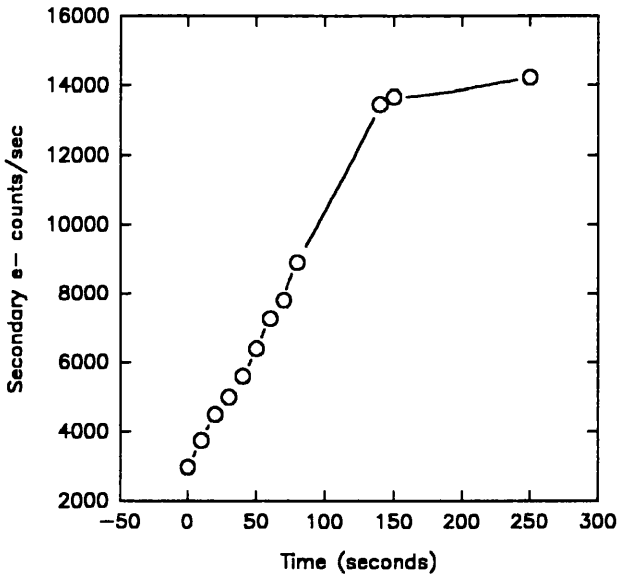

Figure 4.19 β^+ induced secondary e^- yield from an $Ar+O_2$ moderator film as a function of time.

distribution which would not have been observed in the retarding spectra measurments due to the small area of the ^{22}Na deposit.

4.4.6 Conventionally applied electric field

An attempt was made to apply an extraction field to a RGS moderator more directly using, as shown in figure 4.4, a biased grid mounted over the source. A krypton moderator was deposited at a pressure of 10^{-4}Torr for 10 minutes which resulted in a slow e^+ yield of $670\pm80s^{-1}$ corresponding to a moderation efficiency of $0.33\pm0.04\%$.

In the initial investigation the grid was held at -1.7kV whilst the absolute slow e^+ yield was measured. The grid would subsequently be grounded and the 'zero-field' slow e^+ yield measured. This process was repeated four times to obtain good statistics. No significant enhancment in the e^+ beam intensity was observed.

It was not possible to exceed this grid extraction voltage and still meaningfully operate the ceratron detector. This was due to secondary e^-s emitted from the grid being accelerated sufficiently such that they were able to strike the negatively biased (-2kV) ceratron cone and thus cause spurious counts. The NaI detector was unaffected by this process and was henceforth used alone in order to monitor the slow e^+ beam intensity. The grid was biased alternately at 0 and -3.5kV and averaged over four data sets which gave count rates of

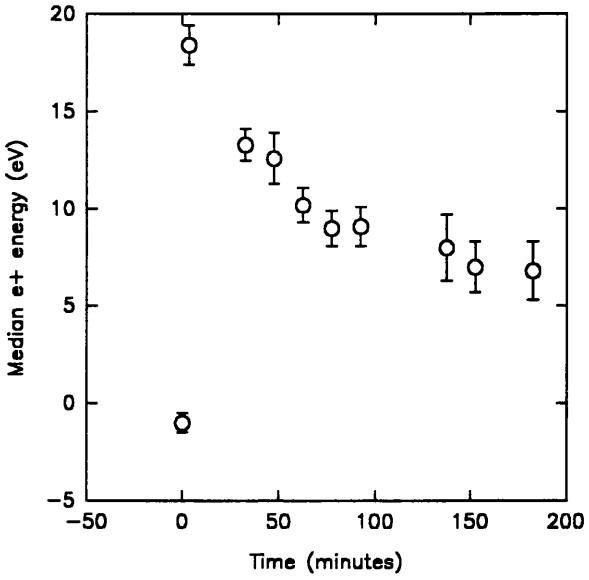

Figure 4.20 Surface charge (e^+ energy shift) as a function of time of an e^- irradiated $Ar+O_2$ moderator film.

$10.6\pm2.8s^{-1}$ and $9.2\pm2.8s^{-1}$ respectively. Again no enhancement was observed with the applied field strength in this case being 2.1kV/mm.

These results were consistent with the results obtained by surface charging since an applied field strength of 2.1kV/mm would be expected, by extrapolating from figure 4.21, to show only an enhancment of 23±16%. Unfortunately it was not possible, using the experimental arrangement described, to apply a higher field intensity than this since it resulted in electrical breakdown.

4.5 **Discussion**

Having deduced the conditions under which this slow e^+ enhancement effect occured, ie a RGS moderator with an overlayer of negative ions, the actual processes involved were considered. It can be argued that the e^+s could either be affected whilst diffusing in the bulk or once they have arrived at the exit surface. If the observed enhancement resulted from a process occuring at the surface then it would be reasonable to assume that this was due to modification of the e^+ work function which is currently quoted for argon as +1.7±0.1eV (Mills and Gullikson 1986). Modification of the work function could result from alteration of the surface electronic structure by bonding of the ions. Conversely if the role of the bulk was of more importance then it would presumably be as a result of the presence of negative surface

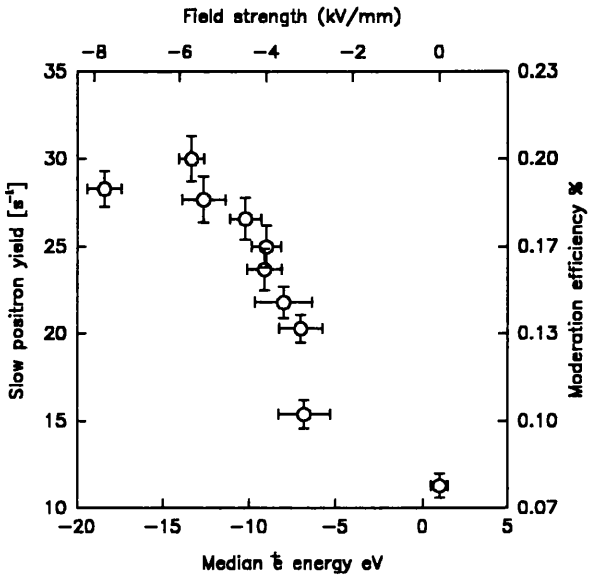

Figure 4.21 Slow e^+ yield as a function of surface charge (and estimated field strength) from an e^- irradiated $Ar+O_2$ film .

charge inducing field assisted extraction.

Several arguments suggest that it is not a surface process. Firstly taking the approximate values of surface potential (-10V) obtained from the emitted e^+ and e^- retarding spectra one can determine the surface charge density and hence the concentration of negative ions which would be required in order to produce such charging (equation 4.1). Carrying out such a calculation a surface concentration of order 1 part in 10^4 is obtained. It does not seem feasible that a concentration of this magnitude could affect the gross emitting properties of the surface to such an extent as to explain the observations outlined in this chapter.

Secondly the diffusion equation solved previously (section 3.1) assumed a perfectly emitting exit surface (ie all of the e^+s reaching the surface were emitted). The approximate agreement with the moderation efficiencies obtained in this investigation suggest that a minor fraction of the e^+s are lost at the surface due to the presence of a positive work function. Assuming this calculation to be valid a minor enhancement could thus be possible by a change in the surface emission properties.

A previous investigation by Simpson (1990) on the possibility of field assisted moderation using RGS involved a Monte Carlo simulation in which essentially the diffusion equation of 4.1 was solved while applying an electric field. This application was performed by adding a time-dependent drift velocity to the random motion of the diffusing e^+s. This drift velocity increased the probability of the e^+s reaching the front exit surface (see section 1.4.2). In this

rather simplified calculation the assumption was made that a e^+ which acquires sufficient energy, from the applied electric field, to excede the positronium threshold (E_{th}) will form stable Ps. No further consideration of this e^+ was subsequently made in the calculation and the particle then contributed to the Ps fraction. This was a crude application of the Ore model for Ps formation within solids.

The results of this calculation predicted that little enhancement would be produced by the application of an electric field to an Ar moderator with the maximum yield occuring at 10kV/mm and giving only a 35% increase in efficiency. For greater field strengths 'heating' of the slow e^+ energy distribution into the Ore gap would rapidly reduce the emitted yield as a result of loss to Ps production. The Ps fraction would rise from a zero field value (measured) of 10% to roughly 80% at 100kV/mm. Both the lack of enhancement in slow e^+ emission and the large increase in Ps formation stem from the assumption that e^+s being accelerated above E_{th} necessarily form Ps. Such an assumption may not reasonably be justified based on the rather small amount of quantitative knowledge (theory or experiment) which is available concerning Ps formation in RGS (section 1.3.5). In fact experiments performed investigating the effect of applied electric fields on Ps production in plastic (Bisi et al 1981) and some gases (eg Charlton and Curry 1985) have observed an initial substantial decrease in Ps formation indicating possibly that a mixture of both Ore and Spur type Ps formation processes occur in insulators and that only at high electric fields does heating into the Ore gap become a dominant effect.

Another factor which could be of importance when considering e^+ dynamics in the presence of an electric field are impurities in the bulk of the RGS. Although the concentration was undoubtedly low in these experiments (10^{-4}-10^{-5}) the long e^+ diffusion lengths in these solids would make interaction more likely. A molecular impurity can allow efficient energy loss (compared to phonon scattering) by the diffusing epithermal e^+s since such impurities have open inelastic channels at energies inside the RGS band gap (below E_{th}). Impurities could therefore act to cool the diffusing hot e^+s and could possibly compete with the heating into the Ore gap induced by the applied electric field and thus reduce e^+ loss due to Ps formation.

It is clear (section 1.4.2) that in principle field assisted moderation enhancement could be of sufficient magnitude to explain the results observed in this study. This would be the case if bulk Ps formation were ignored as a source for loss of free e^+s. To perform a realisitic calculation of the field dependence of a RGS moderator, which could be compared with that

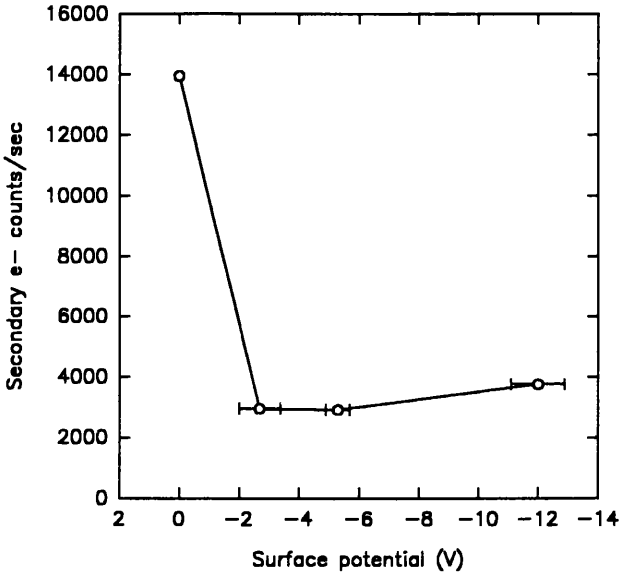

Figure 4.22 β^+ induced secondary e^- yield as a function of surface charge from an $Ar+O_2$ film.

obtained experimentally in this work, it seems clear that a more sophisticated consideration of Ps formation is required than that given in the Monte Carlo simulation performed by Simpson (1990). This might require further experimental as well as theoretical work in this field.

It should be noted that field assisted extraction could also be of sufficient magnitude to explain the secondary e^- yield phenomena presented in this chapter. The estimated magnitude of the electric field required to produce both e^+ and secondary e^- effects observed, about 5kV/mm, is in approximate (order of magnitude) agreement with those expected from solution of the e^+ diffusion equation or consideration of the e^- drift velocity (Spear and LeCombe 1977).

The secondary e^- yield from the moderator was observed to significantly reduce after operating the e^+ beam transport and recovered over a few minutes of transporting e^-s (or negative particles). A proposed explaination for this behaviour was surface trapping of secondary e^-s emitted by the moderator. Slow e^+ retarding spectra measurements indicated a negative surface potential of less than 0.3 Volts caused a reduction of greater than a factor of four in the secondary e^- yield. Even given the low median emission energy (0.5eV) of the secondary e^-s this is a small value of surface potential to produce such a marked effect and corresponds to an electric field strength of less than 0.2kV/mm.

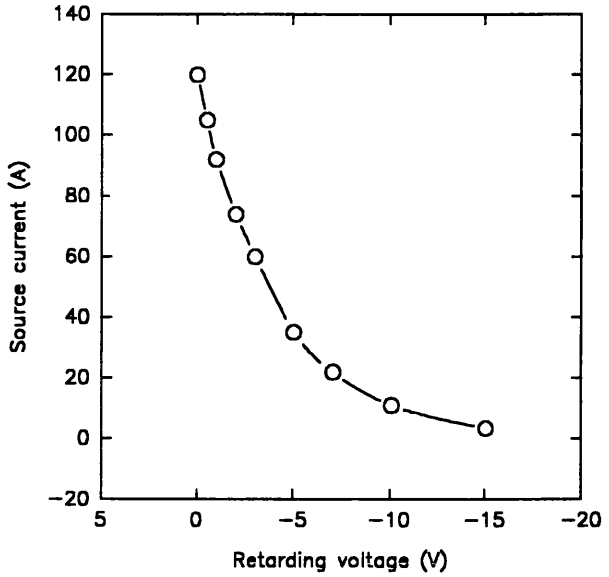

Figure 4.23 Current (e^-s) striking the source mount during filament activation as a function of retarding voltage.

4.6 **Conclusion**

Surface charging of Ar and Kr RGS moderators has been performed by low energy e^- capture at adsorbed impurity sites (eg O_2). An enhancement in the slow e^+ yield of typically a factor of three was observed and a corresponding, usually five fold, reduction in secondary e^- emission. These effects have been interpreted as the field induced drift of diffusing e^+s to (and e^-s from) the exit surface. The field strength within the dielectric RGS film was estimated at approximately 5kV/mm at saturation. The observation of a four fold enhancement in secondary e^- yield and practically total reduction in slow e^+s under positive ion bombardement supports this argument. Secondary e^-s would be drifted towards, and e^+s from, a positively charged exit surface.

The results from this investigation indicate a promising future for research related to surface charging and field assisted e^+ extraction involving the RGS. Several research projects suggest themselves, following naturally from the work presented in this report. Most importantly for e^+ physics would probably be an investigation into slow e^+ (beam) reemission from RGS under the influence of electric extraction. The field could be applied either by surface charging, as demonstrated in this work, or by more conventional methods. Such work would undoubtedly reveal much about e^+ dynamics in these types of insulating materials, including the formation of Ps.

There is scope for much further development of this e^+ moderation enhancment technique which could provide significant improvments on existing technology. The larger e^+ diffusion length and higher E_{th} of solid neon should make field assisted extraction using this material more effective than that observed for argon or krypton. Even if only the roughly factor of three enhancment observed in this study could be recreated using a solid neon moderator then an efficiency of almost 5% would be produced. Such a moderator design could be constructed by applying the electric field using a metal grid. This would hopefully give a controllable and stable system though fabrication could be difficult. It may however also be possible to produce a stable moderator using a surface charge trapping technique whereby adsorbed molecules, lost by stimulated desorption, could be replaced by low ($<10^{-8}$Torr) pressure injection of that impurity (eg oxygen). The charging e^- current could either be supplied along the beam line (from an electron gun) during e^+ transport or, if a sufficiently large radioactive source was used, it may produce sufficient β^+ induced secondary e^-s at the surface in order to charge itself. Field assisted e^+ extraction, despite the wide emission energies from the RGS, could also prove useful in remoderation.

CHAPTER 5

CONCLUSION

The work presented in this thesis has focused on the development of methods to improve upon the quality of current e^+ beam technology. This has included the production of a new method of time resolving a beam using single particle tagging. Also a detailed study of the β^+ moderating properties of the RGS was performed using different source geometries and both electrostatic and magnetic beam transport. Following this work, field assisted e^+ extraction from a moderator was observed for the first time using the RGS and significant enhancements in moderation efficiency were found. This development utilised a novel technique that involved charging of the insulator surface through e^- capture by adsorbed impurities.

The new timing technique tagged the e^+s by detecting secondary e^-s emitted by the moderator as a result of β^+ implantation. This method was expected to be more efficient than conventional β^+ tagging techniques since the efficiencies of both secondary e^- and moderated slow e^+ emission are maximal around the same (lower) implanted β^+ energies. Thus the moderated beam should be preferrentially detected over the higher energy β^+ which penetrate too far into the bulk. This study was performed in poor vacuum (10^{-6}Torr) with metal mesh, foil and powdered MgO samples from which the e^+ and secondary e^-s were magnetically guided to respective detectors which were part of a ToF arrangement. The largest timing efficiencies were obtained using seven tungsten meshes from which $50s^{-1}$ e^+s were detected of which over 20% were timed (Merrison et al 1990). Comparing the timed count rate with that of the total random background a ratio of 5×10^{-4} is obtained which is a factor of 30 greater than that of the more conventional thin plastic scintillator method of β^+ tagging (Coleman 1979). This value is approaching those of 10^{-2}-10^{-1} achieved by the more sophisticated secondary e^- timing technique which uses a remoderation stage (Van House et al 1984). The use of a remoderation stage requires complex experimental apparatus and a UHV system in order to achieve optimal efficiencies. The suitability of a timing method to a particular application depends on several factors. This new technique has the benefits of being simple and rugged with a good timing efficiency, although it is limited by the background to modest intensity beams which can be derived from source strengths of

typically 40MBq. Further work on the technique could significantly improve upon the quoted values with the use of a more efficient moderating/secondary e^- emitting material. One such material could be found in the RGS which possesses the highest currently quoted e^+ moderation efficiencies and have been observed to be highly efficient secondary e^- emitters (Gullikson 1988). Work performed in this thesis showed that typically one e^- per incident β^+ was emitted from the RGS which would indicate a tagging efficiency approaching unity for the emitted slow e^+ fraction. It should be noted though this, again, would lead to source strength limitations due to background considerations.

The e^+ reemission studies performed by Mills and Gullikson (1986) revealed much about the cooling and diffusion of e^+s in such insulating materials and prompted their subsequent use as efficient moderator materials. The high emission efficiency of low energy e^+s reflects the inability of the RGS, due to their large band gap, to rapidly cool the diffusing particles below a few eV. They can thus drift relatively large distances (in one lifetime) and thereby have a good chance of reaching an exit surface. A disadvantage encountered with these moderators when using highly resolved beams is the wide energy and angular distribution of the emitted e^+s. As part of this thesis the efficiencies of several solid Ar, Kr and Xe moderators were measured under different conditions such as depth and source geometry. Comparison was also made between transport using magnetic and electrostatic confinement. The largest efficiencies were those observed using solid Kr deposited on a conical copper source which at optimal depth typical achieved values in excess of 0.5%. This is around an order of magnitude greater than typical metal based moderator designs. It approaches the best quoted moderator efficiency of 1.4% obtained from solid Ne in a conical geometry and requires far less expensive and sophisticated cryogenic systems. In the case of Xe the highest efficiency obtained was 0.35%. Significantly, such a moderator could be operated, although at only moderate vacuum (10^{-6}Torr), using a liquid nitrogen cryostat and might be well suited for low intensity applications.

The RGS moderators employed in these studies were observed to be essentially stable over some days at only modest (10^{-7}Torr) vacuum. The observation of charging effects under e^- bombardment could, however, cause problems with the use of highly active sources given the large number of secondary e^-s generated. Surface charging of RGS has been studied in some depth (eg Sanche 1990) and is seen to occur via low energy e^- capture by overlayered impurities (eg O_2) with the production of stable anions (eg O^- and O_2^-). This method of

surface charging was utilised in the present work in order to study the field assisted extraction of moderated e^+s from Ar and Kr (Merrison et al 1992). The first observations consisted of monitoring the e^+ and β^+ induced secondary e^- yields from air coated RGS moderators. After degassing of an in situ ion gauge, enhancements were observed in the slow e^+ yields. For solid Ar a factor of between 3 and 5 was typically measured and in the case of Kr the enhancement was roughly a factor of 3. A corresponding decrease in β^+ induced secondary e^- yield of between a factor of 5 and 7 was observed. The enhancement decayed to around a half of its initial value over a period of approximately one hour, but could subsequently, in most part, be regained by further activation using the ion gauge. No enhancement effects were observed for samples which did not have an impurity overlayer. With the use of biasing potentials close to the moderator it was possible enhance the β^+ induced secondary e^- yield by over a factor of four while reducing the slow e^+ yield to practically nothing. By consideration of the ion gauge operation and the geometry of the beam it was concluded that the e^+ and β^+ induced secondary e^- yield enhancements were caused respectively by low energy (secondary) e^- and positive ion bombardment.

A more quantitative study of these effects was undertaken using a flat β^+ source upon which an O_2 coated Ar film was deposited. An electron gun was then used to bombard the surface with secondary e^-s of energy between 0 and 20eV. Both e^+ and secondary e^- energy spectra measured before and after surface activation were consistent with a negative surface potential of about 20V. Monitoring the reduction of slow e^+ beam enhancement with the decay of this surface charge allowed the variation of moderation efficiency to be studied as a function of applied electric field. An estimate of the absolute electric field strength within the RGS film was obtained by determinig the Ar film thickness. This was achieved by comparing the moderation efficiency as a function of deposition time (thickness) with theory. The results (figure 4.21) show a rapid rise in moderation efficiency at field strengths between 3 and 6kV/mm above which and up to nearly 8kV/mm the enhancement appears to saturate at about a factor of three. At present there is not a sufficiently sophisticated theoretical treatment of the effect of an electric field on e^+ emission from RGS for comparison to be made with these results. This may partly be attributed to the lack of adequate theoretical or experimental data concerning Ps formation under the influence of an electric field. The possibilty of performing re-emission studies from surface charged RGS following low energy e^+ implantation may provide much useful information on the dynamics occuring within these solids.

The further development of field assisted extraction, whether using this surface charging technique or by more traditional means, could be of significance in the production of more efficient methods of e^+ moderation. This technique provides a virtually cost-free means of increasing moderated slow e^+ yield by at least a factor of three. It requires little adaptation to the design of current RGS moderators, specifically access to some impurity (gas) and a low energy e^- source. If, as suspected, the decay of surface charge results from induced anion desorption, stability of the moderator efficiency may be achieved by some method of continual impurity deposition and e^- bombardment. The estimated field intensity required for field assisted moderation could be achieved by application using a metal grid. This might provide a more controllable and stable moderator design. The results of this study would indicate that the moderation efficiency of solid neon may similarly be increased by this method. Efficiencies of around 5% may thereby be achieved. It is clear that much further work remains to be done on the behaviour of e^+ in surface charged RGS.

REFERENCES

Adachi S, Chiba M, Hirose T, Nagayama S, Nakamitsu Y, Sato T and Yamada T, 1990, Phys. Rev. **A65**, 2634

Anderson C D, 1932, Phys. Rev. **127**, 150.

Baker J A and Coleman P G, 1988, J. Phys. C.: Solid State Phys. **21**, L875

Baker J A, Chilton N B, Jensen K O, Walker A B and Coleman P G, 1991c, Baker J A and J.Phys.:Condensed Matter **3**, 4109

Baker J A, Chilton N B and Coleman P G, 1991b, Appl. Phys. Lett. **59**, 164

Baker J A, Chilton N B, Jensen K O, Walker A B and Coleman P G, 1991a, Appl. Phys. Lett. **59**, 2962

Bardeen J and Shockley W S, 1950, Phys. Rev. **80**, 72

Bass A D and Sanche L, 1991, J. Chem. Phys. **95**, 2910

Beling C D, Simpson R I, Charlton M, Jacobsen F M, Griffith T C, Moriarty P and Fung S, 1986, Appl. Phys. **A42**, 111

Bellotti E, Corti M, Fiorini E, Liguori C, Pullia A, Sarracino A, Sverzellati P and Zanotti L, 1983, Phys. Lett. **B124**, 435

Bergersen B, Pajanni E, Kubica P, Stott M J and Hodges C H, 1974, Solid State Commun. **15**, 1377

Bisi A, Gambarini G and Zappa L, 1981, Lett. Nuovo Cimento **31**, 58

Blackett P M S and Occhialini G P S , 1933, Proc. Roy. Soc. **A139**, 699.

Bodin H A B, 1957, PhD dissertation (University of Glasgow) unpublished

Brandes G R, Mills A P Jr, Voris S S Jr and Zuckerman D M, 1991a, Materials Science Forum vols. 105-110 pt.2, pp.763

Brandes G R, Mills A P Jr and Zuckerman D M, 1991b, Materials Science Forum vols. 105-110 pt.3, pp.1363

Brandt W and Arista N R, 1979, Phys. Rev. **A19**, 2317

Brandt W and Dupasquier A, eds., 1983, International School of Physics 'Enrico Fermi' (1981 Verenna, Italy). Positron Solid State Physics (Procedings of the International School of Physics 'Enrico Fermi'; course 83), (North Holland Amsterdam).

Brandt W, 1982, Lett. Nuovo Cimento **33**, 499

Brandt W and Feibus H, 1968, Phys. Rev. **174**, 454

Brandt W and Paulin R, 1977, Phys. Rev. **B15**, 2511

Canter K F, Brandes G R, Horsky T N, Lippel P H and Mills A P Jr, 1989, in Dorikens-Vanpraet et al, eds., pp18-27

Canter K F, Coleman P G, Griffith T C and Heyland G R, 1972, J. Phys. **B5**, L167

Canter KF, Mills A P Jr., and Berko S, 1975, Phys. Rev. Lett. 34, 177

Caswell W E and Lepage G P, 1979, Phys. Rev. **A20**, 36

Chang T, Tang H, Li Y, 1985, in ICPA 85, p. 212

Charlton M, 1985, Rep. Prog. Phys. 48, 737

Charlton M and Curry P J, 1985, Nuovo Cimento **D6**, 17

Cherry W, 1958, PhD dissertation (Princeton University, unpublished)

Cohen and Taylor, 1973, J. Phys. Chem. Ref. Data, 2, 663

ER BN

Cohen M H and Jortner J, 1969, Phys. Rev. **180**, 238

Coleman P G, 1988, J. Phys. **C21**, L875

Coleman P G, 1979, J. Phys. E: Sci. Instrum. **12**, 590

Coleman P G, Griffith T C and Heyland G R, 1972, J. Phys. **E5**, 376

Coleman P G, Griffith T C and Heyland G R, 1973, Proc. R. Soc. **A331**, 561

Corbel C, Hautojarvi P, Mäkinen J, Vehanen A and Mathiot D, 1989, J. Phys. Condens. Matter **1**, 6315

Curry P J and Charlton M, 1985, Chem. Phys. **95**, 313

Dahl D A and Delmore J E, 1988, "The SIMION PC/PS2 User's Mannual" (Idaho National Engineering Laboratory, 1988)

Deutch B I, Charlton M, Holzscheiter M H, Hvelplund P, Jørgensen L V, Knudsen H, Laricchia G, Merrison J and Poulsen M, 1992, in press

Deutsch M, 1951, Phys. Rev. **82**, 455

Dirac P A M, 1930a, Proc. Roy. Soc. **A126**, 360.

Dirac P A M, 1930b, Proc. Camb. Phil. Soc. **26**, 361

Dupasquier A, 1983, in Brandt W and Dupasquier A, pp510-564

Echt O, 1986, 5th Symposium on Atomic and Surface Physics, Obertraun, Austria

Evans R D, 1955, The Atomic Nucleus, (McGraw-Hill, New York), p.628

Gidley D W, Rich A, Sweetman E and West D, 1982, Phys. Rev. Lett. **49**, 525

Gramsch E, Throwe J and Lynn K G, 1987, Appl. Phys. Lett. **51**, 1862

Gross B, Seggern H and West J E, 1984, J. Appl. Phys. **56**, 2333

Gryziński M, 1965, Phys. Rev. **138**, 305A (part I), 322A (part II) and 336A (part III)

Gullikson E M, Mills A P Jr and McRae, 1988, Phys. Rev. **B37**, 588

Gullikson E M, 1988, Phys. Rev. **B37**, 7904

Gullikson E M and Mills A P Jr, 1986, Phys. Rev. Lett. **57**, 376

Gullikson E M and Mills A P Jr, 1989, Phys. Rev. **B39**, 6121

Gullikson E M, Mills A P Jr and Murray C A, 1988, Phys. Rev. **B38**, 1705

Gullikson E M and Henke B L, 1989, Phys. Rev. **B39**, 1

Heinrich F, 1978, Helv. Phys. Acta **51**, 433

Hutchins S M, Coleman P G, Stone R J and West R N, 1986, J. Phys. **E19**, 282

Ito Y, Axuma T, Sueoka O, Mori S, Katsumura Y, Kobayashi H and Tabata Y, 1985, in **ICPA85**, p.977

Jacobini C and Reggiani L, 1979, Adv. in Phys. **28**, 493

Jacobs H, 1951, Phys. Rev. **84**, 877

Jacobsen F M, 1986, Chem. Phys. **109**, 455

Jacobsen F M, 1983, in Positron Scattering in Gases, Proceedings NATO workshop on e^+ Scattering in Gases (Royal Holloway College, London, 1983), p.85

Jacobsen F M, Charlton M, Chevallier J, Deutch B I, Laricchia G and Poulsen M R, J. Appl. Phys. **67**, 575

Kahana S, 1960, Phys. Rev. **117**, 123

Khatri R, Charlton M, Sferlazzo P, Lynn K G, Mills A P Jr and Roellig L O, 1990, Appl. Phys. Lett. **57**, 2374

Kim L, Pratt R H, Seltzer S M and Berger M J, 1986, Phys. Rev. **A33**, 3002

Knop G and Paul W, 1966, in Alpha, Beta and Gamma Ray Spectroscopy, Siegbahn K, ed., (North Holland, Amsterdam) 1, p.1

Koshida N and Yoshida S, 1978, Appl. Phys. Lett. **32**, 708

Köymen A R, Gidley D W and Capehart T W, 1987, Phys. Rev. **B35**, 1034

Laricchia G and Zafar N, 1992, in Positrons at metallic surfaces ed. A. Ishii (Trans Tech Pub. Ltd, Switzerland) in press

Lennard W N, Schultz P J and Massoumi G R, 1988, Nucl. Instrum. Methods **B33**, 128

Lindhard J, 1976, Nucl. Instrum. Methods **132**, 1

Lynn K G, Chen D M, Nielsen B, Pareza R and Myers S, 1986, Phys. Rev. **B34**, 1449

Lynn K G, Frieze W E and Schultz P J, 1984, Phys. Rev. Lett. **52**, 1137

Lynn K G and McKee B T A, 1979, Appl. Phys. **19**, 247

Lynn K G, Gramsch E, Usmar S G and Sferlazzo P, 1989, Appl. Phys. Lett. **55**, 87

MacKensie I K and Gorayshi P Z, 1985, Solid State Comm. **55**, 125

MacKensie I K, Shulte C W, Jackman T and Campbell J L, 1973, Phys. Rev. **A7**, 135

Madansky L and Rasetti F, 1950, Phys. Rev. **79**, 397

Madey J M J, 1969, Phys. Rev. Lett. **22**, 784

Mäkinen J, Palko S, Martikainen J and Hautojarvi P, 1992, J. Phys. Condens. Matter **4**, L503

Marder S, Hughes V W, Wu C S and Bennett W, 1956, Phys. Rev. **103**, 1258

Märk T D, Leiter K, Ritter W and Stamatovic A, 1986, Int. J. Mass Spectrum. Ion Processes **74**, 265

Marsolais R M, Deschenes M and Sanche L, 1989, Rev. Instrum. **60**, 2724

Massoumi G R, Hozhabri N, Lennard W N and Schultz P J, 1991, Phys. Rev. B **44**, 3486

Merrison J P, Charlton M and Laricchia G, 1991, Meas. Sci. Technol. **2**, 175

Merrison J P, Charlton M, Deutch B I and Jørgensen L V, 1992, J. Phys.: Condens. Matter **4**, L207

Michaud M and Sanche L, 1990, J. Electron Spectrosc. Relat. Phenom. **51**, 237

Mills A P Jr and Pfieffer L, 1979, Phys. Rev. Lett. **43**, 1961

Mills A P Jr, Pfieffer L and Pltzman P M, 1983, Phys. Rev. Lett. **51**, 1085

Mills A P Jr and Murray C A, 1980, Appl. Phys. **21**, 323

Mills A P Jr and Pfieffer L, 1977, Phys. Lett. **63A**, 118

Mills A P Jr and Gullikson E M, 1986, Appl. Phys. Lett. **49**, 1121

Mills A P Jr and Crane W S, 1984, Phys. Rev. Lett. **53**, 2165

Mills A P Jr and Wilson R J, 1982, Phys. Rev. **A26**, 490

Mills A P Jr, 1980, Appl. Phys. **22**, 273

Mills A P Jr and Pfieffer L, 1985, Phys. Rev. **B32**, 53

Mogensen O E, 1983, Phys. Lett. **96A**, 250

Mogensen O E, 1974, J. Chem. Phys. **60**, 998

Mohorovicic S, 1934, Astron. Nachr. **253**, 94.

Mourino M, Löbl H and Paulin R, 1979, Phys. Lett. **71A**, 106

Murray C A and Mills A P Jr, 1980, Solid State Comm. **34**, 789

Musket R G, 1975, J. Vac. Sci. Technol. **12**, 444

Nico J S, Gidley D W, Skalsey M and Zitzewitz P W, 1991, in "Book of abstracts, 9th International Conference on Positron Annihilation", p.132

Nielsen B, Lynn K G and Chen Y C, 1986, Phys. Rev. Lett. **57**, 1789

Obenshain F E and Page L A, 1962, Phys. Rev. **125**, 573

Ore A, 1949, Univ. i Bergen Arbok Natuvidensabelig Rekke, **9**

Ore A and Powell J L, 1949, Phys. Rev. **75**, 1696

Palmer R E and Rous P J, 1992, Rev. Modern Phys. Vol. **64**, 383

Paul D A L, 1958, Can J. Phys. **36**, 640

Pendyala S, 1973, PhD dissertation (University of Western Ontario)

Poulsen M R, Laricchia G, Charlton M, Jensen K O and Walker A B, 1992, Materials Science Forum Vols. 105-110, pp.1431

Rowntree P, Parenteau L and Sanche L, 1991b, J. Phys. Chem. **95**, 4902

Rowntree P, Parenteau L and Sanche L, 1991a, J. Chem. Phys. **94**, 8570

Sambe H, Ramaker D E, Deschenes M, Bass A D and Sanche L, 1990, Phys. Rev. Lett. **64**, 523

Sanche L and Parenteau L, 1990, J. Chem. Phys. **93**, 7476

Sanche L and Deschenes M, 1988, Phys. Rev. Lett. **61**, 2096

Sanche L, Parenteau L and Cloutier P, 1989, J. Chem. Phys. **91**, 2664

Sanche L, 1990, J. Phys. B: At. Mol. Opt. Phys. **23**, 1597

Schou J, 1988, Scanning Microscopy **2**, 607

Schultz P J and Lynn K G, Rev. Mod. Phys. **60**, 701

Schultz P J and Campbell J L, 1985, Phys. Lett. **A112**, 316

Seggern H, 1985, IEEE Trans. Nucl. Sci. vol. **NS-32**, 1503

Sferlasso P, Berko S and Canter K F, 1987, Phys. Rev. **B35**, 5315

Simpson R I, 1990, PhD dissertation (University College London) unpublished

Soininen E, Huomo H, Huttunen P A, Mäkinen J, Vehanen A and Hautojärvi P, 1990, Phys. Rev. **B41**, 6227

Spear W E and LeCombe P G, 1977, Rare Gas Solids Vol. 2, ed. Klien M L and Venables J A (London Academic) ch. 18

Stewart A T, Briscoe C V and Steinbacher J.J, 1990, Can. J. Phys. **68**, 1362

Sueoka O and Koide S, 1976, J. Phys. Soc. Jpn. **41**, 116

Tate J T and Smith P T, 1932, Phys. Rev. **39**, 270

Tong B Y, 1972, Phys. Rev. **B5**, 1436

Tuomisaari M, Howell R H and McMullen T, 1990, J. Phys. B: At. Mol. Opt. Phys. **24**, 1455

Valkealahti S and Nieminen R M, 1984, Appl. Phys. **A35**, 51

Valkealahti S and Nieminen R M, 1983, Appl. Phys. **A32**, 95

Varlashkin P G, 1970, Phys. Rev. **A3**, 1230

Vehanen A, Saarinen K, Hautojärvi P and Huomo H, 1987, Phys. Rev. B **35**, 4606

Vehanen A and Mäkinen J, 1985, Appl. Phys. **A36**, 97

Zafar N, 1990, PhD dissertation (University College London) unpublished

Zafar N, Chevallier J, Jacobsen F M, Charlton M and Laricchia G, 1988, Appl. Phys. **A47**, 409

Zhang C, Tzoar N and Platzman P M, 1988, Phys. Rev. **B37**, 7326

Costello DG, Grove DE, Herring DF and McGowan JW, 1972, Phys. Rev. B5, 1433

Stein TS, Kaupilla WE, Pol V, Smart JH and Jeison G, 1978, Phys. Rev. A17, 1602

Mills A P Jr., Platzman PM, ed Brown BL, 1978, Phys. Rev. Lett. 41, 1076

Mills A P Jr., 1979, Solid state comm. 31, 623

Dale JM, Hulett LD ed Pendyala S, 1980, Surf. Interf. Anal, 2, 199

Vehanen A, Lynn KG, Schultz PJ ed Eldrup M, 1973, Appl. Phys. A32, 163

Lynn KG, Mills A P Jr., West R N, Berko S, Canter K F, Roellig L O, 1985, Phys. Rev. Lett. 54, 1702

Mills A P Jr., 1983, in International School of Physics, 'Enrico Fermi' (1981 Verenna Italy) P.432

Mills A P Jr., 1988, Hyp. Int. 44, 107

Charlton M, Andersen LH, Brun-Nielsen L, Deutch BI, Hvelplund P, Jacobsen F M, Knudsen H, Laricchia G, Poulsen MR, ed Pedersen JO, 1988, J. Phys. B21, L545

Mills A P Jr., Brandes G R, Zuckerman DM, Liu W ed Berko S, 1992, Materials Forum 105, Pt. 2, P. 763

Van Horse J, Rich A, ed Zitzewitz PW, 1984, Phys. Rev. Lett. 53, 953